Silk Cocoons as Composites

Thesis Abstract

Fujia Chen

Jesus College
Michaelmas 2011

Oxford Silk Group
Department of Zoology

Dissertation submitted to the Boards of the Faculty of Life Sciences, in fulfilment for the degree of Doctor of Philosophy in Zoology

This thesis looks at the engineering aspects of silkworm cocoons as a structural biological composite system. A wide range of species of silk cocoons were studied for their morphologies, physical properties and mechanical behaviour. A silk cocoon can be described very broadly as a nonwoven fibre composite made of silk fibres bonded by sericin binder, although the a variety of species can show a diversity of structural features of the layers, porosity, degree of orientation, binding density and presence of crystals etc. These structural differences lead to diverse cocoon mechanical behaviour. Tensile and compressive properties of cocoons are tested and linked to their individual interfibre bonding, connectivity and density. Gas diffusion through the cocoon walls is controlled by the combination of thickness and density.

In addition, a physically realistic quantitative model is developed, which links directly the structure and mechanical properties of silk cocoons. The gradual loss of connectivity of the interfibre bonding is the key mechanism for the deformation of cocoons. It can be quantified as a strain activated function of the bonding up to a failure criterion, where either a percolation threshold of 50% of these bonds or the failure stress of the binder arrives. For *Bombyx mori* cocoon, which has a graded-layer structure, the model was enhanced to include the contribution of interlayer and intralayer bonding in the system. This model can also be applied to other nonwoven fibre and particulate composites using a small number of physically realistic model parameters, and will be a valuable 'bioinspired' tool for the development of new composite systems.

Based on the understanding of structure-mechanical property relationships in silkworm cocoons, an engineering approach was used for examining cocoon as an impact resistant structural material that provides mechanical protection from environmental threats. In addition, silk cocoons were used as a nonwoven reinforcement to develop an engineering composite by increasing the connectivity (more binder) in the cocoon. Using polyurethane or regenerated silk fibroin of medium concentration can increase the toughness of cocoons, and epoxy or regenerated silk fibroin of high concentration binding leads to a brittle system.

Acknowledgements

Firstly, I would like to thank my two supervisors: Dr David Porter for his continual guidance and useful help, his unwavering belief in me, his care and concern for my academic and personal development, his patience in allowing me the freedom to find my own ways, explore my own ideas and make my own mistakes, and his inspiring insight of science and the world; and Professor Fritz Vollrath for giving me the opportunity and support to undertake this novel and interesting piece of work, working through all kinds of difficulties to find the grant which enabled me as an international student to come to Oxford to undertake this doctoral thesis and have the best four years in my life, and introducing me to a new fascinating research field, in which I wish to establish a career.

From Oxford, I would like to thank everyone in Oxford Silk Group for continual help during these four years. My time in Oxford was enhanced by the assistance, friendship and inspiration from this wonderful group. I would particularly extend my gratitude to Ms Juan Guan and Dr Chris Holland for their help with cocoon compressive tests, Mr Maxime Boulet-Audet and Ms Imke Greving for instruction and data analysis of FTIR, Mr Tom Gheysens, Dr Cedric Dicko and Mr Björn Greving for developing cocoon destoning, gas diffusion and fibre diameter measurement methods, Dr Thomas Hesselberg for help with ABAQUS simulation, and Mr Gwilym Davies and Mr Xiafu Shi for the cocoon photographs.

For funding I would like to thank the American Air Force Office of Scientific Research for their generous funding of this project, and thank Jesus College Oxford, The Society for the Advancement of Material and Process Engineering UK, The European Cooperation in Science and Technology, and The Materials Research Society for travel grants.

Finally, I would like to express my deepest gratitude to my family for their unconditional trust, support and encouragement. This thesis is dedicated to my father Haizhong Chen who was denied the higher education I have been able to enjoy because of the dark history, and my mother Xunzhi Yang who gives me a world of opportunities.

Publications

Several chapters of this thesis were revised or partly revised from the following publications.

Chapter 1

Vollrath, F., Chen, F., Porter, D. (2009). Silks and their composites. Transactions of the 14th Fundamental Research Symposium on advances in pulp and paper research, Oxford.

Chapter 2

Chen, F., Porter, D., Vollrath, F. (2012). Morphology and structure of silkworm cocoons. Materials Science and Engineering: C **32**(4): 772-778.

Chapter 3

Chen, F., Porter, D., Vollrath, F. (2012). Structure and physical properties of silkworm cocoons. Journal of the Royal Society Interface. Accepted

Chapter 4

Chen, F., Porter, D., Vollrath, F. (2010). Silkworm cocoons inspire models for random fiber and particulate composites. Physics Review E **82**(4): 041911-041917.

Chen, F., Porter, D., Vollrath, F. (2010). A nonwoven composite model based on silkworm cocoon (*Bombyx mori*). Journal of Materials Science and Engineering **4**(9): 28-33.

Chapter 5

Chen, F., Porter, D., Vollrath, F. (2012). Silk cocoon (*Bombyx mori*): Multi-layer structure and mechanical properties. Acta Biomaterialia. Accepted

Chapter 6

Chen, F., Porter, D., Vollrath, F. (2012). The impact behaviour of silk cocoons. Journal of Experimental Biology. Submitted

Chen, F., Hodgkinson, J. (2011). Impact damage. Encyclopaedia of Composites, Wiley Publishing.

Chapter 7

Chen, F., Porter, D., Vollrath, F. (2012). Silk cocoon as nonwoven biocomposites. Composites, Part A. Submitted

Contents

Chapter 1 1
1.1 Biological composites: structure and mechanical properties 1
1.2 Silk 2
1.3 Historical background of silk cocoon 10
1.4 Chapter introduction 13
1.4.1 Chapter 2: Morphologies of cocoons 13
1.4.2 Chapter 3: Physical properties of cocoons 13
1.4.3 Chapter 4: Structure-property relationship of cocoons 13
1.4.4 Chapter 5: Structure-property relationships of *Bombyx mori* cocoon 14
1.4.5 Chapter 6: Indentation of cocoon 14
1.4.6 Chapter 7: Synthetic cocoon composites 14
1.4.7 Chapter 8: Summary and general discussion 15
1.5 Approach of this thesis 15
Chapter 2 21
2.1 Introduction 21
2.2 Materials and methods 21
2.2.1 Materials collection 21
2.2.2 SEM observation 22
2.2.3 Fourier transform infrared spectroscopy (FTIR) test 22
2.2.4 Density measurement of the cocoons 23
2.3 Results 26
2.3.1 Morphology of the cocoons 26
2.3.2 Cocoon fibres 35
2.3.3 FTIR 36
2.3.4 Density calculation 38
2.4 Conclusion 38
Chapter 3 41
3.1 Introduction 41
3.2 Materials and methods 42
3.2.1 Materials collection 42
3.2.2 Scanning electron microscope (SEM) observation 42
3.2.3 Tensile tests of cocoons 42
3.2.4 Fibre testing 43
3.2.5 Compression tests of the cocoons 44
3.2.6 Gas diffusion test (diethyl ether) 44
3.3 Results and discussion 44
3.3.1 Fibre Properties 45
3.3.2 Tensile Properties 47
3.3.3 Compressive properties 50
3.3.4 Gas diffusion (diethyl ether) 52
3.4 Conclusions 55
Chapter 4 62
4.1 Introduction 62
4.2 Literature Review 63

4.2.1 Bonding failure 64
4.2.2 Shear-lag models 65
4.2.3 Weibull theory 67
4.2.4 Open-cell foam model 68
4.2.5 Summary of Literature 71
4.3 Materials and methods 72
4.4 Cocoon connectivity model development 72
4.5 Application to other cocoons 83
4.6 Application to other materials 86
4.6.1 Nonwovens 87
4.6.2 Particulate composites 89
4.7 Conclusions 93
Chapter 5 97
5.1 Introduction 97
5.2 Experiments: Materials and Methods 99
5.2.1 Materials collection 99
5.2.2 Scanning electron microscope (SEM) observation 99
5.2.3 Fourier transform infrared spectroscopy (FTIR) 99
5.2.4 Tensile tests of cocoons and layers 100
5.2.5 Peel tests 101
5.3 Results and analysis 101
5.3.1 Morphology 101
5.3.2 Component contents 104
5.3.3 Mechanical properties 106
5.3.4 Mechanical properties of cocoon layers 108
5.3.5 Peel tests 112
5.4 Discussion 113
5.4.1 Interlayer bonding energy 113
5.4.2 Layer contribution 114
5.5 Conclusions 117
Chapter 6 121
6.1 Introduction 121
6.2 Experiments 124
6.2.1 Indentation experiments 124
6.2.2 Finite element model 124
6.3 Results 126
6.3.1 Indentation experimental results 126
6.3.2 FEA: Constitutive model for materials 129
6.3.3 FEA simulation results of cocoon samples 132
6.3.4 Indentation: Comparison between experiments and simulations 135
6.3.5 Problems of the FEA modelling 141
6.4 Discussion 143
Chapter 7 149
7.1 Introduction 149
7.2 Background of Composites 150
7.2.1 Resin Matrix 151
7.2.2 Reinforcement 153

7.2.3 Interfacial wettability....154
7.3 Materials and Methods....156
7.3.1 Materials....156
7.3.2 Contact angle measurement....158
7.3.3 Single fibre coating and testing....158
7.3.4 Composites manufacturing....159
7.3.5 Thermogravimetric analysis (TGA)....159
7.3.6 Mechanical testing and scanning electron microscopy (SEM)....160
7.4 Results....160
7.4.1 Fibre-matrix bonding....160
7.4.2 Contact angle measurement....163
7.4.3 Cocoon composites morphology....164
7.4.4 Thermal properties....165
7.4.5 Mechanical properties....167
7.5 Discussion and Conclusions....171
Chapter 8....181
8.1 General summary....181
8.2 General discussion....182

Chapter 1

Introduction

1.1 Biological composites: structure and mechanical properties

Although biology is a mature science, it is only recently that the field has become truly interdisciplinary, enabling physical and materials science to help to explain biological principles and mechanisms [1]. Looking back to 1917, D'Arcy W. Thompson was the first scientist that looked at biological systems as engineering structures, and tried to connect the structures with their basic engineering functionality in his classic work *On Growth and Form* [2]. In the 1950s, materials science and engineering started to evolve and expand rapidly. Currey and Vincent in the 70s and 80s published *Bones: Structure and mechanics* [3] and *Structural Biomaterials* [4], in which they used an engineering approach to study biological materials. Recently, material scientists have performed many studies on biological materials. They intended initially to design or copy materials that impart a biological function. This is also called biomaterials study. This field is now broadening, providing the tools to apply biological mechanisms in the design of materials for non-biological applications. This is so-called biomimetic engineering.

Many biological composites have a highly hierarchical structure down to the nano scale, which enables them to have striking mechanical properties. This is an amazing feature, as they are often made of very weak polymers and mineral compositions, and produced at ambient temperature, pressure and under environmentally benign conditions. These complicated engineering features have arisen from millions of years of evolution to fit their

individual functions. The hierarchical organization of biological materials is inherent in their design. The combination of structure and materials are closely connected to function.

For example, biological ceramic composites are usually comprised of a mineralized hard component, which provides the stiffness, and a softer organic component, which enhances the toughness. Bone has a toughness significantly higher than fully dense hydroxyapatite that makes up 40% of the total volume. Bone has collagen molecules arranged to form triple helix fibrils. These organic components can arrest microcracks ahead of a crack tip if a bone is stressed, which increases the toughness of the composites [1].

Another example is wood, which is one of the most ancient structural materials in the world. Its specific stiffness and specific strength are as high as steel. These outstanding mechanical properties result from its hierarchical structure and optimized reinforcement orientation of cellulose fibrils. Wood has a cellular structure, in which the cellulose is organized into microfibrils, which consist of both crystalline and amorphous regions. Bundles of the microfibrils form macrofibrils that are embedded in an amorphous matrix of lignin, hemicellulose and other components. A microfibril itself has three layers, and the cellulose fibrils in the middle layer (S2 layer) orient in the axial direction with a specific angle, which provides an optimum compromise between energy absorption and the reduction in stiffness [1].

1.2 Silk

Although silk fibre is not the subject of this thesis, a brief introduction is given here as it is one of the key components of silk cocoons. Most silk research has focused on the silk fibre, so it has been extensively studied and understood [5-7].

Silk is not only of interest to the biologist but also materials scientists and engineers, as it has superior mechanical properties that are highly desired by modern industries. Importantly, the material properties of a silk depend not only on the chemistry and subsequent folding pattern of the silk protein, but also on the hierarchical structure of the poly-protein fibre. Both, in turn, depend to a large extent on the conditions under which a fibre has been spun and thus depend on the animal's spinning behaviour. Not surprisingly, this gives the animal a high degree of flexibility in which to use its materials. And if the materials are integrated into structures, the structural materials can then have a range of ultimate properties, depending on the animal's building behaviour. As both materials and structures have evolved over millions of years, much can be learned concerning highly adapted and often optimized structure-property-function relationships on the engineering level [8].

Silk, be it spun by spider, moth, mite or bee is basically one and the same material. True, it has evolved independently in the spiders and the insects and differs in the details of its chemistry and production system. However, by the definition of Vollrath & Porter [5], silk is always spun. That sets silks apart from all other biological materials, which are grown. In essence, all silks are composite nano-structured materials consisting of interspersed regions of high, medium and low order, e.g. protein crystals embedded in a protein matrix. Different silks differ in molecular composition resulting in different spatial configurations with the nano-scale dimensions giving both strength and extensibility. As a rough guide, silk fibres have tensile modulus values in the range 10 kPa for a highly hydrated gel to about 20 GPa for the stiffest dragline silk, and strengths from almost zero values of yield stress to about 1.6 GPa respectively. Commercial textile silk fibres from *Bombyx mori* silkworm cocoon would have a modulus of about 10 GPa with a strength of about 400 MPa. An important strength

parameter is fibre diameter, which might range from about 20 μm down to a few tens of nanometers.

Silk fibres usually have striking toughness compared to other biological or industrial fibres, including Kevlar fibres, which are used as strong fibres in industrial applications (Figure 1.1). This toughness depends not only on the folding of the major silk protein but also on the hierarchical structure of the poly-protein fibre and the conditions under which it is spun. Individual silk fibres range in diameter from 20 to 7000 nm depending on species, spider size, silk type and spinning conditions. The complex hierarchical structure of the fibre is the outcome of a complex spinning process acting on suitable dopants in the polymer feedstock. The complexity of this process suggests that a number of different factors contribute to the extraordinary toughness of spider silk. Silk is spun from a highly concentrated (30-50%) solution of large (several hundred kDa) molecules with a highly repetitive molecular structure consisting of alternating sequences of motifs encoding for both rigid and flexible elements. These sequences appear to be folded into a hydrated nanoscale string-of-beads structure that in turn shows liquid crystalline flow behaviour [5].

A famous of example is the spider silk. All spiders produce more than one kind of silk with the female of the common garden spider having at least seven different kinds, each with its own production system consisting of gland, storage sac, duct, valve and spigot (Figure 1.2). The glands are hidden deep inside the spider's abdomen but the spigots open on nozzles embedded atop highly mobile extremities, the spinnerets [9]. Not all of the garden spider's silks are used in her web. One silk resembles in its function the material of the silk larva, providing the tough covering of the little purse that contains the spider's eggs. Another silk has a double function: fluffed up it cradles the delicate eggs, but when paid out in ribbons it

entangles and enshrouds the unfortunate prey insect. Actually, many silks have multi-purpose: the safety line, trailed at all times, doubles up as material for the frames and radials of the web. The cement that anchors lines to the ground is also used to cement the crisscrossing strands of the egg sac as well as to fix the spirals onto the supporting radials. Spider web silks are re-spun daily, often in large quantities. They are thin enough to be practically invisible. Yet at the same time they are strong enough to catch insects in full flight, no mean feat considering that, pound for pound, the kinetic energy to be absorbed exceeds the impact of a jet landing in the rubber bands of an aircraft carrier. Some of that energy is absorbed by the material itself while some is deflected by the architecture of the web and some, interestingly, discharged by aerodynamic damping due to the low Reynolds number of the thin threads coupled with a self-assembling micro-windlass system.

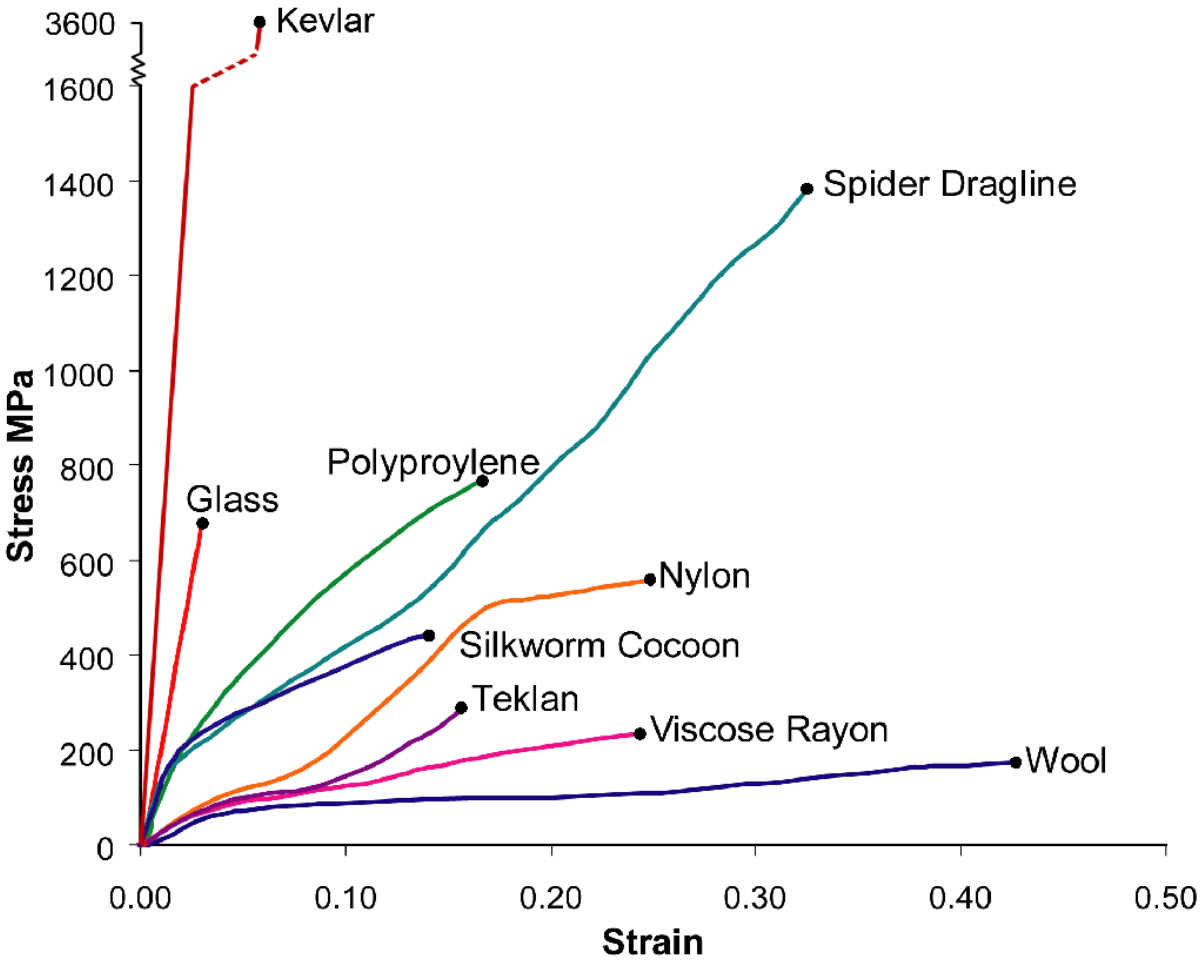

Figure 1.1 Typical stress-strain curves of silk and other fibres [10]. Nylon fibre: Nylon 6,6 medium tenacity from Goodfellow Cambridge Limited (Product No. 325710/1). Polypropylene fibre: medium tenacity PP 305747 fibre from Goodfellow Cambridge Limited. Teklan fibre: a modacrylic fibre which has flam proof qualities from Courtaulds Plc.

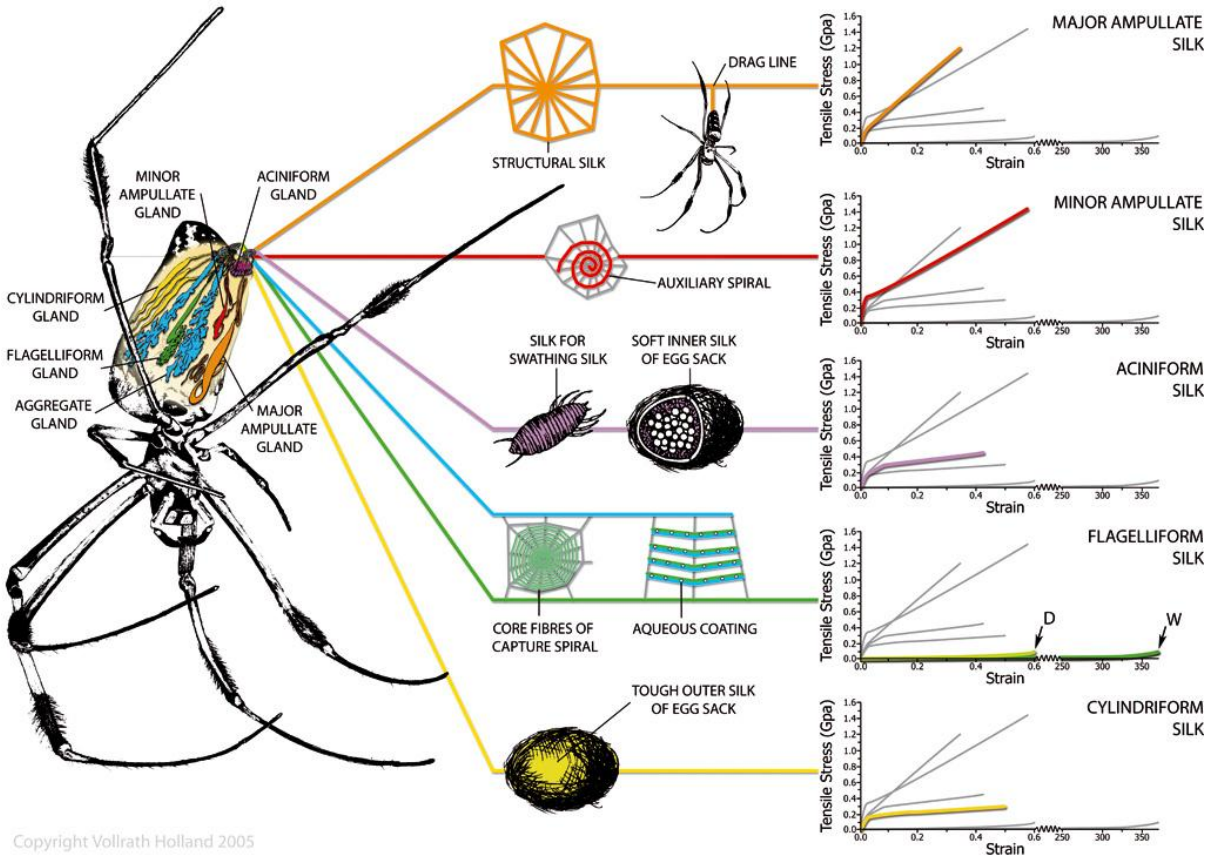

Figure 1.2 The golden orb spider *Nephila* spp with its silk glands, silks and their mechanical properties [11].

On the other hand, silkworms are also skilled craftsmen. Many species from the order Lepidoptera, especially from the family Saturniidae, make delicate cocoons. They devote a considerable proportion of their mass and energy gained from the larva stage to the production of silk for constructing cocoons, and then spend most of their life in them. The cocoon is suggested to provide protection against the environment, parasitism and predators. Chinese silkworm, *Bombyx mori*, is one of the moth species domesticated over millennia for textile silk fibre production. Its cocoons (like those of other silk moths) are natural polymer composite shells with a 3D non-woven structure, consisting of a continuous silk fibroin protein doublet fibre co-extruded with a sericin protein that agglutinates into the composite's

matrix material. A cocoon is a natural polymer composite shell made of a single continuous silk strand with a length in the range of 1000-1500 m and conglutinated by sericin. Each fibre is composed of two fibroins conglutinated by a layer of sericin. Silk fibroin is a natural fibrous protein with a semicrystalline structure. It accounts for about 75 wt.% in the fibre. Sericin is an amorphous protein polymer that accounts for 25 wt.% and acts as an adhesive to maintain the structure of two fibroins in a fibre and the whole cocoon. Figure 1.3 shows a hierarchical set of pictures of the *Bombyx mori* cocoon structure, from the full cocoon to the individual fibre-sericin combination.

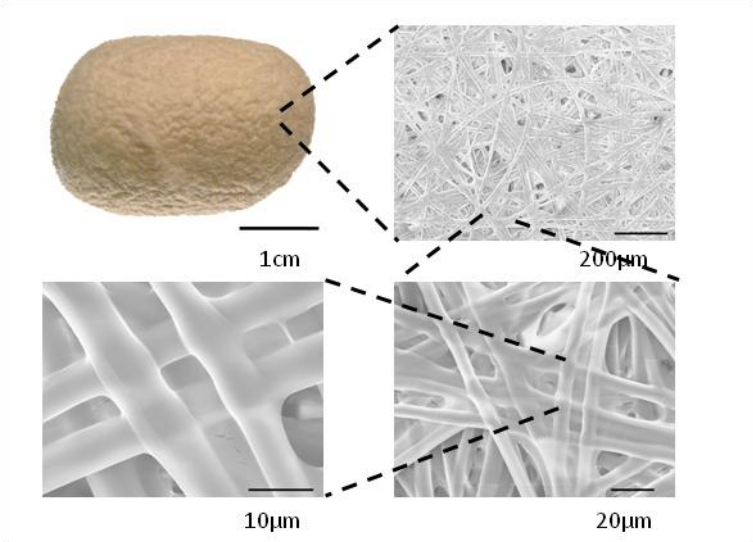

Figure 1.3 Hierarchy of the morphology of a *Bombyx mori* cocoon

The compositions of fibroin and sericin proteins are different. For example, the fibroin of *Bombyx mori* cocoon is composed of a heavy, highly insoluble protein chain (H) and a light (L) chain which are linked by a disulfide bond [12], and another silk core constituent named P25 [13, 14] in a ratio of 6:6:1 [15]. It contains the motif –Gly-Ala-Gly-Ala-Gly-Ser- repeated along its sequence, which forms a high volume fraction of ß-sheet microcrystalline

[16] and acts as a reinforcement to provide the strength and stiffness of the silk [17]. The sericin, on the other hand, mainly consists of three major polypeptides [18] with encoding gene ser1 and ser2, bonded with hydroxyl groups (Ser, Thr and Try) [16, 17]. It is primarily amorphous [19] and soluble, which makes it easy to be removed from cocoon, i.e. degumming, in textile industries. The sericin acts as an adhesive binder to maintain the structural integrity of the fibres and the cocoon [17].

Silk fibres of *Bombyx mori*, *Antheraea. pernyi* and *Anthearea yamamai* have been found to exhibit nanofibrils. The widths of nanofibrils vary from 90 to 170nm according to the types of the silkworms, and are independent of the fibre size [20]. The fibrils lay parallel in layers with a cross angle covering the range of 30-508°C. It is assumed that the nanofibril structure gives the fibres greater flexibility, as the fibre can be accommodated with little stress in the weakly bonded nanofibrils when it is bended. The zig-zag layers can extend the strain to failure of the fibres in tension and compression. Also this structure can help to have more void/flaw tolerance in the fibres [21, 22].

The mechanical behaviour of silkworm silk has been widely studied in engineering and polymer fields. Perez-rigueiro et al. reduced the variability of the tensile properties by engineering methods, and found that they depended on the distribution of microstructural flaws [23]. The differences of initial modulus of fibres were believed to be due to the different condition of the sericin coating, and the two brins in a fibre contribute equally and independently to the tensile load-bearing ability of the material. Sericin contributed to sample cross-section, but added little to the fibre's ability to resist tensile deformation [23, 24]. Silk fibres from *Bombyx mori cocoon* are found to have variations of properties in different layers

[25]. Reddy et al. have tested silk fibres from Saturniidae and found that they have considerably different mechanical properties and diameter [26].

Degumming is used to remove sericin from the silk fibre by a thermo-chemical process. In the textile industry, the cocoons are submerged into water and detergents are added to remove the sericin glue in the cocoon for unravelling the fibres. It has been found that degumming had quantitative effects on the mechanical properties of the fibres: both the initial slope and the proportional limit in the force-displacement plot are decreased [17]. Fractographic analysis on natural and degummed silkworm fibres also shows differences. Morphologies of fracture surfaces of control silk fibres suggested that failure was initiated by the fracture of one fibroin, which leads to a localized overloading of the other fibroin to a failure. Both fibroins of degummed silk deform independently and fracture at different sections [27].

1.3 Historical background of silk cocoon

It is useful to look at the historical background of cocoon studies to give a general overview of cocoon characteristics. In the late 19^{th} and early 20^{th} century, biologists observed and recorded the behaviour of different silkworms and the appearance of cocoons produced from a biological perspective. But in the last ten years, materials scientists moved on to use silkworm cocoons as models for biological composites by studying their morphology, structures and properties using advanced techniques such as SEM, DMTA etc.

In 1867, Trouvelot studied and recorded the cocoon spinning behaviour of American silkworms [28-30]. Yagi in 1926 categorized the cocoons according to their appearance [31]. Yagi divides the Saturnian cocoons (a family in Lepidoptera) into four types according to their modes of attachment and the formation of the exit hole for the adults: 1) stalkless and

closed; 2) stalked and closed; 3) stalkless and opened, and 4) stalked and opened [31]. The cocoons discussed in this paper belong to the first, second and the third type. Some caterpillars spin completely closed cocoons and emerge by secretion of a fluid that softens and dissolves one end of the cocoon, e.g. *Bombyx mori, Antheraea frithi,* while some larvae construct an emergence valve on the cocoon by spinning parallel strands of silk in a conical shape, e.g. *Hyalophora cecropia, Cricula trifenestrata*. The moth can push the strands apart to emerge, but the sticking fibres around the valve resist forced entry from the outside.

Van der Kloot and Williams portrayed cocoon spinning as 'a unique window through which to examine animal behaviour' [32-34]. In their series of interesting papers, they found that the caterpillar has a flexible adaptive response to the structural features of its environment. Usually the larva starts by constructing a macrostructure of a widely spaced supporting network of parallel strands and then stretches and turns its segmented body to survey potential attaching substrates. Twigs or leaves can be pulled around for spinning peduncles or attachments. Within this framework the outermost cover of the cocoon is then built to form a characteristic shape. The larva turns it body around by swinging its head in a figure of eight motion to overlap silk fibres, making layers of silk sheets producing a cocoon with uniform thickness and symmetrical shape.

Tuskes and Paul have defined three main strategies of cocoon placement, although these are not strictly confined to specific species [35]. Cocoons could be suspended from twigs on the host plant by a silk attachment called the peduncle, attach their full length along branches or other supporting substrates, or construct the cocoon among leaves from the host plant without attachment to twigs. Their results show that the construction strategies depend on both the silkworm species and the environments. Danks describes silkworm cocoons in terms of

relative size, robustness, structure and composition of cocoon wall, shape, colour, attachment, and orientation, and tries to relate them to these properties of the biological functions of the cocoon [36].

Some caterpillars, e.g. *Hyalophora cecropia* and *Antheraea pernyi*, pause during the spinning process to secrete a fluid with crystals [33, 37]. It has been suggested that these crystals contribute to the tanning and water resistance of the cocoons, and transform the pliant cocoon into a stiff material with excretory crystals filling the interstices between the silks. An increased stiffness may also act as a defence mechanism, as the ovipositor of the parasitoid cannot penetrate the *Hyalophora gloveri* cocoon once it has tanned [35]. These crystals are calcium oxalate on *Antheraea* [38]. It is also suggested that this plant toxin could irritate the predators, supported by the fact that the larva secretes them in their earlier instars when encountering predators [35].

Recently, work has been done to investigate the structures and properties of the cocoons [25, 39-43]. Researchers have looked into the microstructures of *Bombyx mori* and *Hyalophora cecropia* cocoon using SEM, and measured their mechanical properties and gas diffusability. Such studies will be made on the 27 cocoons presented here to provide a database for bio-mining, and then a more generalised model on structure-property relations for silkworm cocoons, which will be followed by a bioinspired artificial silk composite study.

1.4 Chapter introduction

This thesis will have 8 chapters. Each chapter is a self consistent report about one aspect of silk composites. A brief summary of each chapter is given below.

1.4.1 Chapter 2: Morphologies of cocoons

Cocoons have evolved to use two relatively consistent component materials (fibroin fibres and the sericin binder) to fulfil a variety of functions in a wide range of different environments. This chapter looks at the morphologies and components of 27 species of cocoons to study how cocoons use limited materials to construct a variety of distinct structures.

1.4.2 Chapter 3: Physical properties of cocoons

In order to provide protection against diverse threats and to regulate the inner environment for the silkworm pupae, cocoons have hierarchical structures that have been optimised through evolutionary pressures to provide optimum protection. This chapter will provide comparison of tensile, compressive and permeability properties of 25 species of cocoons, and discuss how modified structures can optimize the physical properties of cocoons.

1.4.3 Chapter 4: Structure-property relationship of cocoons

Importantly for our argument of ‘Learning from Nature’, silk cocoons have similar micro-structures to other technological important stochastic fibrous materials, such as paper, nonwoven textile and electrospun polymer mats. This chapter will develop a quantitative

model to relate the structure and properties of cocoons and further predict properties for other synthetic composites and materials.

1.4.4 Chapter 5: Structure-property relationships of *Bombyx mori* cocoon

The *Bombyx mori* cocoon is a special case in the range of cocoons studied in this thesis. As a textile industrial product, it has been artificially selected for thousands of years to have strong fibres and ease of unravelling. This gives a simple model of nonwoven composites with multiple layer structure for biomimetic study. This chapter will introduce detailed structure and property relationships for *Bombyx mori* cocoon, and develop a more advanced model for its layered structure.

1.4.5 Chapter 6: Indentation of cocoon

In order to provide mechanical protection against parasites and predators, cocoons evolved to have a lightweight and impact resistance structure, which is very similar to the structure of industrial laminated composites. This chapter will use an engineering approach that has been developed to examine composite laminates for cocoon studies by using experiments and finite element simulations to explore the defensive mechanisms of cocoons against mechanical impact attack.

1.4.6 Chapter 7: Synthetic cocoon composites

As an engineering fibre with an optimized combination of strength and toughness, silk fibre is an interesting reinforcement for composites design. On the other hand, silk cocoon, with its cheap price, green nature and good mechanical properties, can be used as a two-dimensional nonwoven fibre assembly for the reinforcement in the composites. This chapter will report

the exploration of using silk cocoons to make synthetic composites. A design of novel synthetic silk composites based on the understanding of natural cocoon mechanisms will be discussed.

1.4.7 Chapter 8: Summary and general discussion

The work arising from this thesis has lead to a general concept about connectivity. I will discuss the impact of this work has on future research on both natural and synthetic materials, also a wider area on general materials on multiscale levels.

1.5 Approach of this thesis

Biology has much to contribute to human designs and applications, and engineering can help in the study of biomechanics and biomaterials. In the example in this thesis, silkworms and composite structural engineers have many common goals and constraints: to design and construct a structure that can withstand expected loads and impact energy with minimum materials and construction time. It is a good starting point to bridge the gap between biology and engineering for a bioinspired study.

My general aims for studying silk cocoons are: firstly, to attempt to understand this natural composite structure from an engineer's point-of-view by using a variety of analytical techniques that have been developed and used by engineers primarily to understand synthetic structural materials; and, secondly, to contribute to the application in synthetic composite design with some of the concepts found in structures that nature has spent millions of years evolving. Nowadays, silk fibres have been studied as engineering fibres and used to make artificial composites mainly for medical use [44-47]. However, without understanding the

biophysics of the cocoon structure and the role of silk fibres in it, it is unlikely to be either effective or constructive to produce a silk composite simply by inserting silk fibres into man-made resins. On the other hand, composite structures with energy-absorbing and tough features have been studied extensively in recent years as composites are in general susceptible to impact damage. Composite engineers have been looking to nature for ideas and new structural forms rather than sticking to conventional fibre reinforced composites. But it would be unwise to copy only the forms from natural structures rather than understanding their mechanism or the scale and function for which they have evolved. This thesis aims to study the fundamental concept of natural silk cocoon composites, and their application to a much broader field for bioinspired design of synthetic composites.

References

[1] Meyers MA, Chen P-Y, Lin AY-M, Seki Y. Biological materials: Structure and mechanical properties. Progress in Materials Science. 2008;53(1):1-206.

[2] Thompson DAW, Bonner JT. On growth and form. Cambridge University Press, 1992.

[3] Currey JD. Bones: structure and mechanics. Princeton University Press, 2006.

[4] Vincent JFV. Structural biomaterials. Princeton University Press, 1990.

[5] Vollrath F, Porter D. Silks as ancient models for modern polymers. Polymer. 2009;50(24):5623-5632.

[6] Porter D, Vollrath F. Silk as a biomimetic ideal for structural polymers. Advanced Materials. 2009;21(4):487-492.

[7] Vollrath F, Porter D, Holland C. There are many more lessons still to be learned from spider silks. Soft Matter. 2011.

[8] Vollrath F, Chen F, Porter D. Silks and their composites. Transactions of the 14th Fundamental Research Symposium on advances in pulp and paper research. Oxford; 2009. p. 1355-1365.

[9] Vollrath F, Knight DP. Liquid crystalline spinning of spider silk. Nature. 2001;410(6828):541-548.

[10] Wynne A. Textiles. Oxford, UK: Macmillan Education, 1997.

[11] Vollrath F, Porter D. Spider silk as archetypal protein elastomer. Soft Matter. 2006;2(5):377-385.

[12] Shimura K KA, Ohtomo K, Katagata Y, Hyodo A. Studies on silk fibroin of Bombyx mori. I. Fractionation of fibroin prepared from the posterior silk gland. The Journal of biochemistry. 1976;80(4):693-702.

[13] Couble P, Moine A, Garel A, Prudhomme J. Developmental variations of a nonfibroin messenger-rna of bombyx-mori silkgland, encoding for a low-molecular-weight silk protein. Dev Biol. 1983;97(2):398-407.

[14] Chevillard M, Couble P, Prudhomme JC. Complete Nucleotide-sequence of the gene encoding the Bombyx mori Silk Protein-P25 and Predicted Amino-acid-sequence of the Protein. Nucleic Acids Research. 1986;14(15):6341-6342.

[15] Inoue S. Silk fibroin of Bombyx mori is secreted, assembling a high molecular mass elementary unit consisting of H-chain, L-chain, and P25, with a 6 : 6 : 1 molar ratio. The Journal of BIological Chemistry. 2000;275(51):40517-40528.

[16] Sprague KU. The Bombyx mori Silk Proteins: Characterization of Large Polypeptides. Biochemistry. 1975;14(5):925-931.

[17] Perez-Rigueiro J, Elices M, Llorca J, Viney C. Effect of degumming on the tensile properties of silkworm (Bombyx mori) silk fiber. Journal of Applied Polymer Science. 2002;84(7):1431-1437.

[18] Takasu Y. Isolation of three main sericin components from the cocoon of the silkworm, Bombyx mori. Bioscience, biotechnology, and biochemistry. 2002;66(12):2715.

[19] Yamaguchi K, Kikuchi Y, Takagi T, Kikuchi A, Oyama F, Shimura K, Mizuno S. Primary Structure of the Silk Fibroin Light Chain Determined by cDNA Sequencing and Peptide Analysis. Journal of Molecular Biology. 1989;210(1):127-139.

[20] Putthanarat S, Zarkoob S, Magoshi J, Chen JA, Eby RK, Stone M, Adams WW. Effect of processing temperature on the morphology of silk membranes. Polymer. 2002;43(12):3405-3413.

[21] Putthanarat S, Stribeck N, Fossey SA, Eby RK, Adams WW. Investigation of the nanofibrils of silk fibers. Polymer. 2000;41(21):7735-7747.

[22] Miller LD. Investigation of the nanofibrillar morphology in silk fibers by small angle X-ray scattering and atomic force microscopy. Int J Biol Macromol. 1999;24(2-3):159-165.

[23] Perez-Rigueiro J, Viney C, Llorca J, Elices M. Silkworm silk as an engineering material. Journal of Applied Polymer Science. 1998;70(12):2439-2447.

[24] Perez-Rigueiro J, Viney C, Llorca J, Elices M. Mechanical properties of single-brin silkworm silk. Journal of Applied Polymer Science. 2000;75(10):1270-1277.

[25] Zhao H-P, Feng X-Q, Shi H-J. Variability in mechanical properties of *Bombyx mori* silk. Mat Sci Eng C. 2007;27(4):675-683.

[26] Reddy N, Yang Y. Morphology and tensile properties of silk fibers produced by uncommon Saturniidae. Int J Biol Macromol. 2010;46(4):419-424.

[27] Poza P, Perez-Rigueiro J, Elices M, Llorca J. Fractographic analysis of silkworm and spider silk. Eng Frac Mech. 2002;69(9):1035-1048.

[28] Trouvelot L. The American silk worm. American Naturalist. 1867:30.

[29] Trouvelot L. The American Silk Worm (Concluded). American Naturalist. 1867:145.

[30] Trouvelot L. The American Silk Worm (Continued). American Naturalist. 1867:85.

[31] Yagi N. The cocooning behavior of a *Saturnian* caterpillar (*Dityoploca japonica*). Journal of Experimental Zoology. 1926;46(2).

[32] Van der Kloot WG, Williams CM. Cocoon construction by the *Cecropia* silkworm. II. The role of the internal environment. Behaviour. 1953;5:157-174.

[33] Van der Kloot WG, Williams CM. Cocoon construction by the *Cecropia* silkworm. I. The role of the external environment. Behaviour. 1953;5:141-156.

[34] Van Der Kloot WG. Cocoon construction by the *Cecropia* silkworm Iii. the alteration of spinning behavior by chemical and surgical techniques. Behaviour. 1954:233.

[35] Tuskes PMP, Paul PM. The wild silk moths of north America : a natural history of the *Saturniidae* of the United States and Canada. Cornell University Press, 1996.

[36] Danks HV. The roles of insect cocoons in cold conditions. E J Entomol. 2004;101(3):433-437.

[37] Lounibos LP. The cocoon spinning behaviour of the Chinese oak silkworm, *Antheraea pernyi*. Animal Behaviour. 1975;23(Part 4):843-853.

[38] Freddi G, Gotoh Y, Mori T, Tsutsui I, Tsukada M. Chemical structure and physical properties of *Antheraea assama* silk. Journal of Applied Polymer Science. 1994;52(6):775-781.

[39] Zhao HP, Feng XQ, Cui WZ, Zou FZ. Mechanical properties of silkworm cocoon pelades. Eng Frac Mech. 2007;74(12):1953-1962.

[40] Zhao HP, Feng XQ, Yu SW, Cui WZ, Zou FZ. Mechanical properties of silkworm cocoons. Polymer. 2005;46(21):9192-9201.

[41] Blossman-Myer B, Burggren WW. The silk cocoon of the silkworm, *Bombyx mori*: Macro structure and its influence on transmural diffusion of oxygen and water vapor. Comparative Biochem Physiol A-Mol Integrative Physiology. 2010;155(2):259-263.

[42] Reddy N, Yang Y. Structure and properties of cocoons and silk fibers produced by *Hyalophora cecropia*. Journal of Materials Science. 2010;45(16):4414-4421.

[43] Weisman S, Trueman HE, Mudie ST, Church JS, Sutherland TD, Haritos VS. An Unlikely Silk: The Composite Material of Green Lacewing Cocoons. Biomacromolecules. 2008;9(11):3065-3069.

[44] Wang L, Li C. Preparation and physicochemical properties of a novel hydroxyapatite/chitosan-silk fibroin composite. Carbo Polym. 2007;68(4):740-745.

[45] Rockwood DN, Gil ES, Park S-H, Kluge JA, Grayson W, Bhumiratana S, Rajkhowa R, Wang X, Kim SJ, Vunjak-Novakovic G, Kaplan DL. Ingrowth of human mesenchymal stem cells into porous silk particle reinforced silk composite scaffolds: An in vitro study. Acta Biomaterialia. 2010;7(1):144-151.

[46] Yuan Q, Yao J, Chen X, Huang L, Shao Z. The preparation of high performance silk fiber/fibroin composite. Polymer. 2010;51(21):4843-4849.

[47] Hardy JG, Scheibel TR. Composite materials based on silk proteins. Progress in Polymer Science. 2010;35(9):1093-1115.

Chapter 2

Morphologies of Cocoons

2.1 Introduction

This chapter looks broadly at the cocoons of 27 different species from different environments in terms of their morphology, composition and structure, on the basis that the cocoons have evolved to use two relatively consistent component materials (fibroin fibres and sericin binder) to fulfil a variety of functions in a wide range of different environments. These structures will provide a solid basis for further study of cocoon physical properties in the next chapters, and bio-inspired design and manufacture of artificial composites based on combinations of natural and synthetic materials in Chapter 7.

2.2 Materials and methods

2.2.1 Materials collection

Bombyx mori silkworms were raised in a laboratory (23±2 °C, 60% relative humidity) and fed with mulberry leaves until they spun cocoons in a dark environment. Their cocoons were collected after the pupae had left them through one end. *Bombyx mandarina* and *Gonometa postica* cocoons were collected separately in wild countryside in Anhui, China and Kenya. All the other cocoons were purchased from Worldwide Butterflies, UK. The selection criterion of cocoons investigated in this section is the availability of the material.

2.2.2 SEM observation

Cocoons were hole punched to make samples with a diameter of 3.5 mm which were glued onto conductive tape and sputter coated with Quorum Technologies SC 7620. Then the coated samples were transferred into the Jeol Neoscope JCM-5000 Scanning Electron Microscope for observation at 15kV voltage. Both the inner and outer sides of cocoons were observed. The fibre bonding length was measured through cocoon layer SEM pictures by measuring the length of the fibre interconnects. 20 measurements were taken for each of three cocoons.

2.2.3 Fourier transform infrared spectroscopy (FTIR) test

FTIR was used to identify the non-protein inorganic crystals on the cocoons found in SEM. A Nicolet 6700 FTIR spectrometer with a MCT-A nitrogen cooled detector (Thermo Scientific, Madison, WI) was used for the infrared spectra acquisition. Attenuated Total Reflectance (ATR) was used to simplify the sample preparation normally necessary for transmission measurements and avoid artefacts caused by probing samples with comparable size as the infrared wavelength. A Golden Gate single reflection diamond ATR accessory (Specac Ltd., London, UK) is embedded in the spectrometer. Spectra were acquired at a 4 cm^{-1} resolution from 500 to 6000 cm^{-1} using a Happ-Genzel apodization, a Metz phase correction and no zero filling. Spectra were obtained from the average of 64 scans at a 5.0632 cm/s mirror speed. The spectra were polarized perpendicular to the plane of incidence (*s*) with a ZnSe holographic wire grid polarizer with 2700 grooves/mm (Thermo Scientific, Madison, WI). The diamond's internal reflectance element (IRE) has a refractive index of 2.417 with an angle of incidence of 45°. For this configuration, the penetration depth of the evanescent

wave for the diamond/air interface is around 1.2 μm at 1650 cm^{-1} (varying with the wavelength). Both sides of each cocoon disc were measured, since the evanescent wave could probe selectively each surface and that the chemical composition of the cocoon can vary depending on the cocoon layer. The pressure applied on the cocoon by the anvil was kept to the minimum necessary to obtain an absolute absorbance value of 0.1. Before each measurement, a new background was acquired to prevent signal fluctuation from the MCT detector response. A cleaning control spectrum was acquired to verify that the puck was free of contamination before acquiring the spectra. The cocoons were punched into circular disc samples of 3.5mm diameter. At least three disc samples from three different cocoons of each species were used for the spectra acquisition (n = 739).

All spectral operations were executed using OMNIC 7.3 controlled using a VBA purpose written code using the OMtalk dialogue protocol (Thermo Scientific, Madison, WI). An offset was first applied from the average of the 1900-1850 cm^{-1} region then normalised to the area integrated from 1800-800 cm^{-1} to compensate for the signal variation due to varying surface contact. A simple ATR correction was applied to correct for the evanescent wave penetration depth dependency on the wavelength. The first differential of the data set was used to highlight the peaks positions for better results. The spectra were not scaled for the variance.

2.2.4 Density measurement of the cocoons

As the cocoon wall has a porous structure, its thickness varies according to force applied to it. This leads to a problem of defining the thickness and calculating the strength of the materials. A compression test of the cocoon wall in the thickness direction has been carried out for

understanding the compressive behaviour of the cocoon materials, and then defining the thickness and density of the cocoon at a constant stress level. A TA Instruments Q800 Dynamic Mechanical Thermal Analyser (DMTA) in compression mode was used to test the compressive behaviour of the cocoons. This is a precision instrument designed to measure viscoelastic properties of materials. It controls and measures five variables: temperature, time, force, position and frequency.

Calibration of the instrument, including (1) position, (2) force and (3) clamps was carried out by Ms Juan Guan as the specialist operator responsible for the machine maintenance.

(1) The position of the drive shaft of the instrument was measured by the optical encoder, whose absolute position was calibrated by using reference objects with known height. The resolution of the optical encoder is 10 nm.
(2) The force was calibrated by following standard calibrating procedures to determine the static force as a function of the position. A slide with a known weight (100g) was loaded. The static force from the ramp moves the slide, and the raw data of force and position were collected continuously during the loading process. These force vs. position data points were generated at even position intervals via a linear fit of the force data in a 5 second window (50 points in total) centred at each position. A cubic spline was used to fit those datum points. Square root of sum of the squares (SRSS) of the discrepancies between the raw data and the fitted cubic spline were calculated and was reported as the Force Calibration Residual, which indicates the goodness of fit of the static force calibration. The force residual is 0.0114 N.
(3) Clamp mass, position and compliance were calibrated. Calibration of the clamp mass is to allow the instrument to compensate for the mass of the clamp adding to the drive

shaft. It weighs 69.9 gm. Zero position of the clamp was essential to determine the point of zero sample thickness in calibration. A position offset was found to be 23.01 μm. Clamp compliance was calibrated for measuring the stiffness of the clamp assembly. A 10 N force was applied to measure the compliance of the moving and frame clamp. Then a reverse 10 N force was applied after removing the first force. The average compliance was calculated based on the steel modulus and the clamp dimensions, which was 0.651 μm/N.

In the compression test of silk cocoons, static (non-oscillating), force-control mode was used to measure the stress-strain curves of the specimens. Cocoons were cut into circular samples with a diameter of 3.5 mm and weighed before tests. A compression clamp (two steel plates) was used to apply a compressive force on the sample. Two raw signals, force and position (which is the measured thickness of the cocoon sample in this case), were recorded in real time. A force ramp rate of 3 N/min was applied. A drive motor delivered force or stress to the moving drive block, which was suspended by an air bearing for a smooth, noise-free and continuous delivery of force. An optical encoder records the displacement of the moving drive block. The tests automatically stopped when the compressive stress reached 1.5 MPa, and the thicknesses of the samples were defined at this compressive stress for further calculations. The data for the force vs. distance of the plate were recorded for analysis. Three samples from each cocoon were tested. The density of the cocoons was calculated from the weight and the defined thickness of the samples.

2.3 Results

2.3.1 Morphology of the cocoons

A summary of cocoon morphology for the 27 species is shown in Figure 2.2. Cocoon morphologies are plotted on the phylogenetic tree, which describes evolutionary relationships among various silkworm species based on their genetic characteristic. Each node in a rooted phylogenetic tree represents the deduced most recent common biological ancestor of the descendants. This phylogenetic tree is generated by using literature data [1-3]. SEM pictures of both outer and inner surfaces of cocoons are shown to make a comparison on their distinctively different morphologies. The cocoon features, e.g. open or closed structure, degree of nonwoven structure, numbers of layer connectivity and extra components such as calcium oxalate (CaC_2O_4) are indicated in the pictures in Figure 2.2. The structural and morphological type of cocoons employed is usually constant with a genus. For example, six *Antheraea* cocoons all have closed cocoons, nonwoven structures and calcium oxalate (CaC_2O_4) crystals, and both *Caligula simla* and *Argema mimosae* cocoons have closed cocoons, lattice structures, single layer and no calcium oxalate crystals.

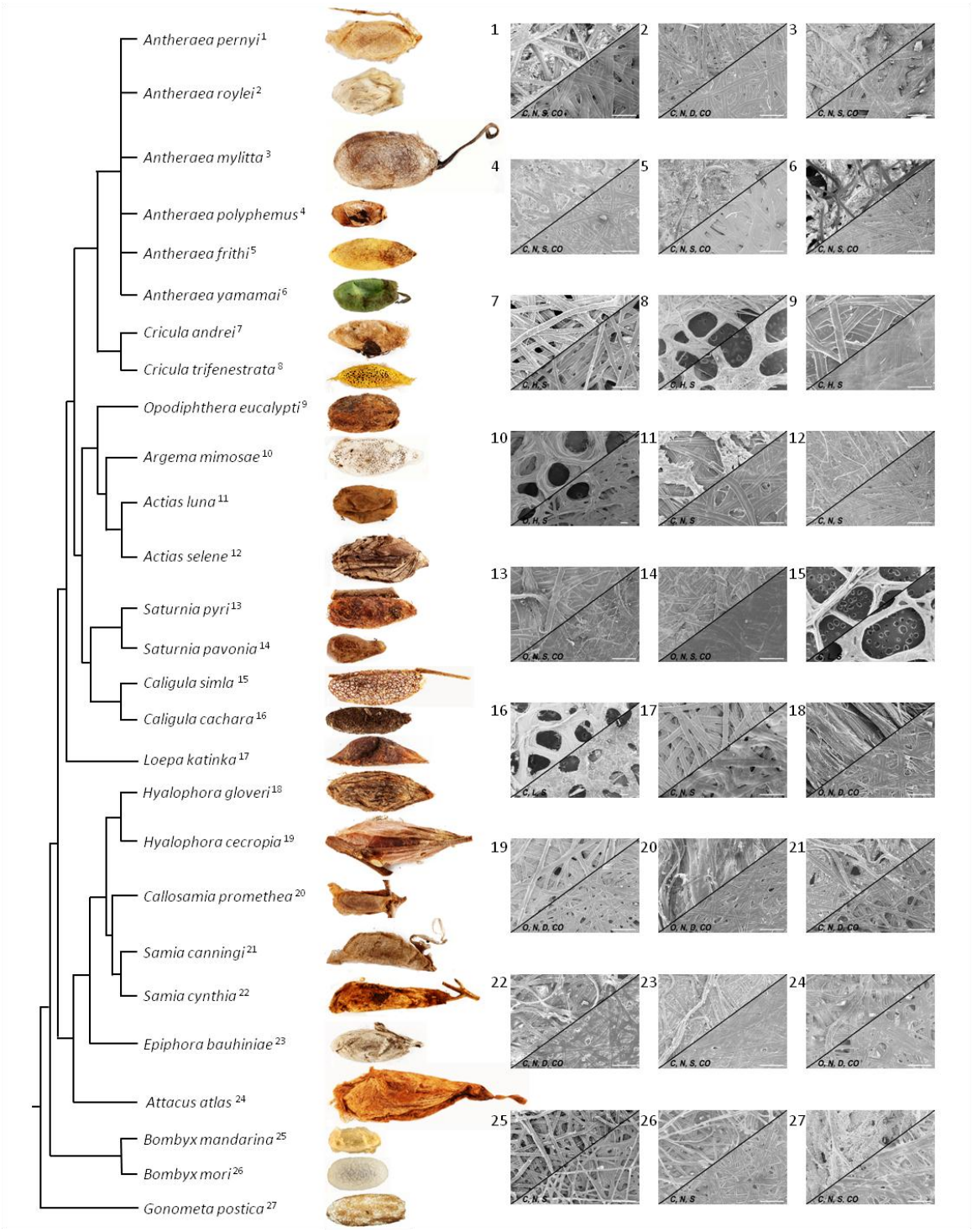

Figure 2.2 Silkworm cocoons in our collection. Left: Phylogenetic tree of silkworm cocoons and pictures [1-3]. Right: SEM pictures of outer (top left) and inner (bottom right) surfaces of silkworm cocoons. Abbreviation: C: Closed cocoon, O: open cocoon, N: Nonwoven structure, H: Nonwoven structure with woven holes, L: woven lattice structure, S: Single layer, D: Double layer, CO: Calcium oxalate crystals. Scale bar: 200 μm.

2.3.1.1 Cocoon layer structure

A cocoon is a hierarchical laminated composite consisting of layers, which can be categorised broadly from their layers into single and double cocoon, as shown in Figure 2.3. The single cocoons can consist of just one single layer (e.g. *Actias* and *Cricula* cocoons), or multiple layers deposited in sequence by the silkworm with either weak or strong bonding between the layers. These multiple layers are parallel to the surface direction, and there are relatively weak bonds by sericin between them. They can be either easily peeled (e.g. *Bombyx mori, Antheraea pernyi*), or can be separated through a degumming method (e.g. *Saturnia pyri*, *Opodiphthera eucalypti*) because of the relatively stronger bonding between the layers. Most of the double cocoons studied in this project have an intervening mesh layer bonded between outer and inner cocoons (e.g. *Hyalophora cecropia*, *Callosamia promethea*). Sometimes the silkworm could also create a large and irregular outer ‘bag’ enclosing an inner cocoon without any bonding between the two cocoons (e.g. *Antheraea roylei*).

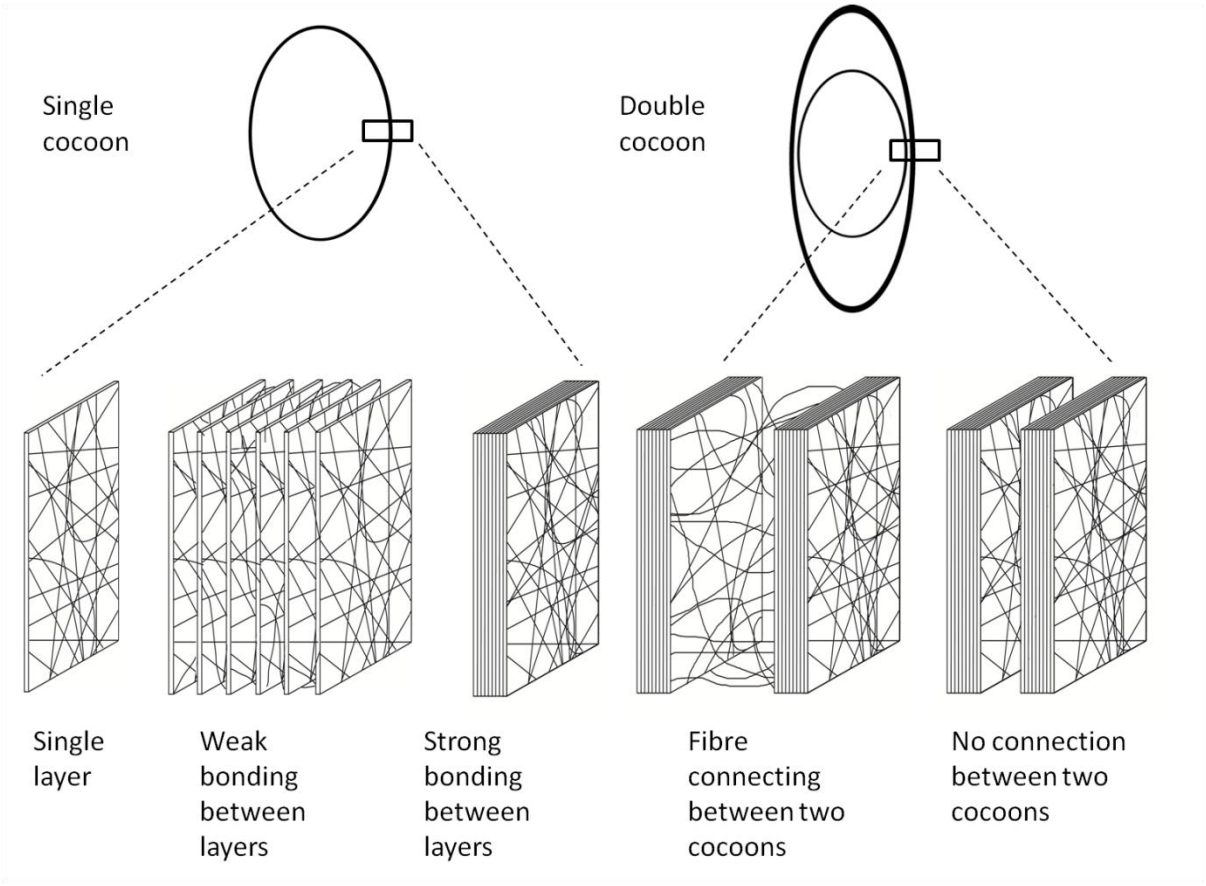

Figure 2.3 Cocoon layer structures

2.3.1.2 Cocoon nonwoven bonding structure

Cocoons have fibres arranged in different degrees of orientation. Here we defined the cocoon structures into 3 categories: fibres randomly arranged in a nonwoven structure, a nonwoven structure with woven holes, and a woven lattice structures with very few fibres randomly arranged. Most of the cocoons studied in this project have a nonwoven porous structure, with the fibres arranged randomly in the plane of the cocoon walls. Figure 2.4 shows different morphologies of nonwoven cocoons. The fibres are bonded by sericin to form a porous network (Figure 2.4A). From SEM pictures, cocoons with this structure always have a graded layer structure, with the porosity decreasing through the thickness direction from outer layer

to inner layer, i.e. the number of interfibre bonds increased from outer layer to inner layer. Sericin granules without bonded fibres exist on the outer layer; probably to promote adhesion of the cocoons in their location (Figure 2.4 B-E for examples of *Bombyx mori* and *Opodiphthera eucalypti*). *Actias* and *Cricula* cocoons, which have a single and thin layer wall, have low porosity and the fibres are strongly bonded by the sericin (Figure 2.4F).

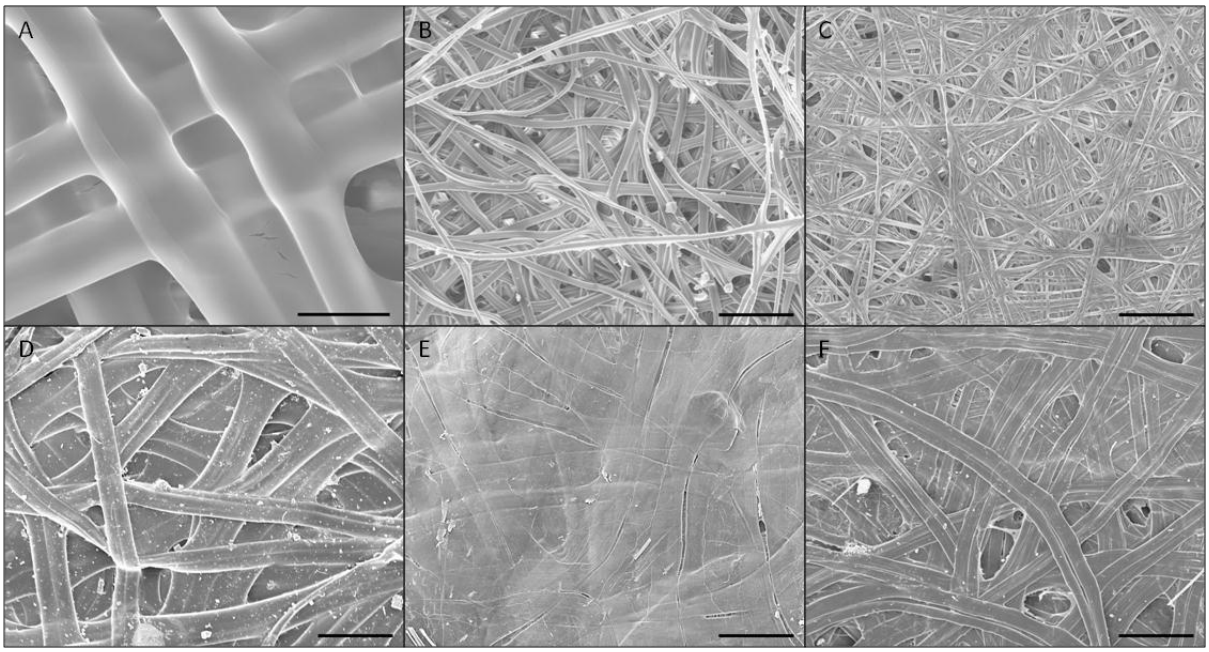

Figure 2.4 Cocoon nonwoven bonding structure (A) Bonding between fibres (*Bombyx mori*) Scale bar: 10μm (B) Multi layer cocoon outer layers (*Bombyx mori*) Scale bar: 200μm (C) Multilayer cocoon inner layers (*Bombyx mori*) Scale bar: 200μm (D) Multi layer cocoon outer layers (*Opodiphthera eucalypti*) Scale bar: 200μm (E) Multi layer cocoon inner layers (*Opodiphthera eucalypti*) Scale bar: 200μm (F) Single layer cocoon morphology (*Actias luna*). Scale bar: 200μm

2.3.1.3 Nonwoven cocoon placement strategies and morphologies

The different strategies of cocoon placement have led to different morphologies of cocoons, which are shown in Figure 2.5. Cocoons made by *Samia canningi* and *Actias luna* attach to the substrate with the sericin flowing along the surface on the substrate. This may increase the bonding area between the fibres (Figure 2.5A and 2.5B for comparison of morphologies between attaching surface and the surface which is not attached to the substrate (free surface)). Usually the attaching surface is thinner than the free surface. Some other cocoons have a long silk peduncle for suspending the cocoon from the host, e.g. cocoons produced by *Samia canningi, Antheraea mylitta*). Those peduncles have most of their fibres aligned parallel to the length directions with some fibres interweaving in other directions (Figure 2.5C and 2.5E). Sometimes the peduncles are covered by moth hairs or other debris (Figure 2.5D for *Antheraea mylitta* cocoon). Open cocoons produced by e.g. *Saturnia pyri* and *Hyalophora cecropia* usually have parallel fibres sticking outwards along the exit, which could be pushed outwards by the silkmoth inside the cocoon (Figure 2.5F).

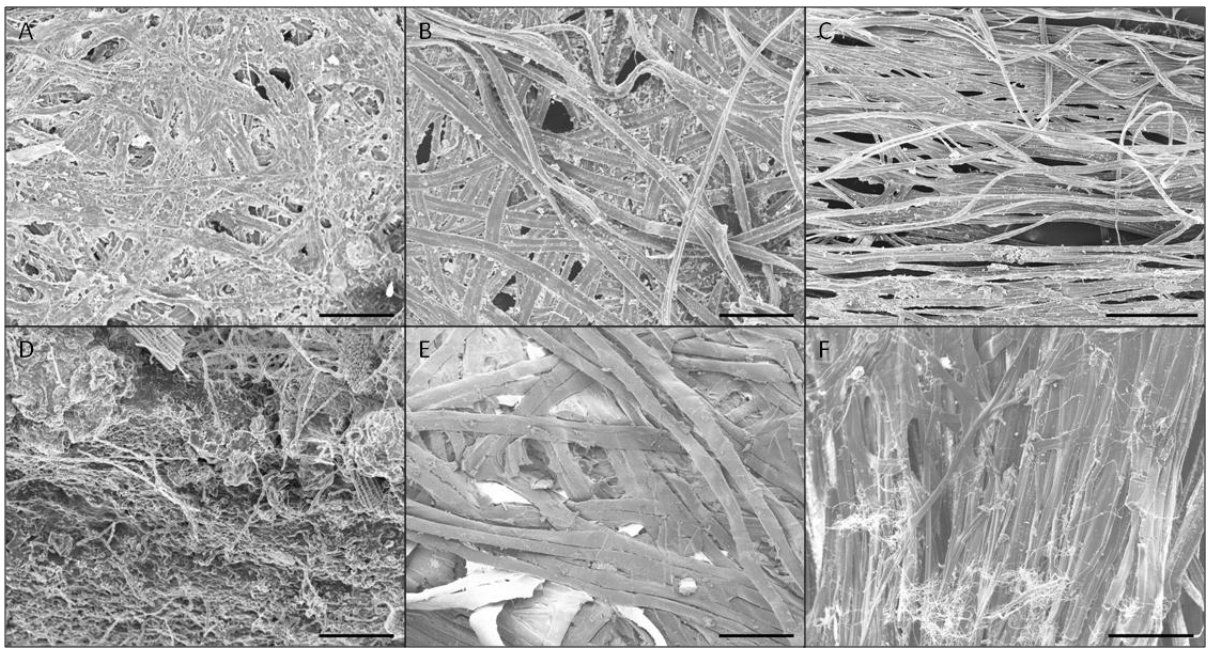

Figure 2.5 Cocoon placement strategies and morphologies (A) Cocoon surface attached to the substrate (*Samia canningi*) Scale bar: 200μm (B) Cocoon surface without attaching to the substrate (*Samia canningi*) Scale bar: 200μm (C) Cocoon peduncle (*Samia canningi*) Scale bar: 500μm (D) Cocoon peduncle surface (*Antheraea mylitta*) Scale bar: 200μm (E) Cocoon peduncle inner structure (*Antheraea mylitta*) Scale bar: 200μm (F) Cocoon exit structure (*Saturnia pyri*). Scale bar: 500μm

2.3.1.4 Cocoons with woven holes or lattice structure

Fabricated holes can be found on some nonwoven cocoons, as shown in Figure 2.6. Fibres are densely packed into concentric structures around the holes for supporting the cocoon frames. *Cricula trifenestrata* (Figure 2.6A) and *Argema mimosae* cocoons have a fibre mesh structure on the large proportion of the cocoon surface, while *Cricula Andrei* and *Opodiphthera eucalypti* (Figure 2.6D) cocoons only have some small holes on the surface not attached to the substrate. The holes of *Opodiphthera eucalypti* cocoon are found to be arranged along the

supporting twig. The rest of the cocoon wall is a nonwoven structure with low porosity, and the fibres are strongly bonded (Figure 2.6A and 2.6B, 2.6D and 2.6E for comparison of morphologies between cocoon holes and free surfaceFigure). *Caligura simla* and *Caligula cachara* cocoons have a lattice structure without any nonwoven cocoon wall (Figure 2.6C and 2.6F). Fibres with higher diameters up to 100μm (Table 2.1) interweave with each other for supporting the cocoon structure. These cocoons can also be found covered by leaves, and the sericin flows along the attaching surface for bonding the cocoons.

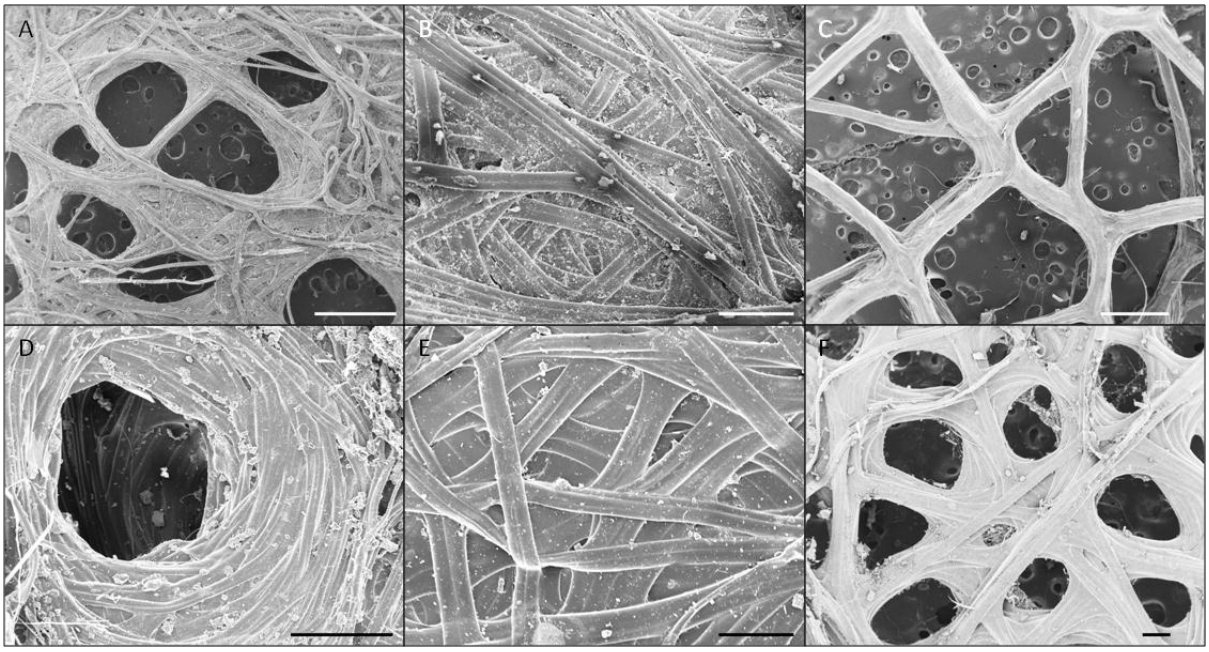

Figure 2.6 Cocoon mesh structure (A) Cocoon with mesh structure (*Cricula trifenestrata*) Scale bar: 1mm (B) The nonwoven wall of cocoon with mesh structure (*Cricula trifenestrata*) Scale bar: 200 μm (C) Cocoon with a lattice structure (*Dictyoploca simla*) Scale bar: 1mm (D) Cocoon with holes (*Opodiphthera eucalypti*) Scale bar: 500 μm (E) The nonwoven wall of cocoon with holes (*Opodiphthera eucalypti*) Scale bar: 200μm (F) Cocoon with a lattice structure (*Caligula cachara*). Scale bar: 200μm

2.3.1.5 Cocoon crystals

Crystals can be found on the surface of the cocoons loosely attached to the silk fibres. Figure 2.7 shows the crystals with different morphologies in different scales. Most crystals on the cocoons in this study have a cubic shape with a side length of 1-3 μm (Figure 2.7A-D for cubic crystals on different cocoons in different scales). Only *Gonometa postica* cocoon has been found to have columnar crystals of 20-30 μm (Figure 2.7E and 2.7F). The crystals are usually on the outermost surface of the cocoons. But for *Antheraea roylei* cocoon, which has a double cocoon structure, the crystals are found on the outer surface of the inner cocoon (Figure 2.3). The crystals are not found on the attached surface.

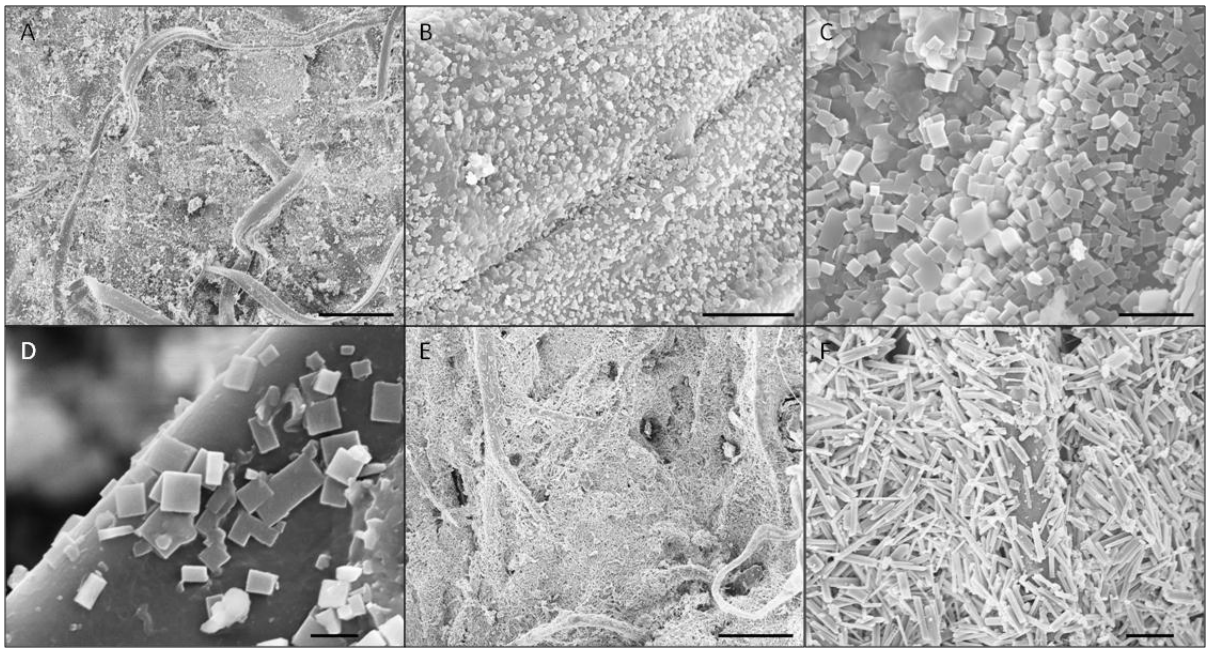

Figure 2.7 Cocoon crystals (A) Cubic crystals on cocoon *Antheraea frithi* Scale bar: 200 μm (B) Cubic crystals on cocoon *Hyalophora gloveri* Scale bar: 10 μm (C) Cubic crystals on cocoon *Bunaea aleinoc* Scale bar: 5 μm (D) Cubic crystals on cocoon *Antheraea pernyi* Scale bar: 2 μm (E, F) Columnar crystals on cocoon (*Gonometa postica*) Scale bar: 200 μm and 20 μm

2.3.2 Cocoon fibres

Figure 2.8 shows the morphologies of silk fibres from different cocoons, which all have two fibroins covered by sericin. Apart from *Bombyx mori* and *Bombyx mandarina*, whose fibres have triangular-shaped cross sections (Figure 2.8A), most of the nonwoven cocoons have fibres with elliptical cross sections (Figure 2.8B for an example of *Antheraea mylitta*). Microfibrils are seen from the silk fibres from *Antheraea* fibres (Figure 2.8C for an example of *Antheraea frithi* fibres). Fibre bonding length were measured in the plane of the cocoon walls as the distance from edge to edge of the single fibres (including two fibroins and sericin

between them) perpendicular to the fibre axis through the bond. This fibre bond length is more meaningful for the cocoon morphology than simply measuring the diameter of reeled individual fibres, which have a large fraction of their diameter as sericin, which redistributes to form the interfibre bonds. This parameter was selected over weight per unit length as a measure of fibre dimensions for the specific discussion on cocoon morphology for the same reason. Usually the lattice cocoon structure or nonwoven cocoons with woven holes has a higher fibre bond length (i.e. higher fibre diameter) than nonwoven cocoons, e.g. *Caligura simla* and *Argema mimosae* compared with *Antheraea* cocoons (Table 2.1). This avoids issues such as the detailed shape of the fibre cross section, and the standard deviation reflects changes in the bond length through the thickness of the cocoon.

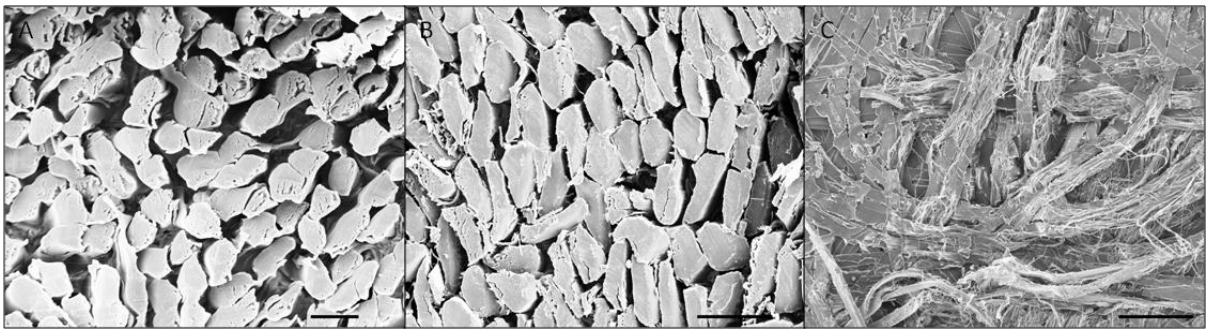

Figure 2.8 Cocoon fibres (A) *Bombyx mori* fibres with triangle-shaped cross sections. Scale bars: 20 μm (B) *Antheraea mylitta* fibres with eliptical cross sections. Scale bars: 50 μm (C) *Antheraea frithi* fibres with multifibrils. Scale bars: 200 μm

2.3.3 FTIR

ATR is well suited for the detection of calcium oxalate since it probes only the superficial layer where the crystals are located. As seen in Figure 2.9, the two main diagnostic bands identified for calcium oxalate hydrate are the O-CO out of phase bonding at 779 cm^{-1} and the

asymmetric C=O stretching at 1315 cm^{-1} [4]. All the crystals observed on the cocoons from SEM pictures are calcium oxalate. The role of bonding between calcium oxalate and silk in the structural properties of cocoons requires further investigation and may open a new field on biomimetic inorganic/organic composites.

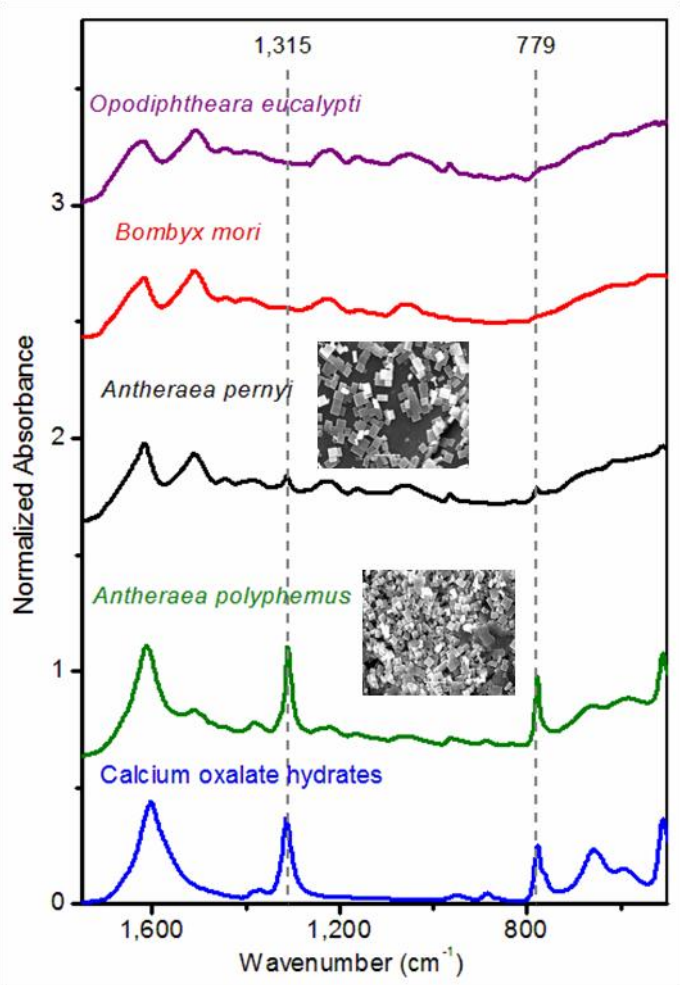

Figure 2.9 Comparison of the FTIR spectrum of commercial calcium oxalate hydrates, cocoons with crystals and cocoons without crystals

2.3.4 Density calculation

Bearing in mind other published thickness measurements of nonwoven materials and papers [5-7], 1.5MPa was chosen as an appropriate stress for our mechanical structure-property relationships where density is a key parameter [8]. Cocoons with multi-microlayer structures have higher thickness, e.g. *Bombyx mori*, *Hyalophora gloveri* cocoons.

The nominal density of a cocoon is calculated from the weight, the diameters of the circular samples, and the thickness, which is defined as the distance between two gauges at 1.5 MPa compressive stress (Table 2.1). The density results have contributions from the silk fibres in the structure and the calcium oxalate crystals on the surface of some cocoons. Cocoons with low porosity from SEM pictures are found to have high density (e.g. *Opodiphthera eucalypti*, *Actias luna*), although the density could be over-estimated due to the re-arrangement of fibres and sericin during the compression tests. On the other hand, calcium oxalate has much higher density than the silk fibres and has a significant effect on cocoon density. Unfortunately, initial analysis indicates that the density results from Table 2.1 do not show good correlation with porosity of the cocoon structures from SEM pictures.

2.4 Conclusion

Silk cocoons are natural polymer fibre composites that have a wide range of structural and morphological features in a hierarchy of dimensional scales from the centimetre size of the cocoons themselves, down through to the micrometer scale of the bonding between silk fibres and sericin binder, which are the main components of the composites. While cocoon morphology can be described very broadly as a nonwoven fibre composite, the 27 cocoons discussed here show a diversity of structural features such as: the number and connectivity of

layers through the cocoon wall thickness, the amount and distribution of sericin binder, the diameter and packing density of the silk fibres, the degree of orientation of the nonwoven structure, the distribution of larger holes within that structure, and the presence of calcium oxalate crystals.

Table 2.1 Measured thickness and density of the cocoon walls, together with the silk fibre bonding length.

	Thickness(μm)	Nominal Density(kg/m^3)	Fibre bonding length (μm)
Bombyx mori	400±10	500±20	25±4
Bombyx mandarina	150±10	830±60	27±4
Cricula andrei	130±30	820±90	54±7
Cricula trifenestrata	220±30	360±80	59±10
Antheraea pernyi	430±70	620±50	61±11
Antheraea roylei	140±10	1410±150	57±8
Antheraea polyphemus	200±10	1010±70	53±3
Antheraea mylitta	380±20	800±30	85±3
Antheraea frithi	400±20	860±20	59±7
Antheraea yamamai	170±10	780±30	43±7
Opodiphthera eucalypti	380±20	1120±170	63±9
Actias luna	35±1	1480±70	40±4
Actias selene	73±31	1190±290	62±9
Saturnia pavonia	120±30	1030±90	46±4
Saturnia pyri	310±10	920±80	83±3
Loepa katinka	140±10	860±30	53±8
Caligula cachara	160±30	650±20	97±8
Caligula simla	360±40	270±30	90±9
Argema mimosae	340±40	700±30	86±12
Attacus atlas	280±80	620±20	46±2
Hyalophora gloveri	300±10	630±60	43±3
Hyalophora cecropia	160±70	900±130	41±4
Callosamia promethea	280±30	870±100	59±7
Samia canningi	340±20	900±100	37±3
Samia cynthia	270±40	900±80	37±3
Epiphora bauhiniae	340±30	760±50	46±2
Gonometa postica	540±60	720±30	33±8

References

[1] Regier JC, Grant MC, Mitter C, Cook CP, Peigler RS, Rougerie R. Phylogenetic relationships of wild silkmoths (*Lepidoptera*: *Saturniidae*) inferred from four protein-coding nuclear genes. Systematic entomology. 2008;33(2):219.

[2] Regier JC, Cook CP, Mitter C, Hussey A. A phylogenetic study of the 'bombycoid complex' (*Lepidoptera*) using five protein-coding nuclear genes, with comments on the problem of macrolepidopteran phylogeny. Systematic entomology. 2008;33(1):175-189.

[3] Regier JC, Mitter C, Peigler RS, Friedlander TP. Monophyly, composition, and relationships within *Saturniinae* (*Lepidoptera*: *Saturniidae*): Evidence from two nuclear genes. Insect Systematics 38; Evolution. 2002;33:9-21.

[4] Silverstein R, Webster F, Kiemle D. Spectrometric identification of organic compounds. In: Bennon D, Yee J, editors. Infrared spectroscopy. New York: John Wiley and Sons, 2005. p. 72-126.

[5] ASTM. Annual Book of ASTM Standards. Standard method for measuring thickness of textile materials. Philadelphia; 1975. p. 477-478.

[6] Li Y, Ma T, Yang S-T, Kniss DA. Thermal compression and characterization of three-dimensional nonwoven PET matrices as tissue engineering scaffolds. Biomaterials. 2001;22(6):609-618.

[7] Wink WA, Baum GA. A rubber platen caliper gage - a new concept in measuring paper thickness. Solutions (Burlington, Vt). 1983;66(9).

[8] Chen F, Porter D, Vollrath F. Silkworm cocoons inspire models for random fiber and particulate composites. Physical Review E. 2010;82(4):041911-041917.

Chapter 3

Physical Properties of Cocoons

3.1 Introduction

A cocoon is a natural silk composite with a nonwoven structure made of continuous silk fibres conglutinated by sericin bonding matrix. As a biological structural material, it has a hierarchical structure that is assumed to have been optimised through evolutionary pressures over millions of years to provide the optimum protection for the silkworm pupae as they transform into moths, and are exposed to a wide range of threats such as physical attack from animals, birds or insects, or more subtle threats such as bacteria or simply harsh environmental conditions. The key point here is that they are all, in themselves, optimised for function and that we should be able to learn from this wide range of optimised structure-property-function relations in cocoons.

Ecologists have suggested that wild silkworm cocoons have evolved (i) for protection against diverse threats and also (ii) to regulate the environment for the pupae as they develop, such as to help conserving/blocking water or regulating the flow of gasses such as oxygen and carbon dioxide [2, 3]. In order to test these hypotheses, a limited amount of research has been conducted recently to investigate the mechanical properties and gas diffusability of silk cocoons from *Bombyx mori* and *Hyalophora cecropia*. For example, Zhao et al. tested the tensile properties of *Bombyx mori* cocoons and found them anisotropic with graded-layer properties [4, 5]. The *Hyalophora cecropia* cocoons and fibres have also been measured by

Reddy et al. [6]. Blossman-Myer et al. have found that *Bombyx mori* cocoon did not obstruct the exchange of respiratory gases between the pupa and the environment [7].

Chapter 2 showed that cocoon materials have evolved and been optimised in their morphology- property combinations with similar silk components. In this chapter, the diverse physical properties of cocoons are studied, and a discussion is presented about how the different structures might control natural tensile, compressive and gas diffusion properties.

3.2 Materials and methods

3.2.1 Materials collection

All materials were collected using the same procedure as stated in Chapter 2.

3.2.2 Scanning electron microscope (SEM) observation

All samples were produced and tested using the standardised protocols as outlined in Chapter 2.

3.2.3 Tensile tests of cocoons

Strips of cocoons in the direction of the long axis were cut for samples into a dog-bone shape due to the nonwoven structure of the materials. The sample had a shortest width of 5 mm and length of 15 mm. Tensile tests were carried out using Instron 5542 with a speed of 2 mm/min and 5 mm gauge length. The stress was calculated from the recorded load from the load cell, and the nominal thickness of the samples which is obtained from tests in section 3.2.5. The displacement of the machine was recorded by a Linear Variable Displacement Transducer (LVDT). Three samples from each cocoon species were tested.

3.2.4 Fibre testing

In the textile industry, *Bombyx mori* cocoons are submerged in water and detergents are added to remove the sericin glue from the cocoon for unravelling the fibres. It has been found that the degumming had quantifiable effects on the mechanical properties of the fibres [20, 25]. In order to understand the underlying contribution of fibres in the cocoon, the tensile behaviour of composite fibres covered with sericin, rather than industrial degummed fibres, was investigated. To do this, a demineralizing method was used for unravelling the cocoons. This method uses EDTA (Ethylenediaminetetraacetic acid) to chemically dissolve the calcium oxalate crystals on the cocoon surface. It has been found to succeed in unravelling the cocoon but causes less damage to both the sericin and the fibres [26]. EDTA powders from Fisher Scientific were dissolved to make a 1 M solution, and sodium hydroxide pellets (Sigma) were dissolved in the liquid to get a pH value of 7. The solution was stirred constantly and heated to a temperature of 60 °C during the dissolving process. When the solutes were fully dissolved, each cocoon was demineralised by immersion in a 1L EDTA solution in an oven at 40 °C for 48 hours. The demineralised cocoons were washed thoroughly in ionized water and then dried in air. Fibres were collected by reeling them in a speed of 80cm/min. For those cocoons which could not be reeled by machine, even after demineralising, the fibres were carefully collected by hand.

Silk fibre tests have been widely studied and investigated in terms of methods and results (See Section 1.2). Here a method is used that has been well validated and widely used in the Oxford Silk Group and other silk communities for measuring silk fibre properties. Fibre samples were well aligned and then mounted on paper frames with 10 mm gauge length and tested in Instron 5542 at 0.18 s^{-1} strain rate. 20 samples from three cocoons in each species

were chosen for tests. All the stress-strain curves of each species were interpolated to zero stress-strain values. Then average stress-strain curves from each speices were calculated with a breaking strain of an average number which is shown in Figure 3.1.

3.2.5 Compression tests of the cocoons

The test was carried out in the protocol which was outlined in Section 2.2.4.

3.2.6 Gas diffusion test (diethyl ether)

An airtight diffusion cell, made from a modified screw-cap centrifuge tube, was used to hold a circular cocoon sample with a diameter of 12 mm. The diffusion cell was filled with 0.35 cm^3 diethyl ether, and was then quickly closed by screwing the cover with the cocoon samples held in-between. A rubber O-ring fitted into the modified lid helps to ensure an airtight seal. The diffusion cell was then placed on an electric balance to measure the reducing weight as a function of time using a connected computer. Any reduction in mass is considered to be the permeation of vaporised ether through the cocoon material as the whole setup is airtight. By recording the change in mass of ether over time, the rate of permeation of the ether vapour through the cocoon sample can be determined. 17 species of cocoons were measured with three samples each. The diffusion of ether with no cocoon in the cell was also recorded for comparison. The test was carried out at 22°C and 51% R.H.

3.3 Results and Discussion

3.3.1 Fibre Properties

Silk fibres which are spun into cocoons are in the form of a bave i.e. a pair of fibroin brins with a sericin covering (See Section 1.2 for more details). This wet or moist covering binds the fibres together and acts as the nonwoven composite matrix phase for the cocoon. Non-degummed fibres with intact sericin coatings unravelled from cocoons were tested in this project for reference in order to examine whether inherent fibre brin properties may play a statistically significant role in cocoon properties. Figure 3.1 (top right plot) shows that the fibre strength has little correlation ($R^2 = 0.2$) with cocoon strength, which is typical of the poor correlation between fibre and cocoon properties. Otherwise, Figure 3.1 (left) shows a few characteristic average stress-strain curves for a number of silk types. All the fibres share a similar initial modulus and a yield at 2 to 4% strain. Importantly, most fibres have a strain to break around 16%. Initial inspection of the data may give the impression of high variability between silk types, but a comparable plot for a single silk type, a *Saturnia pyri* fibre, demonstrates comparable sample variability (Figure 3.1, the bottom-right). It is found that samples taken from different layers in cocoons differ significantly, and even spatially close samples can be very different due to factors such as bending of the fibres in the motion the worm makes while spinning the cocoon. Other observations on *Bombyx mori* report different tensile properties in different parts of the cocoon [17, 18].

Chapter 4 shows that the main fibre parameters that enter models for cocoon properties are low strain elastic modulus and activation strain to break. Here it is suggested that all the different fibres tested have essentially the same effective properties for cocoon fabrication.

It has been amply demonstrated already that the degumming process can have considerable effects on silk fibre properties [19, 20] relieving us from demonstrating the mechanical

behaviour of fibres degummed with different agents. The harsh degumming procedures required for highly bonded cocoons can severely degrade the structure and properties of the fibres themselves [19]. At the simplest level, non-degummed fibres in Figure 3.1 would have larger cross-sectional areas than degummed, leading to a lower strength and modulus values.

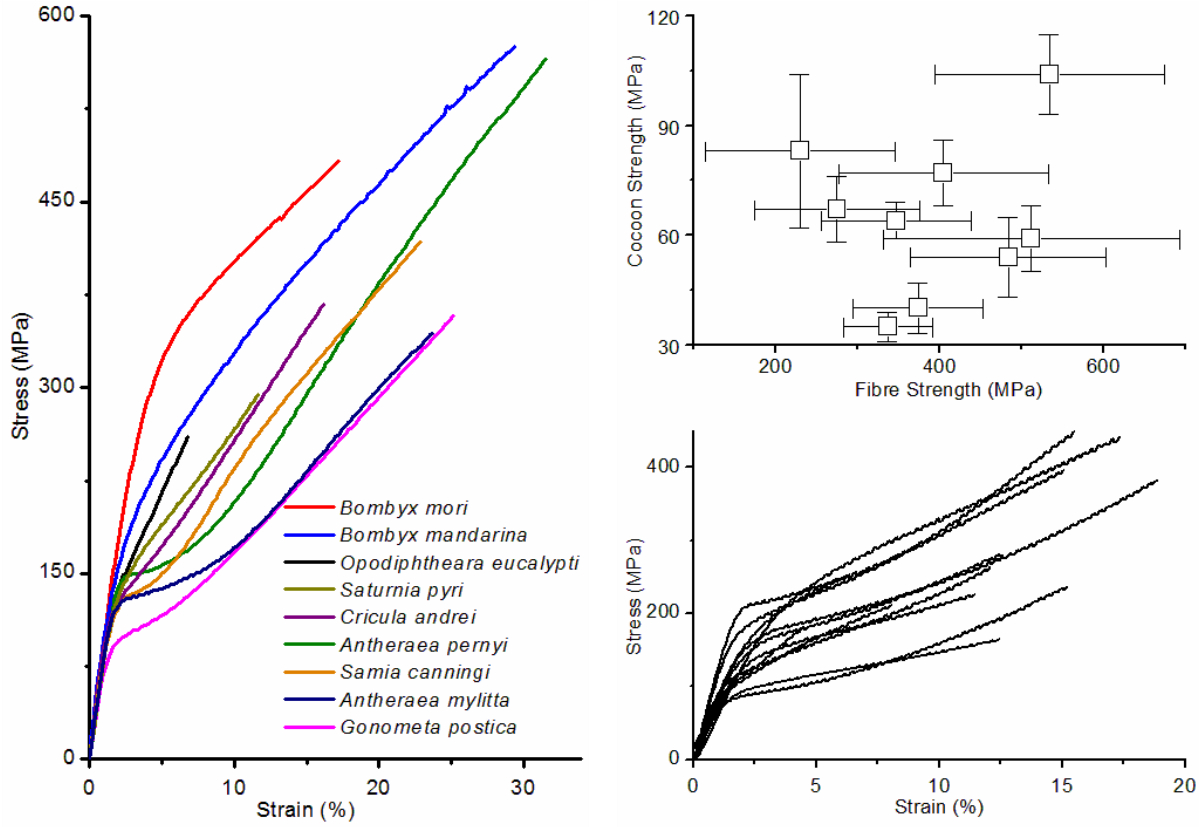

Figure 3.1 Tensile behaviour of single silk fibres. Left: Typical stress vs. strain curves of different silk fibres. Top right: No correlation between cocoon and fibre strength, $R^2 = 0.2$ (Cocoon strengths were calculated in Section 3.3.2). Bottom right: Variation in fibre properties, (*Saturnia pyri* fibre)

3.3.2 Tensile Properties

All our cocoons have a similar general form in their tensile stress-strain deformation profile in the plane of the cocoon wall. The stress rises with strain to a maximum value and the gradient of this curve can change once or twice through apparent yield points until stress falls relatively rapidly after the maximum. Looking at all the stress-strain profiles in Figure 3.2, these yield points are quite consistent in strain across almost all the cocoons, but their combinations and permutations in stress create an interesting diversity.

Here the cocoons are categorized into four types based on their tensile behaviour and their microstructure (Figure 3.2). 'Lattice' cocoons (Figure 3.2A) have only a loose scaffold structure made up of a few fused fibre bundles supporting the cocoon frame with large pores. The fibres sustain the load when the cocoon is stretched and the stress drops rapidly when the fibre bundles break. 'Weak' cocoons (Figure 3.2B) have high porosity and weak interlayer bonding. The inter-fibre bonding breaks gradually with increasing strain, and the stress peaks at 15-20% strain and drops gradually when the unbonded fibres disentangle from the nonwoven structure. 'Brittle' cocoons (Figure 3.2C) usually have a low porosity and strong interlayer bonding or single layer structure. A crack starts from the sericin binding matrix and grows perpendicular to the tensile load, leading to fibre breakage and a dramatic stress drop at 15-25% strain. 'Tough' cocoons (Figure 3.2D) can be grouped into a fourth type, in which the cocoons have medium porosity and interlayer bonding. These cocoons have the most complex stress-strain profiles, with multiple yield points below 20% strain and then a rapid failure in the range 40 to 60% strain, where the sericin binder fragments and the fibres pull apart as a global unravelling.

Future work will add further modelling and attempt to emulate the properties of all types of cocoon in Chapter 4.

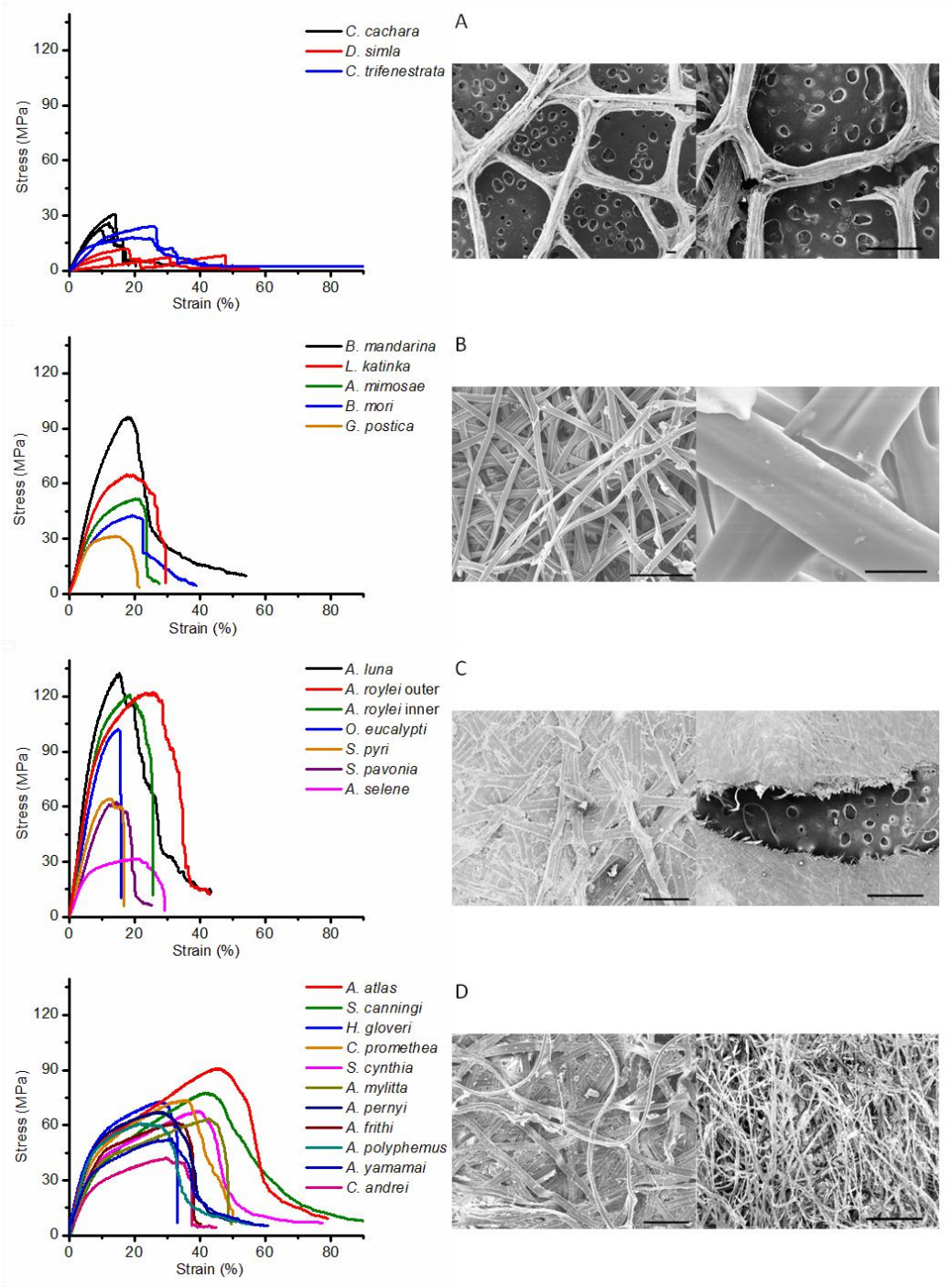

Figure 3.2 Tensile behaviour of silkworm cocoons (A) 'Lattice' cocoons. SEM pictures of *D. simla*. Left: Surface structure, scale bar: 200µm. Right: breaking mechanism, scale bar: 1mm. (B) 'Weak' cocoons. SEM pictures of *B. mori*. Left: Surface structure, scale bar: 200µm. Right: breaking mechanism, scale bar: 20µm. (C) 'Brittle' cocoons. SEM pictures of *S. pavonia*. Left: Surface structure, scale bar: 200µm. Right: breaking mechanism, scale bar: 1mm. (D) 'Tough' cocoons. SEM pictures of *S. cynthia*. Left: Surface structure, scale bar: 200µm. Right: breaking mechanism, scale bar: 1mm.

3.3.3 Compressive properties

All cocoons under compressive stress perpendicular to the plane of the walls have consistent stress-density behaviour. Due to their initial loose structure at the beginning of compression up to about 0.5 MPa, the stress increases slowly with a relatively large increase in density.

The compressive behaviour of cocoons is classified into three categories (Figure 3.3). Of main interest here are cocoons with a porous 3D nonwoven structure, shown as the central block of stress-density curves in Figure 3.3B with structures of a form shown in the micrograph. Either side of this central block are the low density 'lattice' cocoons (Figure 3.3A) and the high density 'brittle' cocoons (Figure 3.3C) which are difficult to compress above the 0.5 MPa level, since compression is against a solid fibre or composite material, with no effective pores to compact in the compression axis.

Between the lower and upper ranges of loose fibre and solid material compaction respectively, the compressive behaviour of nonwoven cocoons is found to follow the mat consolidation model developed by Zhou *et al.* for wood composites [24]. This model treats a composite mat structure as a system of bending beams, in a similar fashion to the open cell foam model used for tensile deformation, but with a different geometry of forces applied to beam segments between the bonded contact points. The number of contact points and the length of the bending segments of fibre decrease with increasing density, thereby increasing the compressive stress in a highly nonlinear manner. The model predicts that compressive pressure, P, should increase in a power 5 of density with a form

$$P = \frac{K\,E_s}{\rho_s}\left(\rho_m{}^5 - \rho_o{}^5\right) \tag{3.1}$$

where E_s and ρ_s are the modulus and density of the fibres respectively, ρ_m is the density of the mat, ρ_o is the initial mat density, and K is a dimensionless proportionality constant.

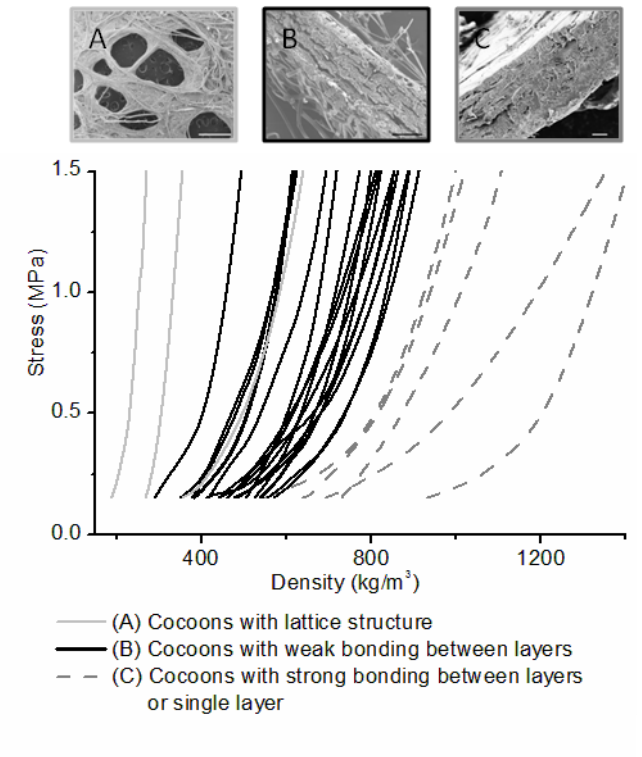

Figure 3.3 Typical stress vs. density curves of silkworm cocoons. (A) Cocoons with lattice structure, *C. trifenestrata* (B) Cocoons with weak interlayer bonding, *B. mori* (C) Cocoons with strong interlayer bonding or single layer, *O. eucalypti*. Scale bar: 200 µm

In the case of these nonwoven cocoons, this power of 5 for pressure on density is found to be a characteristic of the consolidation of the nonwoven structure, as shown in Figure 3.4, where cocoons from the central block of Figure 3.3B are plotted in a log-log pressure-density graph against a reference curve (red) with a power 5 in density. Thus, the model developed for wood-based composites appears to work well for nonwoven cocoon structures, and suggests that the dominant mechanism for compaction resistance is fibre bending.

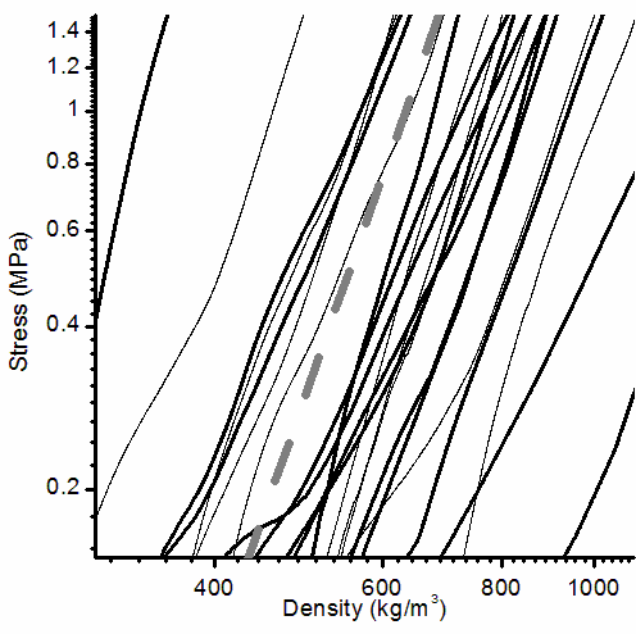

Figure 3.4 Compressive behaviour of silkworm cocoons: Log-log stress vs. density. The dash line is a straight line of 10^5 to illustrate the model relation of equation 3.1.

3.3.4 Gas diffusion (diethyl ether)

It can be assumed that gas and water vapour diffusion must play an important role in the development of pupae in cocoons and perhaps control the barrier characteristic of the cocoon to threats such as bacteria [7]. However, at the moment, we have no quantitative information about the biological role of diffusion. Here the observations on gas diffusion through cocoons as a physical process are reported and an initial attempt is made to demonstrate how the structural and morphological features of different cocoons affect diffusion properties.

As detailed in the experimental section, the rate of gas (diethyl ether) diffusion through a cocoon was quantified by measuring the weight loss of liquid by evaporation and diffusion through a section of cocoon mounted on the end of an otherwise impermeable tube. It was found that the mass loss was almost linear with time, so to compare the different cocoons in

each test, the absolute diffusion rate results were classified in terms of cocoon morphology into 4 groups as shown in the micrographs at the bottom of Figure 3.5 and grouped in the associated bar chart by colour as a guide to the main contributory features that controlled diffusion. Clearly, all the cocoons reduce the speed of ether diffusion with cocoon thickness, porosity and calcium oxalate crystals affecting rate of diffusion. *Actias selene*, *Actias luna* and *Opodiphtheara eucalypti* cocoons all have low porosity which allow them to conserve the ether, and hence the cocoons have lowest ether diffusion rate among the specimens tested. Cocoons with calcium oxalate crystals on the surface also have lower ether diffusion rate, e.g. those produced by *Hyalophora gloveri*, *Antheraea frithi*, *Saturnia pyri*, *Samia canningi* and *Gonometa postica* etc. This may be due to the dense crystals filling the pores. *Actias atlas*, *Bombyx mori* and *Caligula cachara* cocoons have a high-porosity structure, leading to high ether diffusion rate.

Without making a detailed analysis of the diffusion results at this stage in our work, Figure shows that density of the cocoons has a sensible correlation with ether diffusion rate, i.e. a higher density slows down the permeation rate of ether through the cocoon.

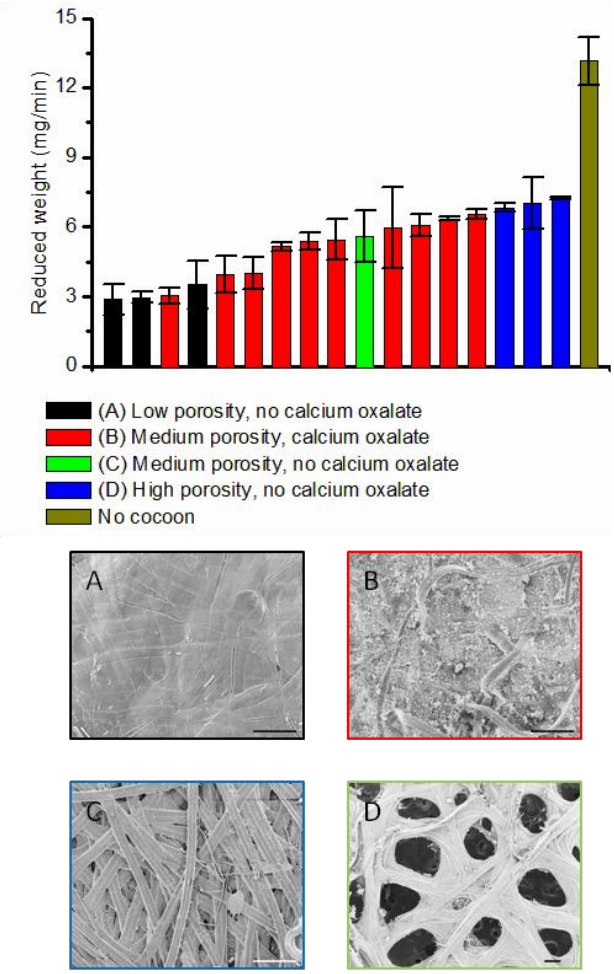

Figure 3.5 Gas diffusability (diethyl ether) of silkworm cocoons. Top: Comparison of diffusability speed of different cocoons. From left to right: *A. luna*, *O. eucalypti*, *S. pyri*, *A. selene*, *H. gloveri*, *A. frithi*, *S. canningi*, *A. mylitta*, *A. pernyi*, *L. katinka*, *A. polyphemus*, *A. yamamai*, *G. postica*, *A. atlas*, *B. mori*, *C. cachara*, *A. roylei*, no cocoon. Bottom: Morphologies of example cocoons. Scale bar: 200 μm (A) Cocoons with low porosity and no calcium oxalate: *O. eucalypti*. (B) Cocoons with medium porosity and calcium oxalate: *A. frithi*. (C) Cocoons with medium porosity and no calcium oxalate: *L. katinka*. (D) Cocoons with high porosity and no calcium oxalate: *C. cachara*.

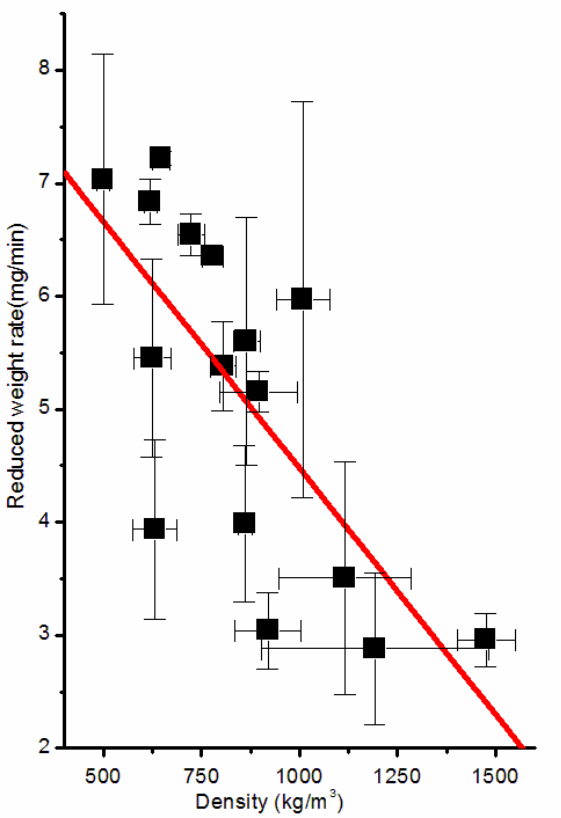

Figure 3.6 Gas diffusion (diethyl ether) rate of silkworm cocoons plotted as the rate of normalized mass loss against the density. R^2=0.51802

3.4 Conclusions

The observations and measurements on 25 diverse types of cocoon is presented in a first attempt to correlate physical properties with the structure and morphology of the cocoons, which appears to be more important than the differences in the properties of the silk fibres themselves. The inter-fiber variability of properties is similar to that of an individual fibre type, and the important fibre properties of low strain modulus and strain to failure for cocoon properties are similar for all the fibre types tested.

Tensile and compressive mechanical properties and gas (diethyl ether) permeation of the cocoon walls were tested. In each case the mechanisms or models that relate these properties to cocoon structure were identified. For tensile properties in the plane of the cocoon walls, four different types of cocoon behaviour were identified. The mechanisms of all types of cocoon will be discussed in Chapter 4.

Compressive properties normal to the plane of the cocoon walls are dominated by density, and a model previously derived for wood mats seems to be applicable and explain the stress-strain behaviour as a power 5 dependence of stress upon density under load. Gas diffusion (diethyl ether) through the cocoon walls is controlled by the combination of thickness and density, and contributions due to features such as calcium oxalate crystals have been identified.

Supplementary Information

Table 3.1 Mechanical properties of cocoons

	Thickness (μm)	Nominal Density (kg/m^3)	Max load (N)	Strength (MPa)	Breaking strain (%)	Modulus (MPa)	Strain at max stress (%)	Fibre bonding length (μm)
Bombyx mori	400±10	500±20	120±40	50±10	35±8	590±110	18±2	25±4
Bombyx mandarina	150±10	830±60	70±10	100±10	53±2	700±100	19±2	27±4
Cricula andrei	130±30	820±90	30±10	40±10	47±7	480±190	24±8	54±7
Cricula trifenestrata	220±30	360±80	30±20	20±10	49±14	210±120	21±6	59±10
Antheraea pernyi	430±70	620±50	100±50	60±10	44±9	790±90	26±3	61±11
Antheraea roylei	140±10	1410±150	90±10	120±10	24±3	1490±370	21±3	57±8
Antheraea polyphemus	200±10	1010±70	60±10	70±10	53±8	920±280	24±3	53±3
Antheraea mylitta	380±20	800±30	150±20	60±10	51±6	760±70	42±3	85±3
Antheraea frithi	400±20	860±20	140±10	60±10	40±2	830±60	32±2	59±7
Antheraea yamamai	170±10	780±30	50±10	60±10	60±8	640±200	34±5	43±7
Opodiphthera eucalypti	380±20	1120±170	140±30	80±20	16±1	630±160	15±1	63±9
Actias luna	35±1	1480±70	20±5	110±20	23±9	1380±440	14±3	40±4
Actias selene	73±31	1190±290	40±10	30±10	24±5	430±160	20±3	62±9
Saturnia pavonia	120±30	1030±90	40±10	50±20	21±7	600±90	11±4	46±4
Saturnia pyri	310±10	920±80	100±40	70±10	21±7	1010±390	15±4	83±3
Loepa katinka	140±10	860±30	50±10	70±10	34±11	690±230	16±1	53±8
Caligula cachara	160±30	650±20	20±10	30±10	18±7	300±40	12±2	97±8
Dictyoploca simla	360±40	270±30	20±10	10±3	44±17	100±70	32±15	90±9
Argema mimosae	340±40	700±30	90±10	50±10	17±4	640±110	22±6	86±12
Attacus atlas	280±80	620±20	160±10	90±10	79±5	950±160	46±1	46±2
Hyalophora gloveri	300±10	630±60	120±20	70±10	41±7	940±140	26±2	43±3
Hyalophora cecropia	160±70	900±130	100±20	100±30	44±5	1120±470	29±4	41±4

Callosamia promethea	280±30	870±100	120±10	70±10	50±4	650±100	33±2	59±7
Samia canningi	340±20	900±100	160±20	80±10	91±2	580±100	43±2	37±3
Samia cynthia	270±40	900±80	100±10	60±10	73±3	610±10	37±2	37±3
Gonometa postica	540±60	720±30	90±20	40±10	22±2	530±140	15±2	33±8

Table 3.2 Mechanical properties of silk fibres

	Maximum Load (mN)	Maximum Stress (MPa)	Strain at max. Stress (%)	Break Stress (MPa)	Break Strain (%)	Initial modulus (MPa)	Breaking energy (J/cm^3)
Antheraea mylitta	400±50	350±50	24±4	200±90	27±5	8700±600	51±13
Antheraea pernyi	260±60	510±130	28±5	370±180	31±6	9500±100	87±25
Bombyx mandarina	110±20	530±110	26±7	310±140	29±6	10700±2100	95±39
Bombyx mori	130±20	480±120	17±7	410±120	17±6	8300±1800	96±17
Cricula andrei	180±40	370±80	17±6	370±80	17±6	10300±1000	36±19
Gonometa postica	220±40	340±50	24±5	340±50	24±5	7800±600	45±14
Samia canningi	110±30	410±100	21±7	330±130	23±8	8400±1900	54±29
Saturnia pyri	260±100	280±110	12±5	290±100	12±5	8300±2000	21±15
Opodiphthera eucalypti	200±80	230±90	7±4	210±120	7±5	8700±1500	12±12

Table 3.3 Results of cocoon gas diffusability (diethyl ether)

	Thickness(μm)	Density (kg/m^3)	Calcium oxalate crystals	Rate of weight loss (mg/s)
Actias selene	73±31	1190±290	N	2.88±0.67
Actias luna	35±1	1480±70	N	2.96±0.24
Saturnia pyri	310±10	920±80	Y	3.04±0.34
Opodiphthera eucalypti	380±20	1120±170	N	3.51±1.03
Hyalophora gloveri	300±10	630±60	Y	3.94±0.79
Antheraea frithi	400±20	860±20	Y	3.99±0.69
Samia canningi	340±20	900±100	Y	5.16±0.18
Antheraea mylitta	380±20	800±30	Y	5.38±0.39
Antheraea pernyi	430±70	620±50	Y	5.45±0.88
Loepa katinka	140±10	860±30	N	5.60±1.09
Antheraea polyphemus	200±10	1010±70	Y	5.97±1.75
Antheraea roylei	140±10	1410±150	Y	6.05±0.48
Antheraea yamamai	170±10	780±30	Y	6.36±0.08
Gonometa postica	540±60	720±30	Y	6.55±0.19
Attacus atlas	280±80	620±20	Y	6.84±0.20
Bombyx mori	400±10	500±20	N	7.03±1.11
Caligula cachara	160±30	650±20	N	7.22±0.06
no cocoon				13.16±1.06

References

[1] Porter D, Vollrath F. Silk as a biomimetic ideal for structural polymers. Advanced Materials. 2009;21(4):487-492.

[2] Danks HV. The roles of insect cocoons in cold conditions. E J Entomol. 2004;101(3):433-437.

[3] Tuskes PMP, Paul PM. The wild silk moths of north America : a natural history of the *Saturniidae* of the United States and Canada. Cornell University Press, 1996.

[4] Zhao H-P, Feng X-Q, Yu S-W, Cui W-Z, Zou F-Z. Mechanical properties of silkworm cocoons. Polymer. 2005;46(21):9192-9201.

[5] Zhao H-P, Feng X-Q, Cui W-Z, Zou F-Z. Mechanical properties of silkworm cocoon pelades. Eng Frac Mech. 2007;74(12):1953-1962.

[6] Reddy N, Yang Y. Structure and properties of cocoons and silk fibers produced by *Hyalophora cecropia*. Journal of Materials Science. 2010;45(16):4414-4421.

[7] Blossman-Myer B, Burggren WW. The silk cocoon of the silkworm, *Bombyx mori*: Macro structure and its influence on transmural diffusion of oxygen and water vapor. Comparative Biochemistry and Physiology - Part A: Molecular & Integrative Physiology. 2010;155(2):259-263.

[8] Chen F, Porter D, Vollrath F. Silkworm cocoons inspire models for random fiber and particulate composites. Physical Review E. 2010;82(4):041911-041917.

[9] I'Anson SJ, Sampson, W.W. Competing Weibull and stress-transfer influences on the specific tensile strength of a bonded fibrous network. Composites Science and Technology. 2007;67(7-8):1650.

[10] Eichhorn SJ, Sampson WW. Relationships between specific surface area and pore size in electrospun polymer fibre networks. Journal of The Royal Society Interface. 2009.

[11] Hoseini M, Bindiganavile V, Banthia N. The effect of mechanical stress on permeability of concrete: A review. Cement and Concrete Composites. 2009;31(4):213-220.

[12] Kothari VK, Das A. Compressional behaviour of nonwoven geotextiles. Geotextiles and Geomembranes. 1992;11(3):235-253.

[13] Rawal A, Anandjiwala R. Comparative study between needlepunched nonwoven geotextile structures made from flax and polyester fibres. Geotextiles and Geomembranes. 2007;25(1):61-65.

[14] Correia NdS, Bueno BdS. Effect of bituminous impregnation on nonwoven geotextiles tensile and permeability properties. Geotextiles and Geomembranes. 2011;29(2):92-101.

[15] Chen F, Porter D, Vollrath F. Morphology and structure of silkworm cocoons. Materials Science & Engineering C-Biomimetic and Supramolecular Systems. 2012;Submitted.

[16] Freddi G, Gotoh Y, Mori T, Tsutsui I, Tsukada M. Chemical structure and physical properties of *Antheraea assama* silk. Journal of Applied Polymer Science. 1994;52(6):775-781.

[17] Zhao H-P, Feng X-Q, Shi H-J. Variability in mechanical properties of *Bombyx mori* silk. Mat Sci Eng C. 2007;27(4):675-683.

[18] Perez-Rigueiro J, Viney C, Llorca J, Elices M. Silkworm silk as an engineering material. Journal of Applied Polymer Science. 1998;70(12):2439-2447.

[19] Jiang P, Liu HF, Wang CH, Wu LZ, Huang JG, Guo C. Tensile behavior and morphology of differently degummed silkworm (Bombyx mori) cocoon silk fibres. Materials Letters. 2006;60(7):919-925.

[20] Perez-Rigueiro J, Elices M, Llorca J, Viney C. Effect of degumming on the tensile properties of silkworm (Bombyx mori) silk fiber. Journal of Applied Polymer Science. 2002;84(7):1431-1437.

[21] Chen F, Porter D, Vollrath F. A nonwoven composite model based on silkworm cocoon (*Bombyx mori*). Journal of Materials Science and Engineering. 2010;4(9):28-33.

[22] Zhu HX. Analysis of the elastic properties of open-cell foams with tetrakaidecahedral cells. J Mech Phys Solids. 1997;45(3):319.

[23] Gibson LJ, Ashby MF. The Mechanics of Three-Dimensional Cellular Materials. Proceedings of the Royal Society of London Series A, Mathematical and Physical Sciences. 1982;382(1782):43-59.

[24] Zhou C, Dai C, Smith GD. A generalized mat consolidation model for wood composites. Holzforschung. 2008;62(2):201-208.

[25] Poza P, Perez-Rigueiro J, Elices M, Llorca J. Fractographic analysis of silkworm and spider silk. Eng Frac Mech. 2002;69(9):1035-1048.

[26] Gheysens T, Collins A, Raina S, Vollrath F, Knight DP. Demineralization Enables Reeling of Wild Silkmoth Cocoons. Biomacromolecules. 2011;12(6):2257-2266.

Chapter 4

Structure-property Relationships of Cocoons

4.1 Introduction

This chapter presents a fundamental quantitative analysis of a variety of silk cocoons which directly links their morphologies and mechanical properties, based on the study of morphologies and physical properties in previous chapters. Most cocoons discussed in this thesis are a natural composite shell constructed by the animal. They consist of a nonwoven structure with a continuous semi-crystalline fibroin silk strand, bonded by about 25%wt amorphous sericin. Their micro-structures are similar to other random fibrous materials such as paper, nonwoven textiles and electrospun polymer mats. Due to the technological importance of nonwoven fibre materials, a number of models for each of these materials of similar structure already exist, particularly paper. A literature survey of the models available is presented below and the models are compared with experimental data for cocoons presented in this thesis. It was found that the models are mathematically complex and require fitting parameters to reproduce the experimental data, rather than predicting properties using a limited number of parameters calculated directly from the component material properties and composite morphology. Therefore, a physical mechanism for cocoon damage behaviour is proposed and described below for the development of the damage and loss of modulus in the cocoons based on my experimental observations. A realistic physical model for cocoons is developed with a first priority (namely including all the observed structural effects under

deformation) to quantitatively calculate cocoon properties using a minimum number of material parameters, which themselves can be calculated independently. This model uses the simple hypothesis that stiffness reduces as the number of bonding sites in a cocoon reduces under increasing load and quantifies this process as loss of connectivity in the composite due to strain-activated bond breaking.

In itself, such a model for silkworm cocoons has limited technological value, and such a bioinspired model needs to be able to predict (rather than just reproduce) the properties of a range of other 'synthetic' materials with similar characteristics. The first obvious set of materials to consider were nonwoven random fibre networks for which previous models had been developed, but they were found to have the shortcoming outlined above. The model was applied to nonwoven materials based on their experimental results. It was then noticed that the simplest form of our model has a remarkable similarity to the stress-strain profiles of particulate composites. Both these types of composite can be linked to the model through the loss of connectivity of bonding under load, and thus a number of such composites are used as examples to both illustrate and validate our bioinspired model in materials of great technological and economic importance.

4.2 Literature Review

Here the mathematical models in the literature that describe the mechanical deformation of cocoons under stress are discussed. Although no specific mathematical models could be found for cocoons in the literature survey, strength models have been developed for other random fibre networks, especially paper materials (presented in sections 4.2.1 to 4.2.3).

Models of open-cell foams are outlined in section 4.2.4, which are relevant to the quantification of cocoons modulus.

4.2.1 Bonding failure

Models for the tensile strength of paper, such as the widely applied semi-empirical theory from Page [1] and the mechanistic theory from Kallmes *et al*. [2], separate the bonding contributions to tensile strength into the influence of the area of inter-fibre bonds, and that of the shear bond strength per unit area acting in these regions. Page [1] proposes a failure process whereby bonds are progressively broken in the failure zone, and the still-bonded fibres take progressively more of the load until they become overloaded and break. This hypothesis leads to the premise that the final sheet strength directly scales with the fraction of fibres that are broken across the rupture zone. Kallmes *et al.* [2] assume that local rupture of a fibre or a bond promotes further failures, rapidly leading to a total failure of the sheet. Bond failures are modelled by removing the contributions from debonded fibres from the integration of the sheet load. Paper with weak bonds is considered to fail due to bond failure rather than rupture of the fibres.

An important independent parameter in many models for the tensile strength of paper is the relative bonded area (RBA); according to Dodson [3] this term was introduced by Kallmes *et al.* who defined it as the fraction of the fibre surface that is bonded to other fibres [2]. RBA exhibits a strong positive correlation with network density and as such can be influenced independently of fibre morphologies. Van den Akker *et al.* [4] suggest that the tensile mode failure of paper involves failure of inter-fibre bonds and fibres themselves. They also propose the fraction of fibre failures increases with increasing density and hence bonding density.

Kallmes *et al.* [2] identified a critical value of RBA at which the initiation of network failure changed from being dominated by bond failure to being dominated by fibre failure. They observed that this threshold occurred between 0.31 and 0.37 for their samples.

Calsson et al. [5] present the mechanism of failure for paper with short fibre length and low RBA is entirely through bond failure with a threshold of half the theoretical maximum strength of the network; above this threshold, both fibre and bond failure are considered to be involved in rupture. Although this model yields reasonable agreement with experimental data from the literature, the assumption of rupture by bond failure only for networks of low RBA is at variance with the experimental observations of Van den Akker *et al.* [4] who observed at least 10% broken fibres along the failure line of even the most lightly bonded networks.

4.2.2 Shear-lag models

In a network under strain, the bonded regions of the fibre surfaces facilitate the transfer of stress between fibre segments. This is the classic shear-lag theory from Cox [6]. Favourable comparisons between Cox's theory and experiments have been reported. Page et al. [7] found the elastic modulus of dense paper samples and highly bonded networks of polyester fibres approached one third of the axial modulus of the constituent fibres, agreeing with Cox. For less dense samples however, the modulus was lower and this was attributed to less efficient stress transfer [8]. Seth et al. [9] demonstrated that when fibres of a given type were subjected to a range of mechanical and chemical treatments prior to or during the forming of networks, the differences in the stress-strain behaviour of the networks could be accounted for entirely by changes in the efficiency of stress transfer. I'Anson *et al.* [10] propose that there is an additional influence of the given mass per unit area, called areal density, on the efficiency of

stress-transfer between fibres. Astrom *et al.* [11, 12] report that the nature of stress transfer in bonded regions influences the elastic and failure behaviour of the network. Carlsson *et al.* [13] indicates the importance of fibre length for weakly bonded sheets, and also the role of RBA as a means for utilizing the strength potential of the fibres.

Shortcomings of the shear-lag model have been voiced. Raisanen *et al.* [14] modelled networks with total fibre length per unit area up to 10 times the percolation threshold and with flexible bonds at regions of fibre intersection. They concluded that the transfer of axial stress in random fibre networks could not be accounted for by the shear-lag approach. Raisanen *et al.* [15] also point out that the network strength is influenced by the mean length of fibre ligaments occurring between crossings. In an experimental study of the strains in individual fibres within a network of cotton fibres, Eichhorn *et al.* [16] observed significant strains at the ends of fibres within the network, contrary to the prediction of Cox that strain would be zero at the fibre ends. It is important to note that the measurements were carried out on fibres that were flat and well bonded at their ends.

I'Anson *et al.* [10] suggest that when a network, in which the number of fibres per unit area is just above the percolation threshold, fails under a tensile stress, the dominant mechanism of failure will be that of bonds rather than fibres because the number of contacts per fibre is typically insufficient to transfer enough stress to a fibre for it to fail. As the number of fibres per unit area increases, so does the expected number of crossings per fibre and thus stress transfer is more efficient, so that fibre failure becomes implicated in network rupture.

4.2.3 Weibull theory

The classic theory of Weibull has been used for predicting the percolation threshold of the fibre network. According to Weibull theory, the strength of a sample without notches is influenced by sample geometry [17]. It predicts an exponential decrease in the specific strength *T* of a sample with increasing volume *V* such that,

$$T = k_w V^{-\frac{1}{m}} \tag{4.2}$$

Where k_w is a constant characterising the strength of the material. This dependence arises because the probability of a 'weak-link' in the material under investigation increases with increasing volume. The nature of the dependence is characterised by the Weibull modulus of the material represented by the parameter *m*.

As the area of material between straining elements is often some tens of square metres, people have sought to relate the strength of paper to its failure by scaling test results from small samples using Weibull's theory. They often consider tensile tests performed on samples of different lengths and widths. For example, Gregersen *et al.* [18] by experiment found the Weibull modulus of a newsprint paper grade to be 28.

An alternative approach to determine the Weibull modulus *m* is to carry out a sufficient number of tests on samples of a single size and compare the distribution of these with the cumulative distribution function for the two parameter Weibull distribution, which gives the probability that a sample will fail under a failure stress, σ, as

$$P(\,fail\,) = 1 - e^{-\left(\frac{\sigma}{\sigma_0}\right)^m} = 1 - e^{-\left(\frac{T}{T_0}\right)^m} \tag{4.3}$$

where σ_0 and T_0 are nominal strengths that are expected to be a characteristic of the material. Using this technique Gregersen *et al.* [18] determined the Weibull modulus of their newsprint sample to be about 18, and Uesaka *et al.* [19] reports values of modulus m between 12 and 25 for newsprint and directory grades of paper.

Wathen *et al.* [20] report a reduction in the Weibull modulus of paper with decreasing structural uniformity; no corresponding influence of uniformity on the mean tensile strength of their samples was observed. They suggest that the Weibull modulus may account for structural inhomogeneities such as in-plane distributions of mass and density.

The key point when using a Weibull approach is that failure probability is quantified as a statistical distribution of failure events (bonds breaking) around a stress value that is characteristic for a given material. For the silk cocoon project in this chapter, a similar approach is used for silkworm cocoons in which the model parameters are quantified in terms of the component material properties and the cocoon network structure.

4.2.4 Open-cell foam model

Cellular materials can include both manufactured materials (e.g. thermal insulation, lightweight reinforcement and filtration) and natural materials (e.g. sponge and wood), which have a cellular structure that optimises performance for each of their specific applications. Open cell foams allow the free passage of gases between the cells, since the cells consist of strands of material with no film between them to enclose the cells. This is important for cocoons, since it allows metabolic processes such as respiration and water exchange to take

place. Many studies have focused on local cell features, such as the effect of disorder and the interaction between cells on a mesoscopic scale. Some models have been developed to provide structure-property relations for cellular solids. Since most foams do not contain straight-through struts, beam bending rather than stretching comes into play, which leads to relatively low modulus of material. A typical model structure for an open cell foam is shown in Figure 4.1.

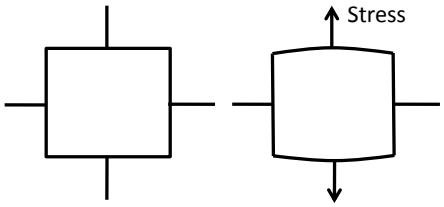

Figure 4.1. A simplified open cell foam model structure, showing bending of the struts under stress for a low modulus.

Gibson *et al.* [21] state that at low densities, the Young's modulus of a cellular solid (E) is related to its density (ρ) through the relation:

$$\frac{E}{E_s} = C\left(\frac{\rho}{\rho_s}\right)^n = Cp^n \tag{4.4}$$

where E_s and ρ_s are the Young's modulus and density of the solid skeleton and $p = \rho / \rho_s$ is the reduced density. The factor $C \approx 1$. Experimental evidence suggests that $n \approx 2$ for open cells. This semi-empirical formula broadly describes data obtained for many different types of foams.

Most theoretical attention has been focused on simple three-dimensional cell structures with straight struts (or walls) arranged in periodic arrays at low densities. If a periodic open-cell solid has 'straight-through' struts that traverse the extent of the sample, deformation occurs along the strut axis, and the modulus varies in direct proportion to the density (n = 1) [22, 23]. If the struts are finite, bending is activated at their intersection points and the Young's modulus can be shown to vary quadratically with the density (n = 2) [22, 24, 25] which agrees with experimental observation. In addition, the importance of strut twisting has also been considered [24].

Zhu *et al*. [25, 26] and Warren *et al.* [24] derive analytical results for an open-cell tetrakaidecahedral model packed in a body centred cubic array, a generalised geometrical form that should be a good representation of a random fibre composite. The results demonstrate incompressible behaviour ($\nu \to 0.5$) at low densities. The results of Zhu *et al.* [25, 26] for the Young's modulus, Y, and Poisson's ratio, ν, for strain parallel to the 100 axis are,

$$\frac{Y_{100}}{Y} \approx \frac{2}{3} C_z \left(\frac{\rho}{\rho_s}\right)^2 \left(1 + C_z \frac{\rho}{\rho_s}\right)^{-1} \qquad \nu_{12} = \frac{1}{2} \frac{1 - Cz\left(\rho/\rho_s\right)}{1 + Cz\left(\rho/\rho_s\right)} \tag{4.5}$$

where C_z =1.06 for equilateral triangles. The foam is relatively stiff under uniform compression, with the bulk modulus varying linearly with density.

Warren *et al.* [27] also derive analytical relations for the properties of a foam comprised of isotropically oriented tetrahedrally arranged struts. The geometry can be visualised as a node located at the centre of a tetrahedron with equilateral faces, the four struts connecting the

central node to the vertices. There are eight nodes of this type adjacent to the central node. The results are

$$\frac{E}{E_s} = \frac{C_w p^2 (11 + 4C_w p)}{10 + 31C_w p + 4C_w^2 p^2} \tag{4.6}$$

where $p = \rho / \rho_s$ and C_w = 0.827 for a circular cross-section. The definition of the model shows that beam bending is the primary mode of deformation for uniaxial compression.

To make a quantitative estimate for a cocoon we use an open cell foam as the analogy and apply the relation of Zhu et al. [26]

$$\frac{Y}{Y_f} \approx \frac{2}{3} C_z \left(\frac{\rho}{\rho_f} \right)^2 \left(1 + C_z \frac{\rho}{\rho_f} \right)^{-1} \quad \text{where } C_z = 1.06 \approx 1 \tag{4.7}$$

This is an extension of the simpler Gibson-Ashby [27] proportionality in density squared and shows how the elastic modulus of the composite is controlled by porosity, where ρ is composite density relative to that of the solid, ρ_f.

4.2.5 Summary of Literature

The models described suggest failure mechanisms for paper, which has a random fibre structure similar to that of cocoons. When a network in which the number of fibres per unit area is just above the percolation threshold fails under a tensile stress, the dominant mechanism of failure will be that of bonds rather than fibres breaking, because the number of contacts per fibre is typically insufficient to transfer enough stress to a fibre for it to fail. The specific tensile strength is obtained in these models from the competing effects of the

efficiency of stress-transfer between fibres, and a change in network strength that arises due to the probability of network failure with different sample volumes, as given by the Weibull theory.

Most of the open-cell foam models work on the density and microstructure dependence of the Young's modulus. The modulus of foam is low due to bending of beams (fibres) normal to the strain axis, rather than simple stretching of the fibres.

4.3 Materials and methods

All samples were produced and initially tested using the standardised protocols as outlined in Chapter 3. The specifics of each experiment will be introduced as they are encountered in the chapter.

4.4 Cocoon connectivity model development

Figure 4.2 shows overall cocoon structure as well as central layer morphology of 3 different moth species (*Bombyx mori, Antheraea pernyi, Opodiphthera eucalypti)* alongside measured stress-strain plots for the full cocoon walls, which are good examples of properties at the lower, middle, and upper limits of mechanical properties ('Weak', 'Tough' and 'Brittle' cocoon in Chapter 3) across a wide range of cocoon types in Chapter 3 respectively. Stress rises with a reducing modulus as strain increases and the binding points between fibres break progressively. After a peak stress, there is a rapid fall in stress, indicating a state without a continuous bonded pathway through the sample, which by now is held together simply by entangled fibres.

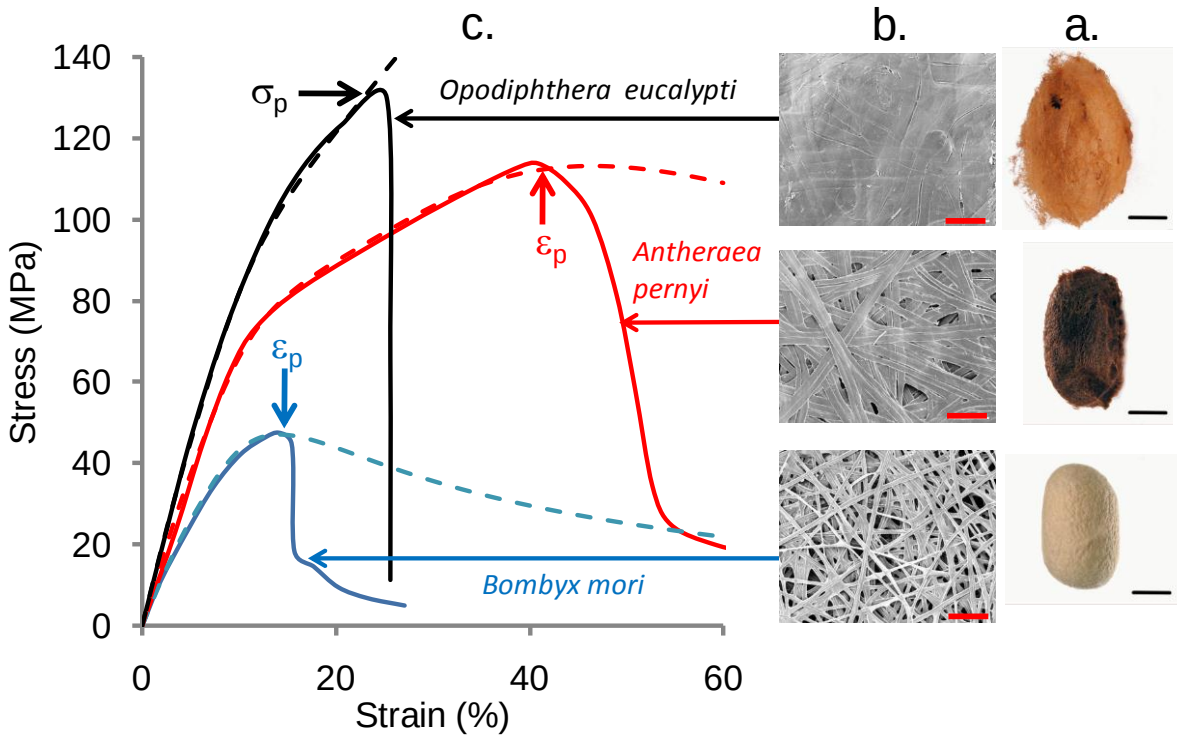

Figure 4.2 The stress-strain curve for three silkworm cocoons with their different nonwoven network structures,. a. The cocoons of *Bombyx mori, Antheraea pernyi, Opodiphthera eucalypti* (scale bar 10 mm) b. Typical bonded nonwoven structure of the middle layers of the cocoons (scale bar 200 μm). c. Stress-strain profiles for the cocoon walls, with solid lines showing experimental measurements and dashed lines as model calculations, with failure conditions shown as arrows in either stress (σ_p) or strain (ε_p).

A physically realistic model for nonlinear mechanical properties of the cocoon walls in terms of the component materials and the composite morphology can be derived from those data. While silk fibre properties were measured experimentally in Chapter 3, the sericin properties were derived by Prof David Porter by detailed modelling calculations [28, 29]. Sericin was modelled by assuming an amorphous structure to get a modulus of 3.5 GPa and a yield strength at around 130 MPa using Group Interaction Modelling [30]. The brittle failure stress was estimated using empirical correlations with the average cross-sectional area of the polymer chain [29] to give a stress of 135 MPa. It shows sericin polymer is right on the border between brittle and ductile within reasonable accuracy levels of the models. Figure 4.3 shows the stress-strain characteristics of the component materials for *Bombyx mori*. For our model, the key material parameters are a silk fibre modulus $Y_f \approx 5 – 9$ GPa and strength of about 400 MPa as well as a sericin matrix modulus of 3.5 GPa and a failure stress of 130 MPa.

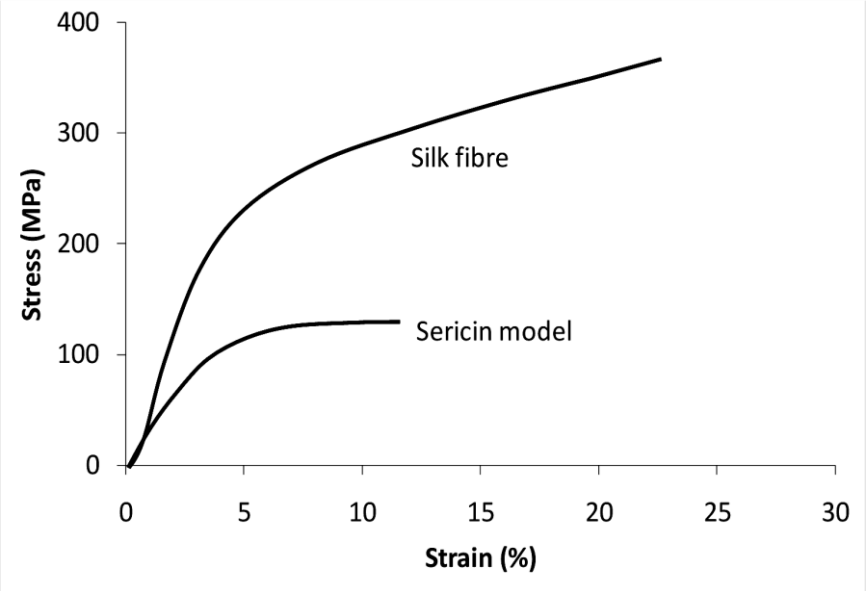

Figure 4.3 Typical observed stress-strain profile for a *Bombyx mori* fibre and predicted profile for sericin.

The initial elastic modulus of the cocoon walls, Y, is significantly lower than that of the fibres and binder due to bending of the circular cross section of fibre with a radius of about 2 mm spun by the gyrating silkworms [2,25] and was found to follow the open cell foam model of Zhu [26] with $\rho_s \approx 1300$ kgm^{-3}.

$$\frac{Y}{Y_f} \approx \frac{2}{3}\left(\frac{\rho}{\rho_s}\right)^2\left(1+\frac{\rho}{\rho_s}\right)^{-1} \tag{4.8}$$

Observations presented in this work suggest that damage through loss of connectivity of bonding between fibres gradually reduces the stiffness of the composite with increasing strain. Accordingly, a pragmatic fracture mechanics approach is adopted and scale modulus linearly with the active fraction of bonded fibres that sustains load. In this radically simple connectivity model, the fraction of broken bonds is quantified by using an Arrhenius

activation function in mechanical energy of deformation in strain, ε, relative to an activation strain, ε_a, squared, since elastic energy density is proportional to elastic strain squared.

Assuming a number of different activation effects, i, with fractional contribution f_i the relation for stress, σ, with initial composite modulus, Y, becomes

$$\sigma = Y\ \varepsilon\left[1-\sum_i f_i \exp\left(-\left(\frac{\varepsilon_{ai}}{\varepsilon}\right)^2\right)\right] \quad \text{where} \quad f_i = \frac{Y_i}{Y} \tag{4.9}$$

and the normalized (ε_a = 1, Y = 1) stress contribution of a single fraction is shown in Figure 4.4 to illustrate the relation.

The typical three-layer morphology of cocoons of outer, central and inner first led us to expect three different activated bond breaking effects to be associated with the different binder concentrations in layers. However, a more detailed analysis of further cocoon types and their component layers demonstrated that the three different activated processes seem to be directly associated with the component materials and bonding morphology.

The model parameters for equation (4.8) were determined by fitting the experimental data shown in Figure 4.2 for the three cocoon types and first using the very consistent values of activation strain which is defined by the change in slope of the stress-strain curves to give values of 0.05 (i), 0.16 (ii) and 0.6 (iii) for the three types of cocoons in Figure 4.2. The activation strain appears to be linked to the breaking strain of the sericin and fibroin fibres and which allows the uncoiling of the fibre. It was then noticed that most of the cocoon data could be best fitted by taking the two lowest modulus values of 130 and 425 MPa, which correspond very well with the failure stress values for the sericin and fibroin fibres,

respectively. Finally, only one modulus value of Y_3 was needed to complete the parameter sets, and this value increased with increasing density and bonding connectivity between the fibres, and corresponded remarkably well with values that fit the simple relation $Y = Y_2 + Y_2 + Y_2$. Since models such as that of Zhu equation (4.8) allow calculation of the initial cocoon modulus, and Y_1 and Y_2 are known, the final model parameter $Y_3 = Y - (Y_1 + Y_2)$ can be determined independently.

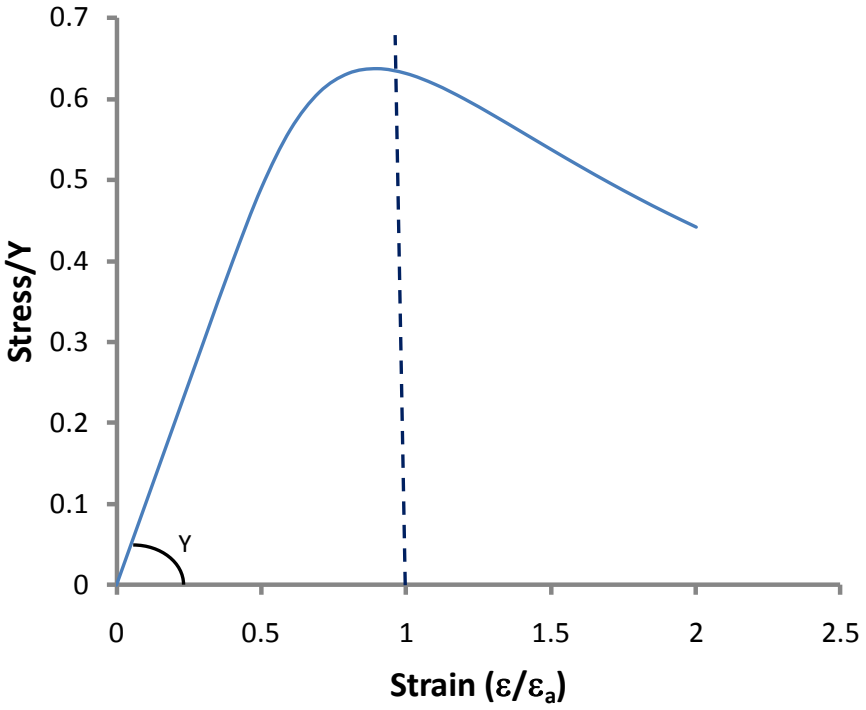

Figure 4.4. Simplest model normalised stress-strain profile for a single component contribution of equation (4.9) with an activation strain, $\varepsilon_a = 1$, and initial modulus, Y = 1, showing how damage to the materials and bonding through ε_a leads to loss of stiffness.

Table 4.1 Parameters for the cocoon model and other examples.

Material	ε_{ai}			Y_i (MPa)		
i	1	2	3	1	2	3
Bombyx mori cocoon	0.05	0.16	0.6	130	425	10
Antheraea pernyi cocoon	0.05	0.16	0.6	130	425	240
Opodiphthera eucalypti	0.05	0.16	0.6	130	425	400
Nonwoven cloth	0.06	0.23	-	260	260	-
Paper	0.025	0.077	-	700	700	-
Nanomat	-	0.11	0.7	-	40	40
Polymer bonded explosive (at 1 s^{-1})	0.033	-	-	900	-	-
Concrete (compression)	0.0025	-	-	12200	-	-

The model parameters used to fit the cocoons and the example composite materials of the paper in section 4.6 are given in Table 4.1. Thus, all the parameters in equation (4.8) can be calculated directly from the cocoon structure and model predictions (dashed lines) are compared with observation (solid lines) in Figure 4.2. The important differentiating parameter is Y_3, which increases to the limiting value of fibre strength of about 400MPa as the amount of interfibre bonding increases and more fibre sustains load directly. Any relation between the model parameters and failure properties of the components will need to be investigated more thoroughly in future work.

The model provides important insights into how structural changes with increasing strain control properties. Equation (4.9) gives the fraction of elastically active material (in square brackets) at any strain relative to ε_a, which gives the recoverable strain, ε_r, as the material relaxes back from any applied total strain, ε. Ignoring nonlinear viscoelastic relaxation rate effects in this initial treatment, the cyclical loading of cocoon wall can be calculated for *A. pernyi* (shown in Figure 4.5b), where applied strain is increased in 10% increments and then relaxed back to zero stress through σ_r. The recoverable stress-strain is taken here to be linear with a modulus Y_r given by σ_r/ε_r at any point below an applied total strain. Once that strain has been exceeded and more cumulative damage develops, the recoverable strain again follows the overall envelope. The observed cyclical response is shown in Figure 4.5b for comparison, and includes more complex viscoelastic relaxation effects. However the trends are well reproduced by the model.

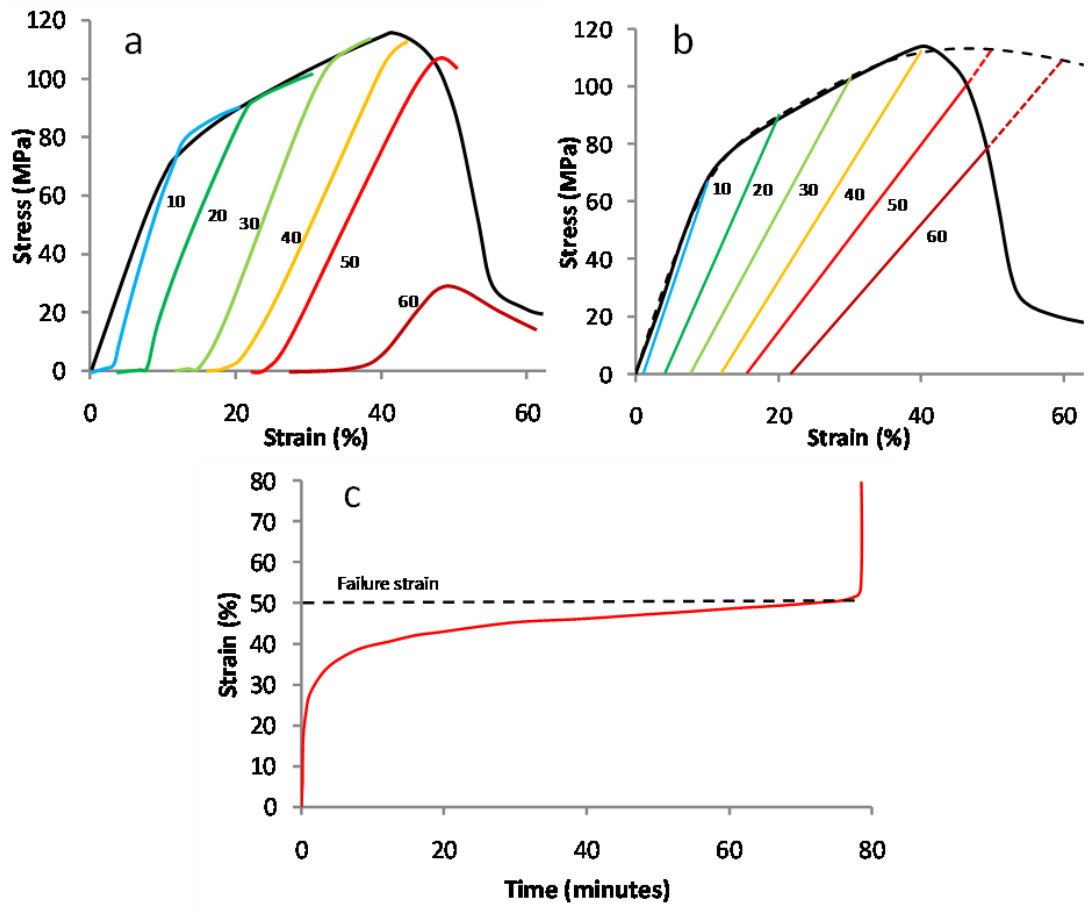

Figure 4.5 Demonstration that strain is the key activation parameter for damage effects on mechanical properties using recoverable elastic and plastic strain effects in *A. pernyi* cocoons. a. Measured recoverable strain after deformation to a given total strain, as labeled. b. Predicted recoverable elastic strain to the same series of total strains as in a. c. Evolution of strain with time in a creep experiment after an initial elastic strain of 18%, showing the cocoon fails at a relatively constant value of strain.

Importantly, failure is seen to be rapid after a critical strain, above which there appears to be no continuous bonding path to sustain load. This condition was found to correspond to the stress-strain point where $Y_r \approx Y/2$ as a bond percolation condition [28] or (for *O. eucalypti*, for example) the failure stress of the weaker sericin binder component at about 130 MPa,

whichever is the lower. This condition is marked in Figure 4.2 as ε_p or σ_p for the three cocoons and agrees well with observation. A general plot of the predicted failure conditions of percolation strain and failure stress are shown in Figure 4.6 as dashed lines superimposed upon the predicted stress-strain profiles of cocoon with different values of Y_3 as marked.

That strain appears to be the dominant activation parameter for bond breaking, and hence for mechanical properties is shown by examination of stress relaxation and time dependence of creep strain under constant load. Figure 4.5 c shows strain as a function of time under a constant stress of about 80 MPa for *A. pernyi*, where strain increases with an exponential relaxation form from the short time elastic value of 18% with a relaxation time of 150 s, and the sample breaks at the same value as in the standard stress-strain curve in Figure 4.2, indicating that damage is directly linked to strain.

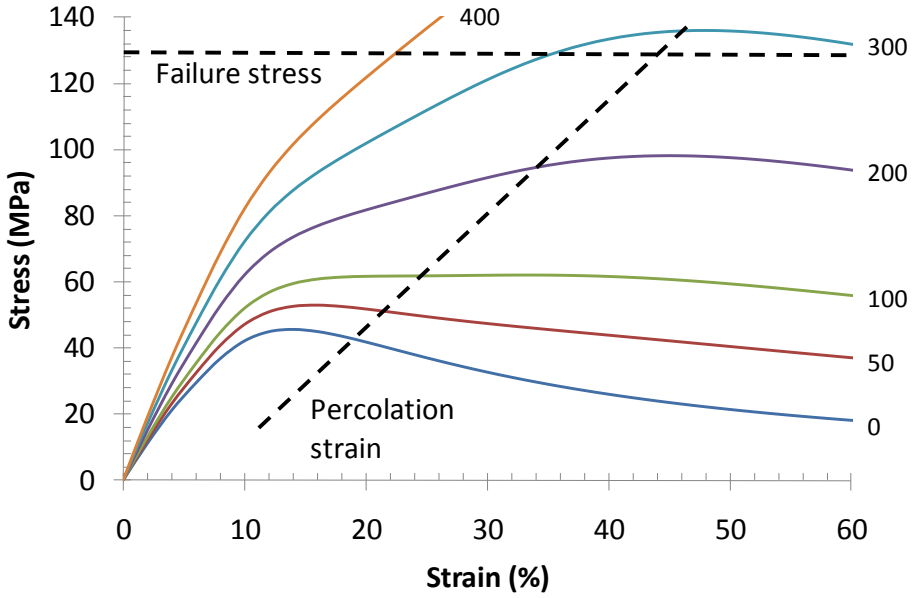

Figure 4.6 Predicted stress-strain profiles of cocoons with different values of the parameter Y_3 (marked), with predicted failure criteria of stress and percolation strain shown as dashed lines.

4.5 Application to other cocoons

Here the connectivity model is applied to analyze the general cocoon properties measured in Chapter 3. As the fibres have very similar modulus values and density from the experimental results in Chapter 3, the 25 species of cocoons tested in that chapter simply follow a Gibson-Ashby type [23] of relation approximately in density squared, which is plotted in Figure 4.7 to illustrate the general overall trend in our dataset.

The data displayed in Figure 4.6 demonstrates the limits of cocoon strength, as the dashed line envelope bounded by the percolation strain for loss of bonding connectivity and the upper stress bound of the individual strength of the sericin binder. While the model is very simple and does not consider detailed features of cocoon morphology, comparison with

experimental observations in Figure 4.8 from Chapter 3 shows it captures the key features of most of the cocoon stress-strain profiles. All the samples have a gradual reduction of the modulus as connectivity is lost and a percolation threshold follows. Two critical strains, 6 % and 16%, are observed in all of the curves, which represent sericin and fibre failure individually according to the model.

The ’tough’ cocoons (Figure 4.8D) would have a third higher activation strain at around 60 % associated with the interfibre bonding connectivity, depending on their individual morphologies. However, this activation strain is not usually observed directly as a yield point because global failure usually precedes it. The ‘brittle’ cocoons (Figure 4.8C) with low porosity and a high bonding area, in contrast, usually fail by crack propagation through the compact combination of fibres and matrix, and their strength often has an upper limit of about 130 MPa, which is the strength of the sericin matrix. I also note that fibres break during the catastrophic failure of the material at their model characteristic failure strain of about 16%. On the other hand, the ‘weak’ cocoons (Figure 4.8B) have a high porosity and the structure fails when about half of the bonding between fibres breaks, and the unbonded fibres are pulled out with hardly any fibre breaks, which is represented as a long tail in the stress-strain curves.

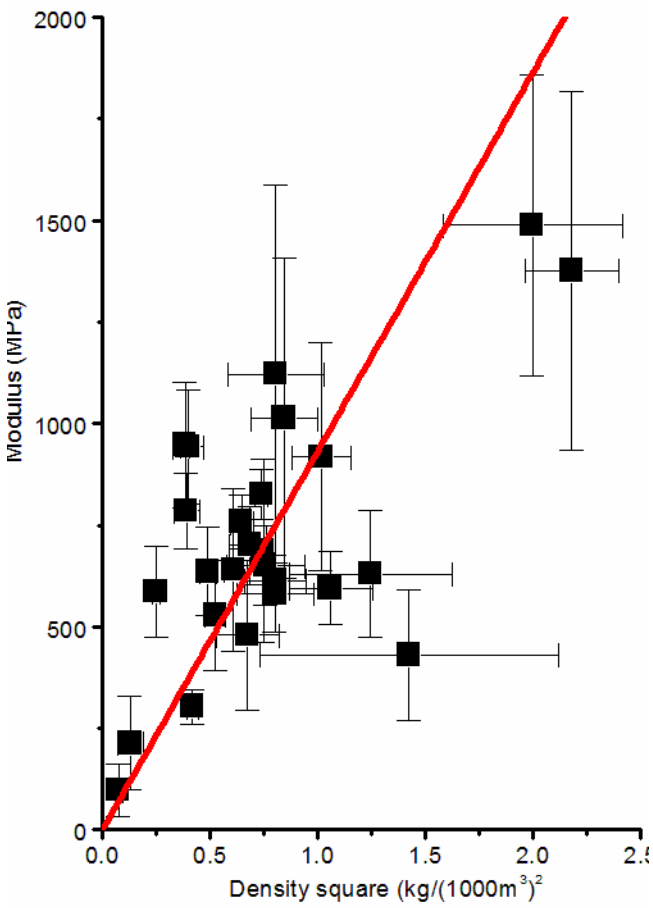

Figure 4.7 Tensile behaviour of silkworm cocoons: Modulus vs. density square. R^2=0.41862.

It shows the tensile properties of cocoons fit the Zhu model [26].

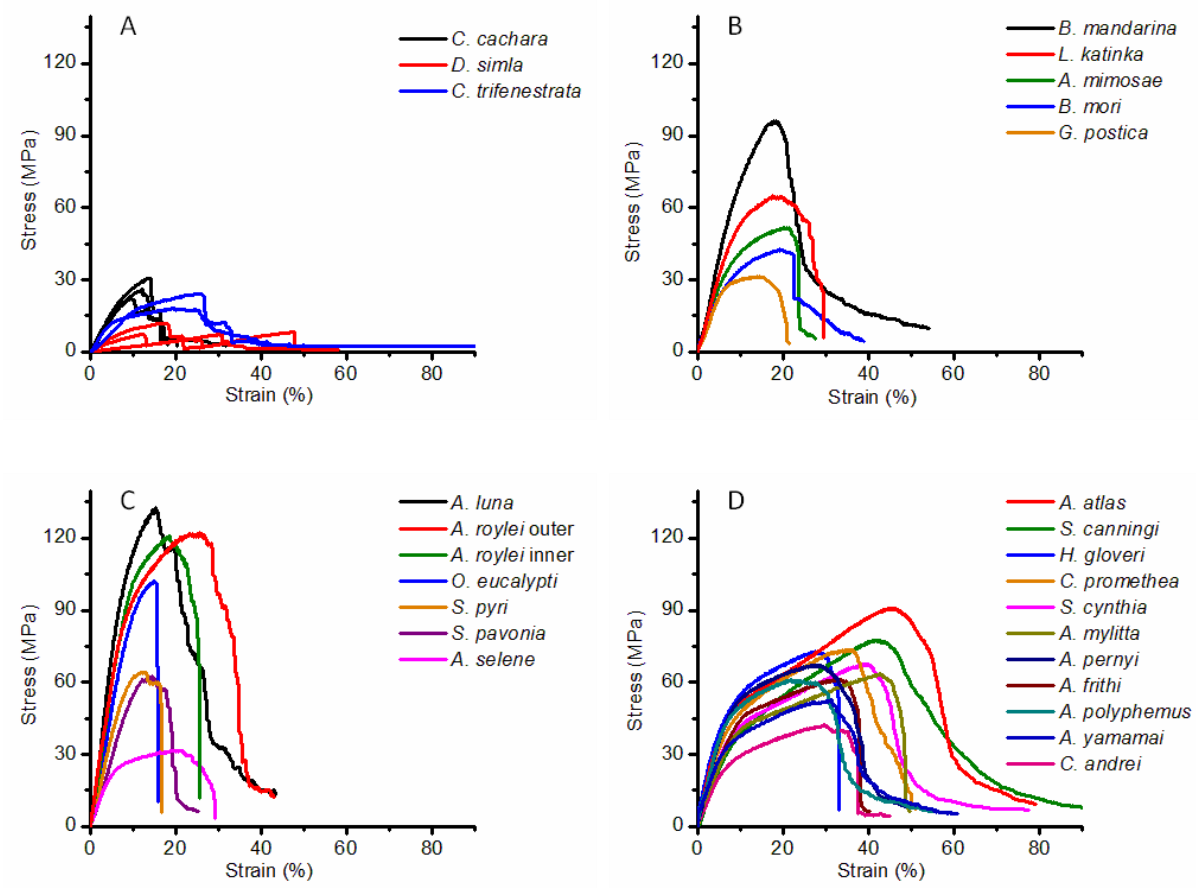

Figure 4.8 Tensile behaviour of silkworm cocoons from Chapter 3 (A) 'Lattice' cocoons. (B) 'Weak' cocoons. (C) 'Brittle' cocoons. (D) 'Tough' cocoons.

4.6 Application to other materials

The bonding connectivity in cocoon walls provides an excellent quantitative description of detailed nonlinear mechanical properties in a natural non-woven composite. However, such a model has limited interest unless it has broader applicability. It is noted that a wide range of very different composite materials have stress-strain profiles that have the same form as those of our cocoons, while noting also that current models for these materials are mathematically complex, quite narrow in scope, and largely empirical. Here, too, the main feature shared is the apparent control of mechanical properties by loss of connectivity of bonding between the component materials. Such loss occurs, either via fibre-fibre bonding for random fibre or via

particle-matrix bonding for particulate composites. Here, the cocoon connectivity model is applied to a range of nonwoven fibre and particulate composites to illustrate how the model can be used with other materials. All the model parameters for other materials are shown in Table 4.1.

4.6.1 Nonwovens

Nonwoven cloth was purchased from a retailer and is simply a standard household cleaning cloth with a nonwoven structure made from regenerated cellulose fibres, as shown in Figure 4.7. The 'modulus' parameter values equivalent to fibre strength are 260 MPa, with activation strains of 0.06 and 0.23 (Table 4.1). These are consistent with properties of Viscose regenerated cellulose fibres with a tensile strength of about 300 MPa and a failure strain of about 8% [31]. The nonwoven structure shows less bending of the fibres relative to cocoons with semicircular bends, suggesting a lower value for the upper activation strain for the uncoiling process, relative to 0.6 for cocoons.

Paper samples were taken from a standard office laser printer with a weight of 80g/m^2 and has low values for activation strains of 0.025 and 0.077, with modulus or component failure stress values of 700 MPa. These strains are due to the non-coiled morphology of the paper fibres, which does not therefore have an upper activation strain for uncoiling. The strength of processed cellulose fibres in the paper could be compared with that for more crystalline Lyocell regenerated cellulose fibres, with a tensile strength of 700 MPa at a failure strain of about 8% [31]. The lower activation strain of 0.025 would then simply be that of the cellulosic binding matrix between the fibres, analogous to the sericin binder matrix in the cocoons.

The Nanomat properties were taken from literature [32, 33], and the specific nanomat scaffold was made from dry electrospun PLGA fibres with fibre diameters in the range 500 to 800 nm with a high porosity (92%) structure of highly coiled fibres, which give an upper activation strain comparable with the cocoons at 0.7. The strength of the PLGA polymer fibres is observed to be about 45 MPa [34], in good agreement with the modulus parameter value (Table 4.1). The high modulus at very low strain is probably due to strong intrafibre hydrogen bonding, but has not been included here.

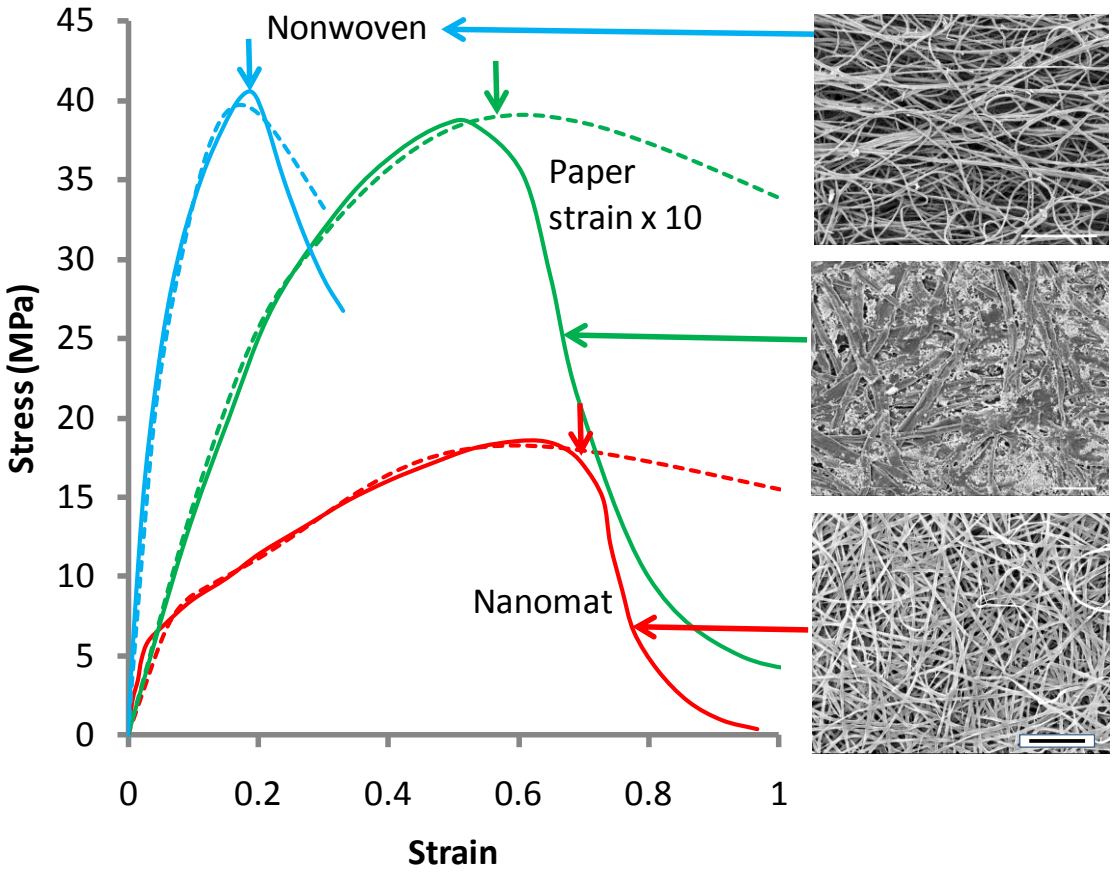

Figure 4.9 (colour online) Comparison of model (dashed lines) and observed (solid lines) stress-strain relations for nonwoven fibre materials as labelled, with percolation condition marked as arrows. Scale bar length: 80 g/m^2 office printer paper 'paper' 100 μm, nonwoven household cleaning cloth 'nonwoven' 500 μm, and a nanomat scaffold 10 μm.

4.6.2 Particulate composites

Figure 4.10 plots stress-strain relations for two important examples of particulate composites as polymer bonded explosive (PBX) [35] and concrete [36, 37] under compression. The particulate composites are notably simple, in that they have only one activation process for particle-matrix debonding. These composites also show the same form of cyclical loading response as outlined for cocoons above.

For the particulate composites studied in this work so far, they appear to follow a very simple form of the connectivity model with a single component effect that follows the model equation form very well. In general, particulate composites should follow the standard additivity rules to calculate the composite elastic modulus from their component properties. The main problem comes in calculating the activation strain, ε_a. For the two examples in Figure 4.10, I do not know the exact composite composition, so simply demonstrating the form of the model with realistic parameter values is all we can do at this stage. We suggest that debonding between the particles and matrix components follows a fracture mechanics form of debonding stress or strain being dependent upon the size of the particles, or more specifically, the distance between the particles, d. Using an energy equivalence of elastic energy density of modulus, M, inside a cube of side length d with the energy to create 6 free surfaces with an energy per unit area of $\Gamma \approx 0.15$ Jm^{-2}, we can write an expression for the local strain to cavitation, ε_c, with a form [38]

$$\varepsilon_c \approx \sqrt{\frac{12\Gamma}{Md}} \tag{4.10}$$

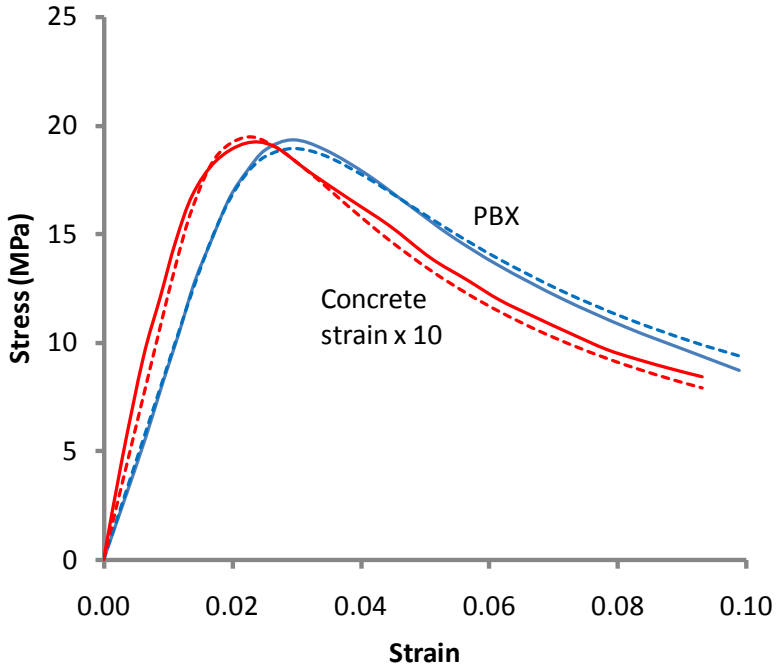

Figure 4.10 Particulate composites of polymer bonded explosives [35] and concrete [36, 37] under compression, which show a single activated process like that in Figure 4.6. Solid lines are reported experimental data, dashed lines are model calculations.

If the volume fraction of rigid particles is ϕ, then the active fraction of matrix in any axis can be approximated as $\phi/3$, such that the tensile strain on the composite to generate the local strain ε_c will be $\varepsilon_c\,\phi/3$, which we then equate to the activation strain for loss of bond connectivity in the model as a compressive strain scaled by $1/\nu$, where ν is Poisson's ratio

$$\varepsilon_a \approx \frac{\phi}{3\nu}\sqrt{\frac{12\Gamma}{M\,d}} \tag{4.11}$$

Polymer bonded explosives, PBX, stress strain curves were taken from literature, in the form of experimental data for a standard mock composition 900-21 used at LANL to simulate PBX 9501 [35]. The parameters can be taken in two ways: either they are simply seen as best fit

parameters for an excellent fitting function with a modulus of 900 MPa and an activation strain of 3.3% under compression, or they can be considered at a more fundamental level as design parameters that need to be quantified in terms of their chemical and morphological composition. By way of illustration for a non-specific PBX, if we consider 100 μm particles of energetic material with a volume fraction of 0.1 in a binder matrix with a tensile modulus of 2 MPa and a Poisson's ratio of 0.5, we can estimate the distance between particles, $d \approx 3.3$ μm, to give an activation strain from equation (4.9) of $\varepsilon_a = 0.035$. The activation strain is in good agreement with the experimental example as a reasonable parameter value with physical relevance.

Concrete is a particulate composite of sand bonded by cement, which is in turn the matrix binder for larger aggregate particles [36]. We again see in Figure 4.4 that the model function gives an excellent fit to concrete properties, which are taken from literature [37]. The modulus value of 12 GPa is slightly low for cement and silica materials (20-30GPa might be expected for silica materials) and the small activation strain of 0.0025 under compression is characteristic of highly brittle silica materials.

Again as a hypothetical example for illustration, consider the concrete example with a modulus of 12 GPa that is a concrete with 25% cement paste with filler modulus of about 30 GPa comprising sand particles with a medium grade particle size of about 0.2 mm and average separation distance therefore of about 17 μm. The inverse fraction additivity rule for modulus suggests a cement matrix modulus of about 4 GPa. The Poisson's ratio of these materials is low at about 0.2. Equation (4.9) then suggests a compressive activation strain for this model concrete of about $\varepsilon_a \approx 0.0022$, which is a realistic estimate for concrete.

4.7 Conclusions

In this chapter a bioinspired model is presented, which uses the highly evolved natural composites of silkworm cocoons provides a physically realistic and quantitative predictive model framework that can be used for analysis, design, or optimization of important new composite materials. The observed mechanism for the loss of stiffness in cocoons is a gradual loss of connectivity through sericin bonding, between load bearing silk fibres. This loss of connectivity can be quantified as a strain activated fission of the interfibre bonds up to a failure criterion where either a percolation threshold of about 50% of these bonds (quantified as modulus reaching half of its initial value) or the failure stress of the sericin binder is reached, whichever is lower. The connectivity model can be applied to other nonwoven fibre and particulate composites using a small number of physically realistic model parameters.

References

[1] Page D. A theory for the tensile strength of paper. Tappi Journal. 1969;52(4):674-681.

[2] Kallmes O BG, Perez M. A mechanistic theory for the load elongation properties of paper. Pap Tech Ind. 1977;18(7,8,9,10):222-228,243-225,283-225,328-331.

[3] Dodson CTJ. The nature of bonds in paper and the behaviour of paper under mechanical strain. Rep Prog Phys. 1970;33(1):1.

[4] Van den Akker JA, Lanthrop AL, Voelker MH, Dearth LR. Importance of fiber strength to sheet strength,. Tappi Journal. 1958;41(8):10.

[5] Carlsson LA. A shear-lag approach to the tensile strength of paper. Composites Science and Technology. 2005;65(2):183.

[6] Cox HL. The elasticity and strength of paper and other fibrous materials. British Journal of Applied Physics. 1952;3:72.

[7] Page DH, Seth RS, De Grace JH. The elastic modulus of paper, I. The controlling mechanisms. Tappi Journal. 1979;62(9):3.

[8] Page DH, Seth RS. The elastic modulus of paper, II. The importance of fiber modulus, bonding and fiber length. Tappi Journal. 1980;63(6):4.

[9] Seth RS, Page DH. The stress strain curve of paper. In: J B, editor. VIIth Fund Res Symp. Cambridge; 2003. p. 32.

[10] I'Anson SJ, Sampson, W.W. Competing Weibull and stress-transfer influences on the specific tensile strength of a bonded fibrous network. Composites Science and Technology. 2007;67(7-8):1650.

[11] Åström J. Microscopic mechanics of fiber networks. Journal of Applied Physics. 1994;75:2383.

[12] Åström JA. Elasticity of Poissonian fiber networks. Physical review C, Nuclear physics. 2000;61(5):5550.

[13] Carlsson LA, Lindstrom T. A shear-lag approach to the tensile strength of paper. Composites Science and Technology. 2005;65(2):183-189.

[14] Raisanen VI, Alava, M.J., Niskanen, K.J., Nieminen, R.M. . Does the shear-lag model apply to random fiber networks? Journal of Materials Research. 1997;12(10):2725.

[15] Räisänen VI. Effect of texture on fracture of fibrous materials. Computer methods in applied mechanics and engineering. 1998;161(1-2):103.

[16] Eichhorn SJ. Deformation micromechanics of natural cellulose fibre networks and composites. Composites Science and Technology. 2003;63(9):1225.

[17] Weibull W. A statistical theory of the strength of materials. Stockholm: Ingeniorsvetenskapsakademiens Handlingar 1939.

[18] Gregersen, A H, T. H. Evaluation of newsprint strength and runnability by using Weibull statistics. *Progress in Paper Physics Seminar*. Vancouver, Canada; 1998.

[19] Uesaka T, M F, D H, N D, C. M. Factors controlling pressroom runnability of paper. *The Science of Papermaking, Trans XIIth Fund Res Symp, .* Oxford; 2001.

[20] Wathen R, Niskanen K. Paper web strength distributions and formation. *Progess in Paper Physics Seminar*. Syracuse, USA; 2002.

[21] Gibson LJ, Ashby MF. Cellular solids: structure and properties. Cambridge University Press, 1999.

[22] Ko WL. Deformations of Foamed Elastomers. Journal of Cellular Plastics. 1965;1(1):45-50.

[23] Christensen RM. Mechanics of low density materials. J Mech Phys Solids. 1986;34(6):563-578.

[24] Warren WE. Linear elastic behavior of a low-density Kelvin foam with open cells. Journal of applied mechanics. 1997;64(4):787-794.

[25] Zhu HX, Mills, N.J., Knott, J. F. Analysis of the high strain compression of open-cell foams. J Mech Phys Solids. 1997;45(11-12):1875.

[26] Zhu HX. Analysis of the elastic properties of open-cell foams with tetrakaidecahedral cells. J Mech Phys Solids. 1997;45(3):319.

[27] Warren WE, Kraynik AM. The Linear Elastic Properties of Open-Cell Foams. Journal of applied mechanics. 1988;55(2):341-346.

[28] Porter D. Predictive nonlinear constitutive relations in polymers through loss history. International journal of solids and structures. 2009;46(9):1981.

[29] Seitz JT. The Estimation of Mechanical-Properties of Polymers from Molecular-Structure. Journal of Applied Polymer Science. 1993;49(8):1331-1351.

[30] Porter D. Group Interaction Modelling of Polymer Properties. New York: Marcel Dekker, 1995.

[31] Gindl W. Strain hardening in regenerated cellulose fibres. Composites Science and Technology. 2006;66(13):2049.

[32] Li WJ, Laurencin, C.T., Caterson, E.J., Tuan, R.S., Ko, F.K. . Electrospun nanofibrous structure: a novel scaffold for tissue engineering. Journal of biomedical materials research Part A. 2002;60(4):613.

[33] Huang ZM. A review on polymer nanofibers by electrospinning and their applications in nanocomposites. Composites Science and Technology. 2003;63(15):2223.

[34] Wang L, Zhang Z, Chen H, Zhang S, Xiong C. Preparation and characterization of biodegradable thermoplastic Elastomers (PLCA/PLGA blends). Journal of Polymer Research. 2009.

[35] P. Rangaswamy RMH. A computational viscoelasticity/damage/plasticity model for high-explosive materials WIT Transactions on Modelling and Simulation. 2007;45:12.

[36] Della RM. New Strong Cement Materials: Chemically Bonded Ceramics. Science. 1987;235(4789):651-658.

[37] Caner FC. Microplane model M 4 for concrete. II: Algorithm and calibration. Journal of engineering mechanics. 2000;126(9):954.

[38] Porter D. Multiscale Modelling of Structural Materials, Chapter 9 In: Guo X, editor. Multiscale Materials Modelling: Woodhead Publishing 2007.

Chapter 5

Structure-property Relationships of *Bombyx mori* Cocoon

5.1 Introduction

The previous chapters have focussed on a wide range of wild species to study the biodiversity of cocoon properties for their very diverse hierarchical structures and optimized properties. In Chapter 4, a connectivity model was developed to understand the structure-property relationships of silk cocoons as nonwoven fibre composites. This has provided us with a unique tool for investigating the design of silk cocoons.

Bombyx mori cocoon is a special case in the range of cocoons studied in this thesis. As a composite cultivated for its commercial function of providing silk fibres for industry, the *B. mori* cocoon has been selected to have strong fibres, ease of unravelling, and attractive optical properties. Figure 5.1 shows the hierarchy of the morphology of a *B. mori* cocoon, both in the plane of the cocoon wall and through its thickness. *B. mori* cocoon is a natural polymer composite shell made of a single continuous silk strand with a length in the range of 1000-1500m and conglutinated by sericin. Each fibre is composed of two fibroins coated by a layer of sericin. The cocoon has a 3D nonwoven structure with multiple layers. Sericin acts as an adhesive to maintain the random fibre and the multi-layer structure in the whole cocoon.

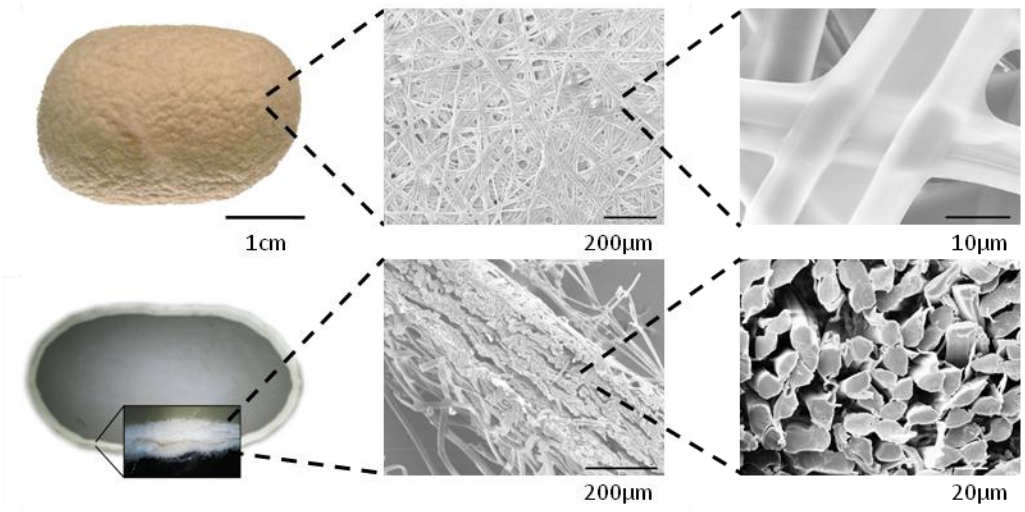

Figure 5.1. Hierarchy of the morphology of a *B. mori* cocoon. Above: cocoon surface morphology with nonwoven structure. Below: cocoon multi-layer morphology.

Compared to the cocoons of 'wild' (as opposed to domesticated) silkworm species, the *B. mori* cocoon has a relatively large thickness, low strength but high toughness and a distinct graded layer structure (See Chapter 2). While wild cocoons use crystals or leaves for strengthening the structures, the *B. mori* cocoon has a delicate random fibre arrangement, which acts as a simple 3D nonwoven composite structure [1]. While the fibres and sericin of *B. mori* cocoons have been studied extensively [2, 3], the cocoons themselves have been researched in far less detail, and consequently the relationships between their structure and morphology are poorly understood.

This chapter presents our investigation of *B. mori* cocoons in terms of their multiple layer structure and its relationship with mechanical properties. A solid understanding of such a highly selected cocoon can provide important lessons for the design of new composite materials with an interesting balance of porosity, strength and toughness.

5.2 Experiments: Materials and Methods

5.2.1 Materials collection

All cocoon samples were collected using the standardised protocols as outlined in Chapter 2.

5.2.2 Scanning electron microscope (SEM) observation

Cocoons were hole-punched to make samples with a diameter of 3.5mm and glued on superconducting tape. The samples were sputter coated in Quorum Technologies SC 7620 and then transferred into the Jeol Neoscope JCM-5000 Scanning Electron Microscope for observation at 15 kV. After mechanical testing the samples were collected for SEM observations with the same procedure.

5.2.3 Fourier transform infrared spectroscopy (FTIR)

A Golden Gate single reflection diamond ATR accessory (Specac Ltd., London, UK) embedded in a Nicolet 6700 FTIR spectrometer with a MCT-A nitrogen cooled detector (Thermo Scientific, Madison, WI) was used for the infrared spectrum acquisition. Spectra were acquired at a 4 cm^{-1} resolution from 500 to 6000 cm^{-1}. Static spectra were obtained from the average of 64 scans at a 5 cm/s mirror speed. Both sides of each cocoon disc were measured. The sericin powder spectrum was acquired from washed-out sericin from the cocoon. The converted fibroin spectrum was obtained for *B. mori* silk gland posterior part that was sheared, converted and dried. All spectral operations were executed using OMNIC and a VBA purpose written code using OMtalk. An offset was first applied from the average of the 1900-1850 cm^{-1} region then normalised to the area integrated from 1800-800 cm^{-1} to compensate for the signal variation due to surface contact.

A Principal Component Analysis (PCA) was performed afterwards using the Pearson method (XLstat, Addinsoft, France) by Mr Maxime Boulet-Audet. An infrared spectrum contains thousands of data points depending of the resolution. However, they are not all inter-dependent and large data sets are not always easy to visualise. For this reason a PCA was executed to reduce the number of significant variables. This method was developed more than 100 years ago [4] and is the most used multivariate method. It is commonly performed on infrared spectra datasets [5-7]. PCA is an orthogonal linear transformation projecting the observations from an initial dimensional space with *n* variables to a final dimensional space with fewer variables; preserving the maximum amount of variance in the first dimensions. If the 2 or 3 first components represent most of the variability, a 2 or 3D plot can be used to illustrate the variations between samples. As a result, the dataset can be simplified to fewer variables using most of the information available in the spectra. PCA can be used to reduce number of variables in preparation for another multivariate analysis like Linear Discriminate Analysis. PCA is used to analyse the fibre/sericin content of cocoon layers from FTIR spectrum in this Chapter.

5.2.4 Tensile tests of cocoons and layers

Strips of cocoons were cut for samples with a width of 5 mm and length of 15 mm. Tensile tests were carried out using an Instron 5542 with a speed of 2 mm/min and 5 mm gauge length. For the examination of cocoon layers, the layers were very carefully separated using a sharp blade to maintain the fibre structure without damaging it. Although it was possible that layer separation could introduce damage and reduce the properties of the undivided layer, the damage caused by layer separation should not be too great to influence our conclusion from the paper as the layers were mainly bonded only by the sericin glue. For evaluating the

effect of different split layer numbers, samples were collected from the same cocoon and split into different numbers of layers. The mechanical testing of the layers was the same as that of the cocoon, and the modulus and strength of each layer were calculated from its individual cross-section area.

5.2.5 Peel tests

Peel tests was carried out to measure the interlayer bonding force in the cocoons and evaluate its contribution to the mechanical properties of the cocoon multilayer system. Cocoons were cut into strips with a 20 mm length and a 5 mm width. The sample was then peeled at the same point through the cocoon thickness to create an interlayer crack 5 mm long with the same method used in section 5.2.4. The separated parts of the samples were clamped and peeled at an angle of 90° in an Instron 5542 with a tensile speed of 2.5 mm/min. The tested samples were themselves peeled again to investigate interlayer bonding through the whole thickness of a cocoon.

5.3 Results and analysis

5.3.1 Morphology

Although *B. mori* cocoon has a 3D nonwoven structure that is made from a single continuous strand, it has also a multi-layer structure with fewer fibres connecting layers than aligned in the individual layers. The inter-layer bonding is much weaker than the intra-layer bonding, which makes it easy to separate individual cocoon layers.

Figure 5.2 shows the graded morphologies of cocoon components in different layers throughout the thickness of a cocoon wall. From the inner to the outer surface, the porosity

and amount of sericin increases while the amount of bonding between fibres decreases. Although sericin is a bonding agent between the fibres and thus maintains the cocoon's structure, it was found that in the outer layer the sericin coating does not interconnect the fibres, so it does not form additional bonding between fibres. In the inner layers, the sericin covers the surface of fibroins efficiently to form a highly bonded network.

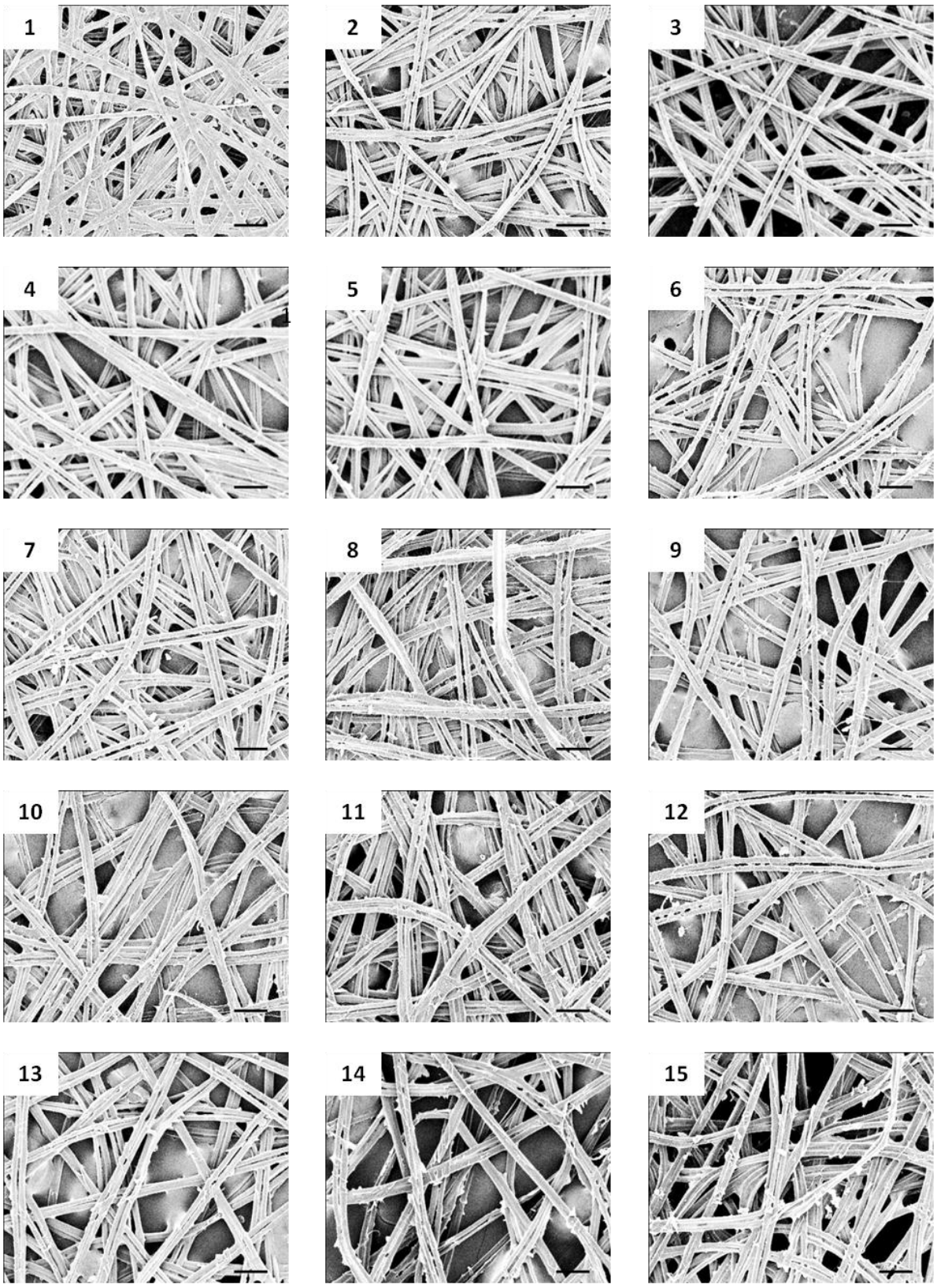

Figure 5.2. Morphologies of cocoon layers from inner (1) to outer (15) of the cocoon surface.

Scale bar: 100 μm.

5.3.2 Component Analysis

FTIR spectroscopy was used to analyse the amount of sericin on the cocoons. Attenuated Total Reflectance allowed the selective probing of the inner and outer surfaces of the cocoon. To assign the sericin and fibroin bands, spectra of pure sericin powder and converted fibroin were acquired.

The fibroin and sericin spectra have very distinctive infrared signatures (Figure 5.3). The main differences are due to the presence of β-sheets peaks present in the converted fibroin at 1700, 1617, 997, and 975 cm^{-1} [8-13]. In contrast to sericin, fibroin also shows the asymmetric bending mode 441 cm^{-1} and the symmetric bending mode of CH_3 at 1334 cm^{-1} [8, 14]. The 1160 cm^{-1} band assigned to the N-C_α (the first carbon on the backbone) stretching is absent in the fibroin mode[8]. On the other hand, sericin has distinctive bands at 1394 cm^{-1} and 1041 cm^{-1} due to C-H and C-C bending vibrations vibration respectively[15]. Since not all the frequencies vary independently, a principal component analysis has been performed on the dataset (n = 30) to extract the principal components explaining the main differences between the samples and remove the co-linearity [16]. All the spectra were offset with the average of the 1800-1750cm-1 spectrum region. No bands are present. The first principle component (PC1) is the most important factor expressing most of the variability from the principle component analysis. As shown in Figure 5.3, PC1 has negative peaks at frequencies representative of sericine and positive bands at the wavenumber of fibroin modes. The relative amount of both proteins can be linked to the score of the first principal component representing 50 % of the spectra variance.

In Figure 5.4, the first principal component (PC1) score from inner and outer surface of cocoons are completely resolved. The uni-dimensional test of equality of the means of the classes proves that the two side of the cocoon have significantly different infrared spectra and chemical composition ($p < 0.0001$). Since the peaks of the first principal component peaks match those observed for the pure proteins, it is concluded that the inner surface has significantly less sericin than the outermost surface.

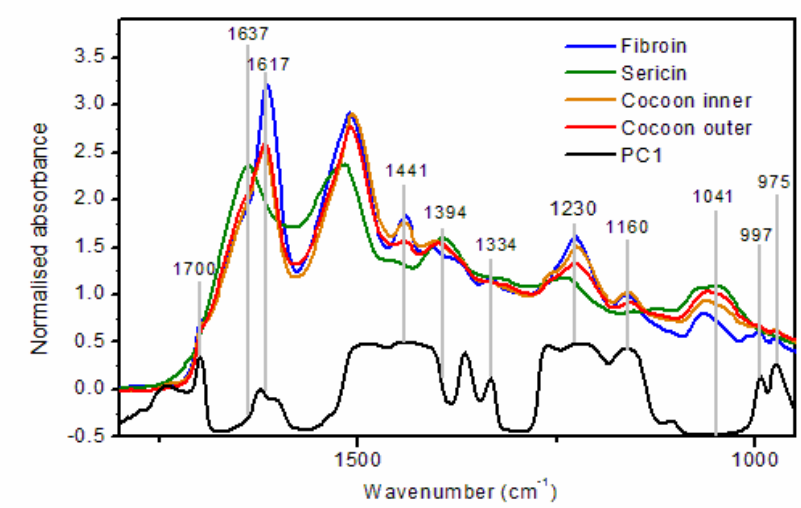

Figure 5.3 FTIR spectra of *B. mori* cocoon inner and outer part, sericin powder, fibroin, and first principal component of the inner and outermost of the *B.mori* cocoon FTIR spectra.

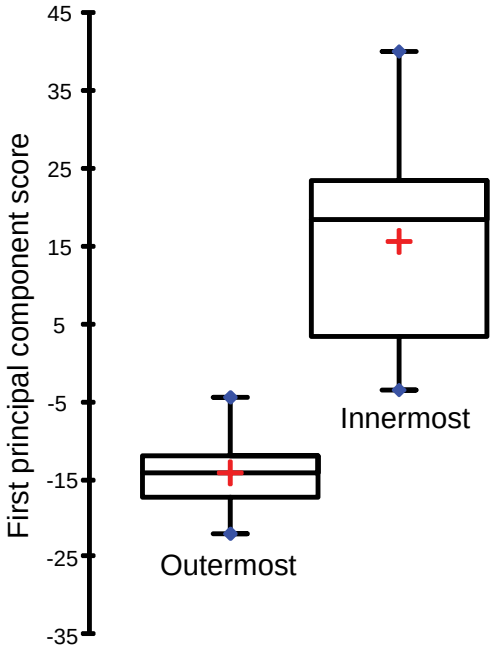

Figure 5.4 First principal component score for the innermost and outermost part.

5.3.3 Mechanical properties

The in-plane mechanical behaviour of silk cocoons is generally similar in the different directions of cocoon surfaces (Figure 5.5 Left). The stress rises initially linearly with the increase of strain until about 6% strain and then reduces as the strain increases before a dramatic drop of the stress followed by a long tail in the stress-strain curve. Cocoon samples cut from the 90° direction (transverse direction) have slightly lower modulus, which could be due to the natural curvature of the samples. The mechanical properties of *B. mori* cocoons are shown in Table 5.1.

A model was developed in Chapter 4 to describe mechanical behaviour of a wide range of cocoons with their non-woven morphology; the study in this chapter included only cocoons of *B. mori*. Most such cocoons conform to the open cell foam model developed by Zhu et al.[17], whereby the elastic modulus of the cocoon is controlled by fibre density and the

elastic modulus of the fibres through a process of bending of the fibres between bonding junctions. The bonding connectivity between the fibres reduces with increasing strain to reduce modulus. The cocoon structure then fails at a percolation threshold when about half of the bonding breaks, and the unbounded fibres are then pulled out, which is represented as a long tail in the stress-strain curves.

At small strains in tensile tests, the sericin bonds between the fibres generally crack first because sericin has a lower breaking strength than the fibres. In the outer layers, which have lower bonding density, the fibres de-bond and gradually disentangle as strain increases. In the inner layers, where there is strong bonding between the fibres, the failure of sericin propagates into the fibres, resulting in fracture of the layers and breakage of the fibres (Figure 5.5 Right).

Table 5.1 Mechanical properties of *B. mori* cocoon

Thickness (mm)	Nominal Density (kg/m^3)	Max load (N)	Strength (MPa)	Breaking strain (%)	Modulus (MPa)	Strain at max stress (%)	Fibre cross-section area (μm^2)
0.40	499±16	115±36	54±11	35±8	586±111	18±2	278±55

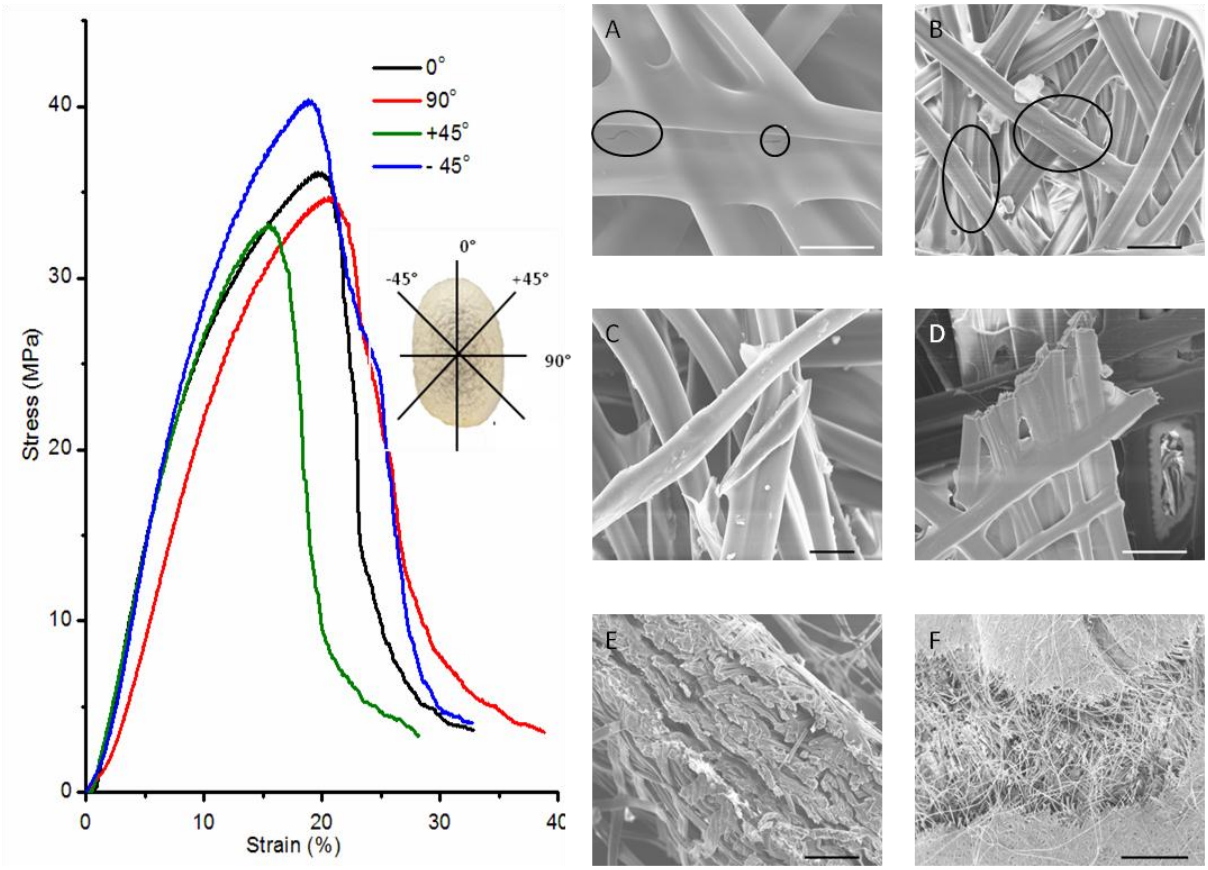

Figure 5.5 Tensile tests of cocoons (*B. mori*). Left: stress vs. strain curves of cocoon samples cut from different directions (0° is the longitudinal direction of the cocoon). Right: breaking mechanisms of cocoons (A) Sericin cracks at small strains, scale bar: 10 µm. (B) Inter-fibre bonding breaks, scale bar: 50 µm. (C) Fibres de-bond, scale bar: 20 µm. (D) Fibres break at innermost layer, scale bar: 20 µm. (E) Cocoon delamination, scale bar: 100 µm. (F) Fibres break at innermost layer and disentangle in the outer layers, scale bar: 1mm.

5.3.4 Mechanical properties of cocoon layers

The general shape of stress-strain curves of samples taken from individual layers is similar to that of samples taken from a whole cocoon wall (Figure 5.5), as shown in Figure 5.6 for different degrees of layer separation. Because the porosity ranges from being highest at the

outer surface and decreases into the interior, a general modulus and strength decrease from the inside to outside layers would be expected. However, Figure 5.6 shows that a simple comparison of the stress-strain curves of the different layers gives no clear trends with bonding density in the plane of the cocoon walls, as shown in Figure 5.2. Qualitative differences in the curve shape to different failure mechanisms can be loosely attributed to various effects, such as longer tails at high strain due to more fibre pull-out with lower bond density towards the inside, and sharper falls in stress at failure due to cracks developing with high bond density.

The example for a cocoon that has been separated into 9 layers is given in Table 5.2, where no clear trends in mechanical properties are seen through the thickness. However, if modulus and strength are normalised by dividing by the thickness of each layer to be corrected to be specific modulus and strength parameters, there is a clear trend of decreasing properties from inside to outside, as shown in Figure 5.7 for the example in Table 5.2. This implies that the removal of interlayer bonding reduces the modulus and strength of the composite structure, bearing in mind that modulus and strength are themselves already normalised per unit area.

Table 5.2 Mechanical properties of cocoon layers in an example of 9 layers split from a cocoon

Layer number (from inner to outer)	Max Stress (MPa)	Strain at Max Stress (%)	Modulus (MPa)	Thickness (mm)	Normalized Modulus (MPa/mm)	Normalized Strength (MPa/mm)
1	18.8	7.9	480.4	0.02	24.0	938.5
2	59.7	15.4	914.9	0.08	11.4	746.3
3	28.6	9.9	439.1	0.06	7.3	475.7
4	14.6	10.9	289.4	0.04	7.2	364.6
5	28.4	15.0	439.5	0.09	4.9	315.3
6	14.8	10.8	261.8	0.08	3.3	185.4
7	19.1	11.8	351.0	0.07	5.0	272.6
8	24.5	14.2	393.4	0.11	3.6	222.7
9	22.3	21.3	220.9	0.14	1.6	159.4

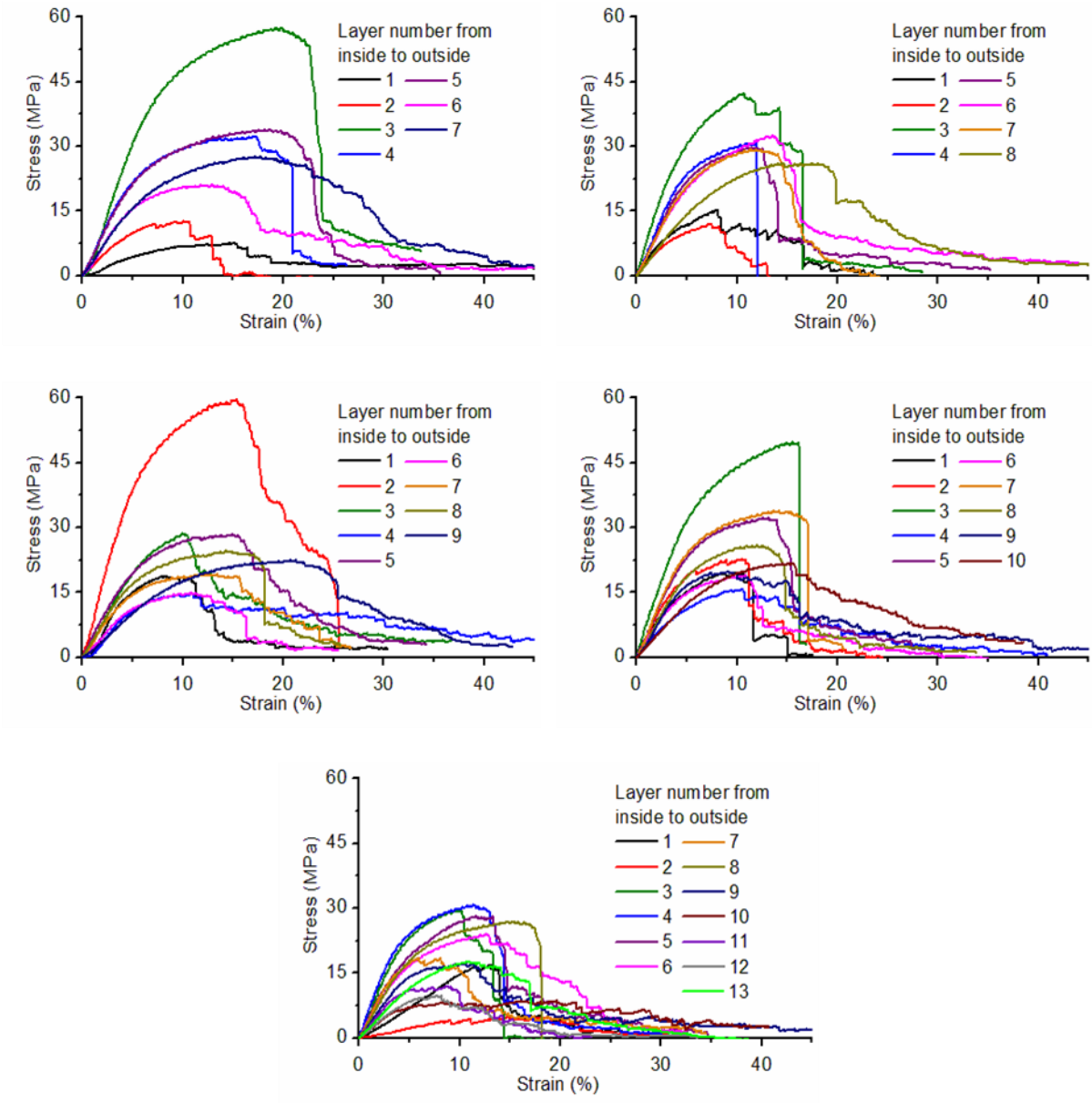

Figure 5.6 Stress-strain curves of cocoon layers with different split numbers: Stress vs. strain curves of individual layers from inner to outer side of cocoon. No clear trend can be seen between the cocoon layer properties and layer positions.

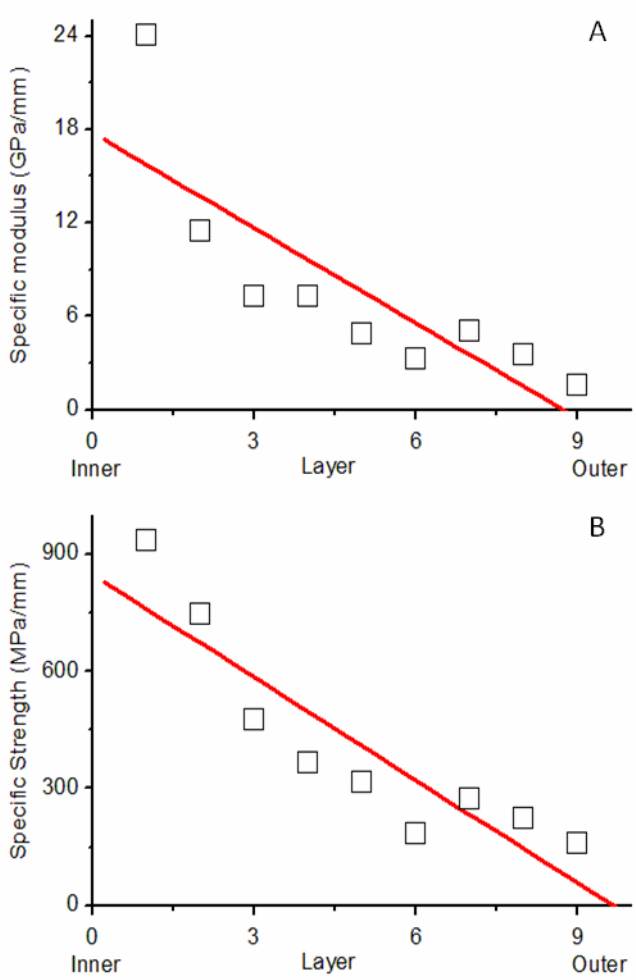

Figure 5.7 Mechanical properties of cocoon layers in an example of 9 layers split from a cocoon. (A) Normalized modulus (modulus/thickness) vs. layers from inner to outer side of cocoon. (B) Normalized strength (strength/thickness) vs. layers from inner to outer side of cocoon.

5.3.5 Peel tests

The peel test results in Figure 5.8 show that the interlayer connectivity at different positions in the cocoon thickness share a generally similar nonlinear load-displacement relation, with an average peel force of 0.32 N and the peel energy is 61 J/m^2. The large fluctuations in load

with displacement are simply due to the uneven spatial distribution of sericin bonds, but a detailed statistical analysis of the results is beyond the scope of this work.

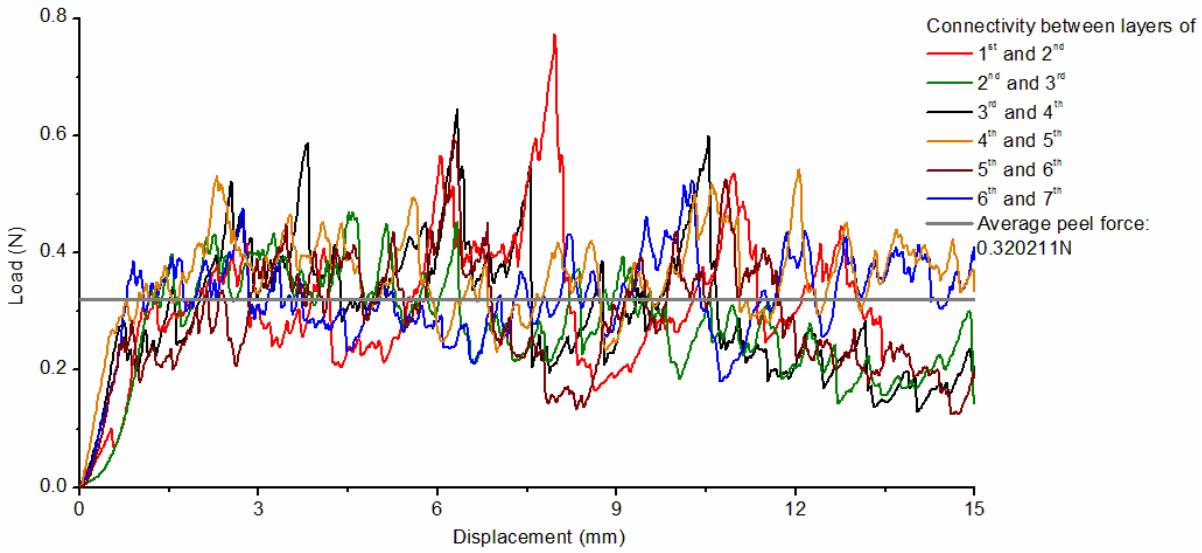

Figure 5.8. Load vs. displacement curve of *B. mori* peel tests. In this test, a cocoon sample was separated into 7 layers, as the layer could become too thin to be employed on the machine if more layers were separated. The 1st layer is on the inner surface of the cocoon and the 7th is on the outer surface.

5.4 Discussion

5.4.1 Interlayer bonding energy

Peel tests suggested an interlayer bonding energy of 61 Jm^{-2}, which it is taken here as a first hypothesis as being due to breaking of sericin bonds. It is interesting here to test this hypothesis by trying to predict this bonding energy from the properties of sericin.

When creating a fracture surface, the energy absorbed is the binding energy density around the crack to a depth, d, that is involved in the elastic energy density storage under a stress, σ,

required to create a free surface. An equation was derived for this previously for solid polymers by Prof David Porter [18], which relates the failure strength, σ, to the size of a cavitation site, d, by the following equation in terms of tensile modulus, E, free surface energy, $\Gamma = 0.15$ J/m^2 for most polymer types

$$\sigma = \sqrt{\frac{12\,\Gamma\,E}{d}} \tag{5.12}$$

Since the sericin strength $\sigma \approx 130$ MPa and modulus $E \approx 3$ GPa [18], the dimension d can be estimated to be $d \approx 0.3$ μm. Using polymer group contributions gives a binding energy density, E_{coh}/V (cohesive energy divided by volume), for sericin of about 0.5 GJ/m^3 [19]. So the energy per unit area of solid sericin failure, H_{solid}, is predicted to be

$$H_{solid} = \frac{E_{coh}}{V}\,d = 160\ Jm^{-2} \tag{5.13}$$

It was calculated that the nominal density for *B. mori* cocoon is 499 kg/m^3[20], such that if it is assumed that the void area in each porous plane of fibres is the same as the volumetric void fraction of 499/1300 = 0.38, then the actual energy per porous area for delamination will be about 160 x 0.38 = 61 J/m^2. This fits well with the experimental results and supports the hypothesis that the delamination is mainly through brittle fracture of the interlayer sericin bonds.

5.4.2 Layer contribution

In order to evaluate the contribution of interlayer bonding to the properties, a cocoon has been split into different numbers of layers for tensile testing, and the stress-strain curves of

the individual layers were summed to compare with the mechanical behaviour of the whole cocoon. The more layers split in the cocoon, the more the interlayer connectivity is lost. From the experimentally calculated sum of the individual stress-strain curves, the cocoon strength, strain at max stress and breaking energy are all reduced when more layers were split, although the modulus (gradient of the stress-strain curve at low strains) is less affected (Figure 5.9A).

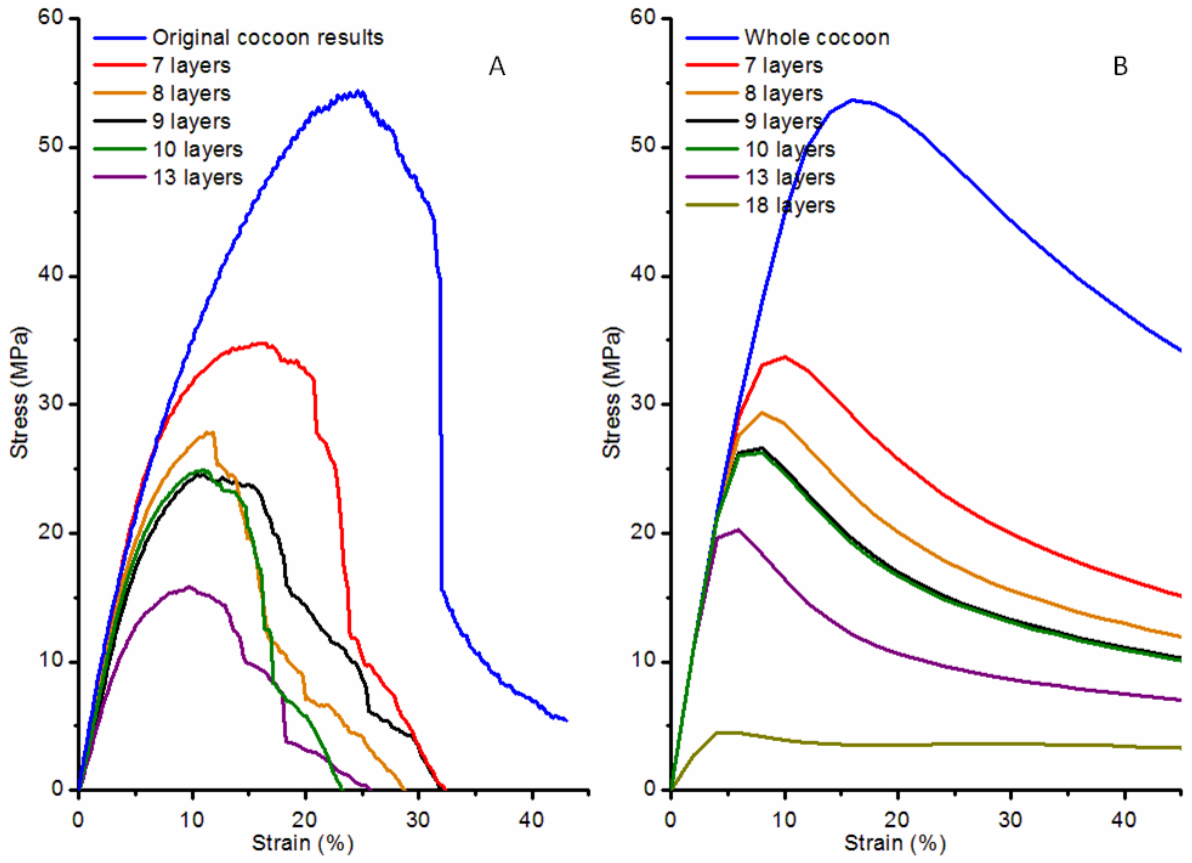

Figure 5.9. Mechanical properties of a cocoon with reduced interlayer connectivity. Cocoons were split into different numbers of individual layers, and their stress-strain curves were summed for comparison with the whole cocoon. A. experimental results. B: model prediction from Eq. 5.3.

A quantitative model was developed to describe the damage mechanism for nonwoven cocoons including *B. mori*, which is detailed in Chapter 4. It proposed a general tensile mechanism for nonwoven composite cocoons in which the bonding connectivity reduces gradually with increasing strain. Three activated bond-breaking processes were identified that are associated with sericin and fibre breaks and uncoiling of the fibre turns. An activation strain associated with each failure process and the total fraction of broken bonds is quantified using an Arrhenius activation function in mechanical energy of deformation in strain, ε, relative to an the activation strain, ε_a, squared, since elastic energy density is proportional to elastic strain squared. Assuming the number of different activation effects, i = 3, with fractional contribution f_i the relation for stress, σ, with initial composite modulus, Y, is given by

$$\sigma = Y\,\varepsilon\left[1-\sum_i f_i \exp\left(-\left(\frac{\varepsilon_{ai}}{\varepsilon}\right)^2\right)\right] \quad \text{where} \quad f_i = \frac{Y_i}{Y} \tag{5.14}$$

It is noticed from the experimental observations that there is a linear relationship between the number of split layers and the loss of strength (Figure 5.10A), which suggests that each layer contributes a similar amount. Assuming a single layer of cocoon consists only of one single fibre thickness of about 22 μm and a cocoon has an average wall thickness of 0.4 mm, the cocoon would have roughly 18 layers in total. The possibility is explored that the activation strain reduces linearly with the loss of each interlayer bond. For the experimental curves in Figure 9A, the activation strain for fibre breaks was determined to be 0.18 (same method as stated in Chapter 4), which suggests that this activation strain should reduce by 0.01 per layer split. Figure 5.10B shows the model predictions using this simple hypothesis, which agree very well with the experimental observations. The final model curve with all 18 layers

separate leaves only the intra-layer sericin bonding terms active for strength, and that each interface bonding layer contributes a similar level of additional strength to the cocoon as this individual layer.

5.5 Conclusions

The layer structure of *B. mori* cocoon was investigated for the graded layer properties in terms of : morphological structure, component contents and mechanical properties. It emerged that that the inner layers of cocoons have less sericin but more interfibre bonding compared to the outer layers. Because of this morhpology and component contents, the strength and modulus reduces from inner to outer layers. The mechanism of the individual layer and the interlayer bonding which are responsible for the mechanical behaviour is identified and quantitatively modelled.

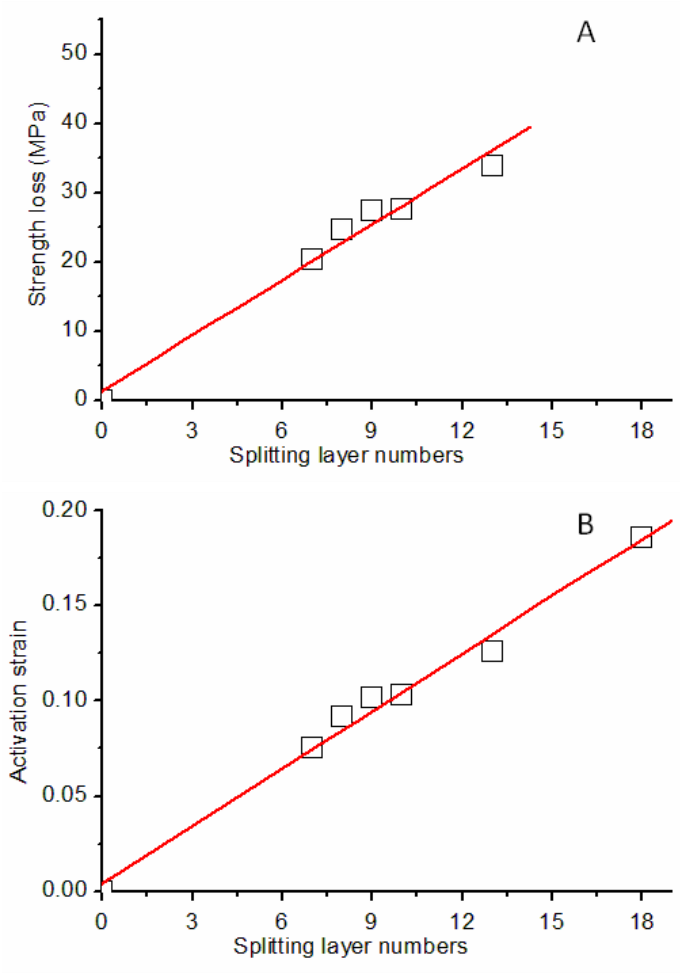

Figure 5.10. Interlayer connectivity (activation strain) vs. Number of split layer (the degree of loss of interlayer connectivity) in the cocoon (A) Experimental loss of strength vs. number of split layers (B) Modelling of activation strain of cocoon losing partial interlayer connectivity vs. Splitting layer numbers

References

[1] Chen F, Porter D, Vollrath F. Morphology and structure of silkworm cocoons. Materials Science & Engineering C-Biomimetic and Supramolecular Systems. 2012;32(4):772-778.

[2] Vollrath F, Porter D. Silks as ancient models for modern polymers. Polymer. 2009;50(24):5623-5632.

[3] Fu C, Shao Z, Fritz V. Animal silks: their structures, properties and artificial production. Chem Commun. 2009(43):6515-6529.

[4] Pearson K. On Lines and Planes of Closest Fit to Systems of Points in Space. Philosophical Magazine. 1901;2(6):559-572.

[5] Czarnik-Matusewicz B, Matusiak-Kucharska M, Hawranek JP. Principal Components Analysis of Infrared Spectra of Liquid Acetylacetone. Polish Journal of Chemistry. 2009;83(5):999-1011.

[6] Zhang LP, Noda I, Wu YQ. Principal Component Analysis Based Interconversion Between Infrared and Near-Infrared Spectra for the Study of Thermal-Induced Weak Interaction Changes of Poly(N-Isopropylacrylamide). Appl Spectrosc. 2009;63(6):694-699.

[7] Hu Y, Li BY, Sato H, Noda I, Ozaki Y. Noise perturbation in functional principal component analysis filtering for two-dimensional correlation spectroscopy: Its theory and application to infrared spectra of a poly(3-hydroxybutyrate) thin film. J Phys Chem A. 2006;110(39):11279-11290.

[8] Moore WH, Krimm S. Vibrational Analysis of Peptides, Polypeptides, and Proteins .2. Beta-Poly(L-Alanine) and Beta-Poly(L-Alanylglycine). Biopolym. 1976;15(12):2465-2483.

[9] Garside P, Lahlil S, Wyeth P. Characterization of historic silk by polarized attenuated total reflectance Fourier transform infrared spectroscopy for informed conservation. Appl Spectrosc. 2005;59(10):1242-1247.

[10] Teramoto H, Miyazawa M. Molecular orientation behavior of silk sericin film as revealed by ATR infrared spectroscopy. Biomacromolecules. 2005;6(4):2049-2057.

[11] Miyazawa T, Blout ER. Infrared Spectra of Polypeptides in Various Conformations - Amide I and II Bands. J Am Chem Soc. 1961;83(3):712-719.

[12] Muller WS, Samuelson LA, Fossey SA, Kaplan DL. Formation and Characterization of Langmuir Silk Films. Langmuir. 1993;9(7):1857-1861.

[13] Taddei P, Monti P. Vibrational infrared conformational studies of model peptides representing the semicrystalline domains of Bombyx mori silk fibroin. Biopolym. 2005;78(5):249-258.

[14] Barth A. The infrared absorption of amino acid side chains. Prog Biophys Mol Bio. 2000;74(3-5):141-173.

[15] Barth A. The infrared absorption of amino acid side chains. Prog Biophys Mol Biol. 2000;74:141-173.

[16] Li G, Thomson M, Dicarlo E, Yang X, Nestor B, Bostrom MPG, Camacho NP. A chemometric analysis for evaluation of early-stage cartilage degradation by infrared fiber-optic probe spectroscopy. Applied Spectroscopy. 2005;59(12):1527-1533.

[17] Zhu HX. Analysis of the elastic properties of open-cell foams with tetrakaidecahedral cells. J Mech Phys Solids. 1997;45(3):319.

[18] Chen F, Porter D, Vollrath F. A nonwoven composite model based on silkworm cocoon (*Bombyx mori*). Journal of Materials Science and Engineering. 2010;4(9):28-33.

[19] Porter D. Predictive nonlinear constitutive relations in polymers through loss history. International journal of solids and structures. 2009;46(9):1981.

[20] Chen F, Porter D, Vollrath F. Silkworm cocoons inspire models for random fiber and particulate composites. Physical Review E. 2010;82(4):041911-041917.

Chapter 6

Indentation of Cocoon

6.1 Introduction

Cocoon properties may be of great interest in the biomimetic development of flexible damage-resistant light weight composites. As stated in Chapter 2, many silkworms have silk cocoons with a laminated structure (see examples of *Bombyx mori*, *Antheraea pernyi* and *Opodiphthera eucalypti* cocoons in Figure 6.1). Although each species of cocoon has its own individual features, they all have a multi-layer structure with fewer fibres connecting layers than aligned in the individual layers. The interlayer bonding is much weaker than the intralayer bonding. The porosity of the cocoon layers decreases from inner to outer layers (See Chapter 5). This structure shares a morphological similarity with conventional laminated composites, in which the fibre prepregs are stacked and bonded by resin matrix between the layers. Furthermore, the cocoons are, in themselves, optimised for functions to have a wide range of structures (and therefore properties) across the species with a limited number of components, usually only silk fibre and sericin. Some cocoons also have specific features, such as extra calcium oxalate crystals on the cocoon surface in *A. pernyi* cocoons and larger holes in the walls of *O. eucalypti* cocoons (Figure 6.1 inserts), which will be relevant for discussions later in this chapter.

In order to understand structural biological materials, some questions must be answered: what is their function, how are they used, and what loading conditions are present? For our materials, the preponderance of silk cocoon clearly attests to its biological success. All

cocoons appear to be multifunctional and possible functions include camouflage [1], thermo-regulation [2] and humidity control [3]. However, despite surprisingly little experimental data, the main function of all cocoons is likely to be to offer the enclosed pupae mechanical protection from predators [4, 5], similar to the protection against both general and specialised predators provided by the silken cocoons enclosing spider egg sacs [6]. The exact way in which the cocoon offers protection depends on the nature of its main predators.

Literature shows that three main strategies to penetrate the cocoons are employed by predators: (1) Penetration of the cocoon wall by drilling. This strategy is employed by ichneumonid wasps which lay eggs in or on the pupae that develops into larvae that parasitize the pupae [7]. (2) Creating a hole in the cocoon by removing silk by tearing and shearing movements. This strategy is employed by mice and other small mammals [4]. (3) Creating a hole in the cocoon by breaking individual fibres and the cocoon wall by making an indentation in the cocoon. This strategy is employed by birds which either use their beaks to compress the cocoon walls or like woodpeckers attempt to directly hack holes in the cocoons [5].

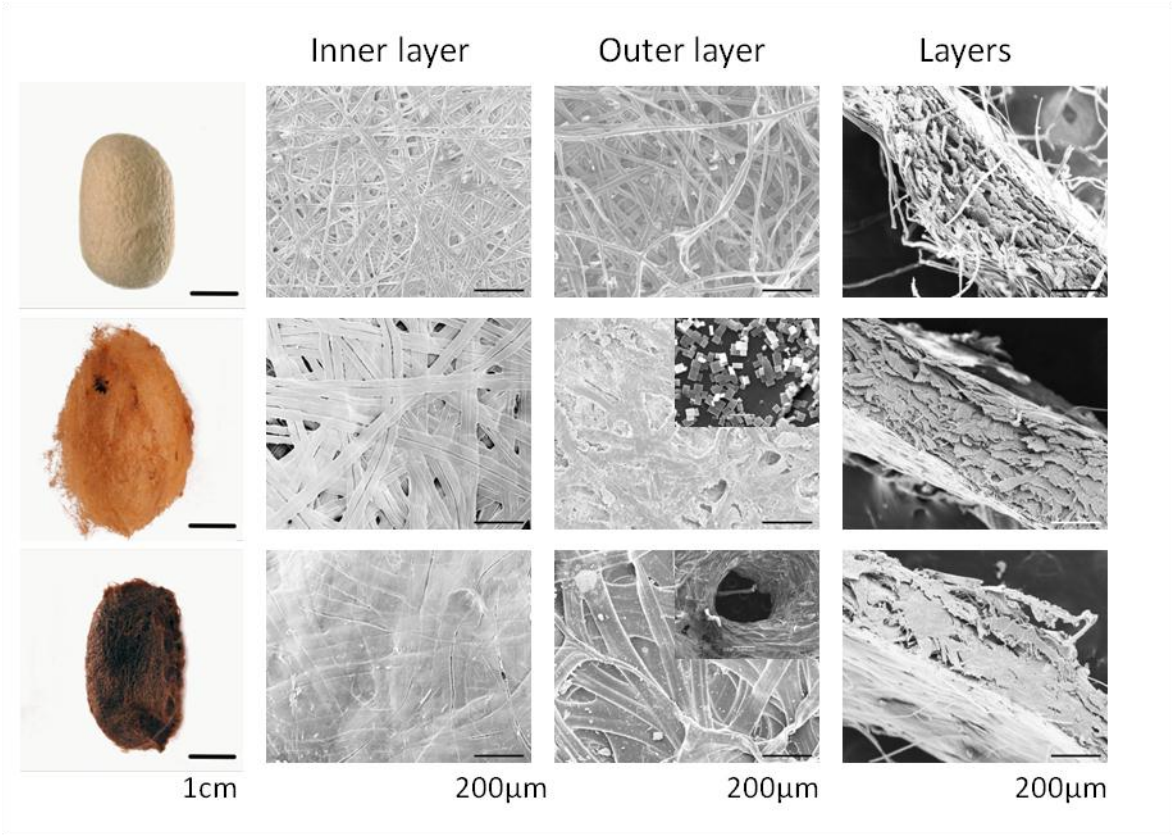

Figure 6.1 The morphologies of the layer structure of the cocoons of *Bombyx mori* (first row), *Antheraea pernyi* (second row) and *Opodiphthera eucalypti* (third row). First column shows photographs of the cocoon, while SEM photographs of the inner and outer layer structure are shown in columns two and three. Porosity is found to decrease from inner to outer layers. Insert of *A. pernyi* cocoon: calcium oxalate crystals found on outer cocoon surface. Insert of *O. eucalypti* cocoon: fabricated hole structure found on cocoon surface. Column 4 shows SEM photographs of cross sections of layer structures of the cocoons.

All of the above three strategies involve impact strike on cocoons. Defence against these strategies would include the ability to either resist the impact with little damage, or tolerate the damage by maintaining the structure. As a cocoon acts as a protective structure for the pupa, it should evolve to have engineering benefits like impact resistance and damage tolerance by combining the structure and material properties for fulfilling its biological functions. This chapter focuses on how cocoons have evolved counter-measures against the

third strategy using an engineering approach. It is described how cocoons deform during quasi-static localized indentation and develops a simple finite element method to simulate this behaviour. Then the model is used to investigate the defensive strategy of silk cocoons by optimizing its structure and materials properties for achieving their superior impact resistance and damage tolerance.

6.2 Experiments

6.2.1 Indentation experiments

Each half of the cocoon samples was superglued at its cut edge onto a glass slide. The central points of the cocoon halves were measured and marked to be the compressive points. *O. eucalypti* cocoon samples were cut to avoid the fabricated holes on the cocoon wall. Both *A. pernyi* and *O. eucalypti* cocoon specimens did not have consistent geometries due to the variation of their natural sizes. The tests were carried out in a Zwick/Roell Z0.5 test machine under displacement control at a loading rate of 5 mm/min. The indentation load was applied through a steel rod with a round flat end (1.56 mm diameter). The unloading was performed at a speed of 15 mm/min. The samples flexed back but did not recover completely their undeformed shape. The cocoon samples respond to form a concave area under the indenter. The shapes of cocoon crush during the indentation until the indenter reached the slide underneath the sample were recorded.

6.2.2 Finite element model

The aim of finite element modelling in this work is to perform simulations of the quasi-static response of cocoons in order to understand the failure modes caused by the local indentation

described above. Based upon the success of our models for the mechanical properties of cocoons based upon open cell foam structures, it was noted that previous work on simulating deformation in foam materials has used the finite element package ABAQUS software [8-10]. Since the software was available in the group on a different project to simulate spider web deformation, we used ABAQUS/CAE 6.8-4 to simulate the indentation behaviour of cocoon materials.

An axisymmetrical idealization was used for the geometry of the three cocoon types. The mesh consisted of 94,400 finite elements with 2 elements through the wall thickness (due to the limited speed of the modelling computer and time of this project) (Figure 6.2). All degrees of freedom at the boundary of the specimen bottom were constrained, simulating a rigid fixed support. The indenter was modelled as a force applied to a circular area on the outer surface of the cocoon in the program. All degrees of freedom of the indenter were constrained, except in the vertical direction.

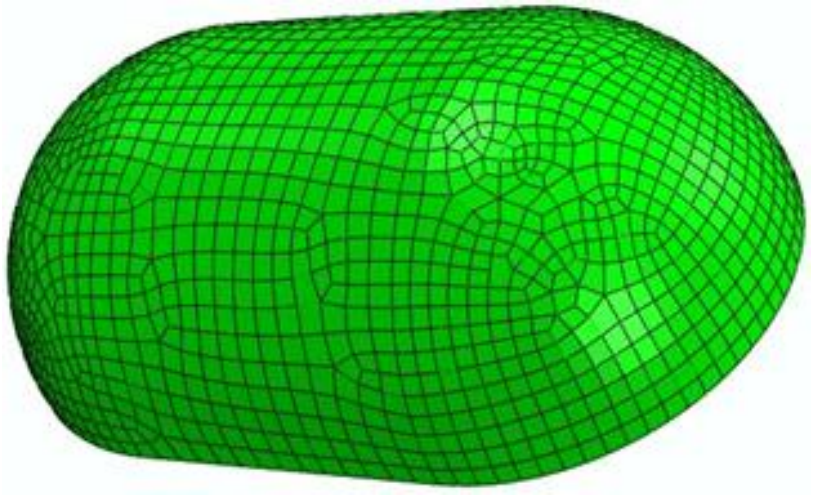

Figure 6.2 Geometry model of the cocoons. The length of this cocoon model is 3.5 mm.

6.3 Results

6.3.1 Indentation experimental results

Typical load-indentation curves for the three cocoon types are shown in Figure 6., with deflection given as a fraction of the maximum strain until the indenter reached the glass plate and load is shown on the same scale for all the cocoons for comparison. The *B. mori* cocoon load-deflection curve has a gradual decrease of the stiffness before the stress reaches a plateau level with the emission of a noise (cracking sounds), which was attributed to extensive sericin breakage and delamination in the cocoon sample (Figure 6.3). The damage process is also reflected in the fluctuations in the load response. *B. mori* cocoon has the largest delamination areas among the three cocoons and nearly all the interconnectivity between layers in the concave area are broken (Figure 6.5). The *B. mori* response is relatively consistent, and the five curves shown in Figure 6.4 reflect the full range of responses, which we attribute to relatively consistent size and shape of the cultivated cocoons, compared with the other wild cocoons.

The indentation behaviour of *A. pernyi* and *O. eucalypti* cocoons has much more variation. We attribute this to their inconsistent geometrical shapes and sizes, as they are spun in wild environments that have much less control than cultivated *B. mori* cocoons. Due to the limited time in this project, only three samples of each species were tested for a preliminary study. Generally, both cocoons also have nonlinear behaviour (Figure 6.4). The onset of interlaminar delamination of the cocoons was associated with the gradual decrease in the slope of the load-deflection curves. After that, the cocoons were extensively damaged, which can be seen from the pronounced fluctuations in the load-deflection curves. *A. pernyi* cocoon

has extensive sericin breakage and some delamination after indentation tests. However, general fibre and layer breakages are found in *O. eucalypti* cocoon with less damage propagation and large scale failure can only be found close to the indentation area. The indentation terminates with a clear penetration of fibre and layer breakage in *O. eucalypti* cocoon (Figure 6.5).

One of each of the three experimental tests from both *A. pernyi* and *O. eucalypti* cocoons has been selected for simulation. Their geometrical data were collected for FEA calculations, and their specific experimental curves were used for comparison with the simulation results.

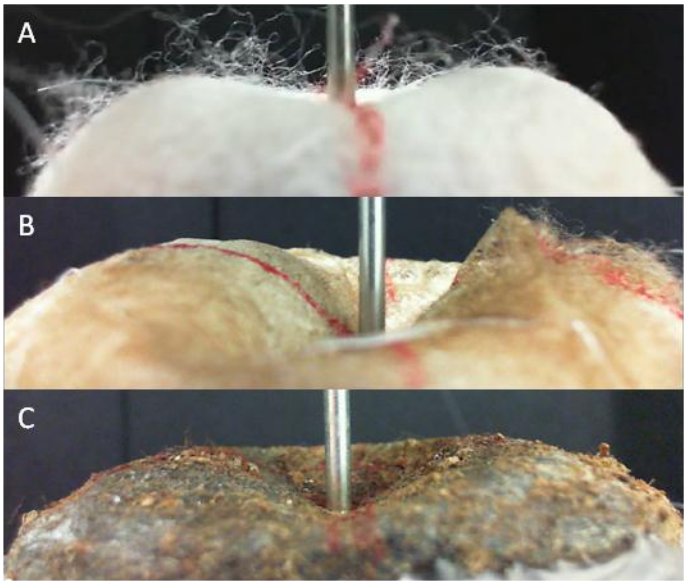

Figure 6.3 Photographs of the quasi-static impact tests of three cocoons showing their deformation. A. *Bombyx mori*. B. *Opodiphthera eucalypti*, C, *Antheraea pernyi*. Scale: the length of the picture is 3.5 mm.

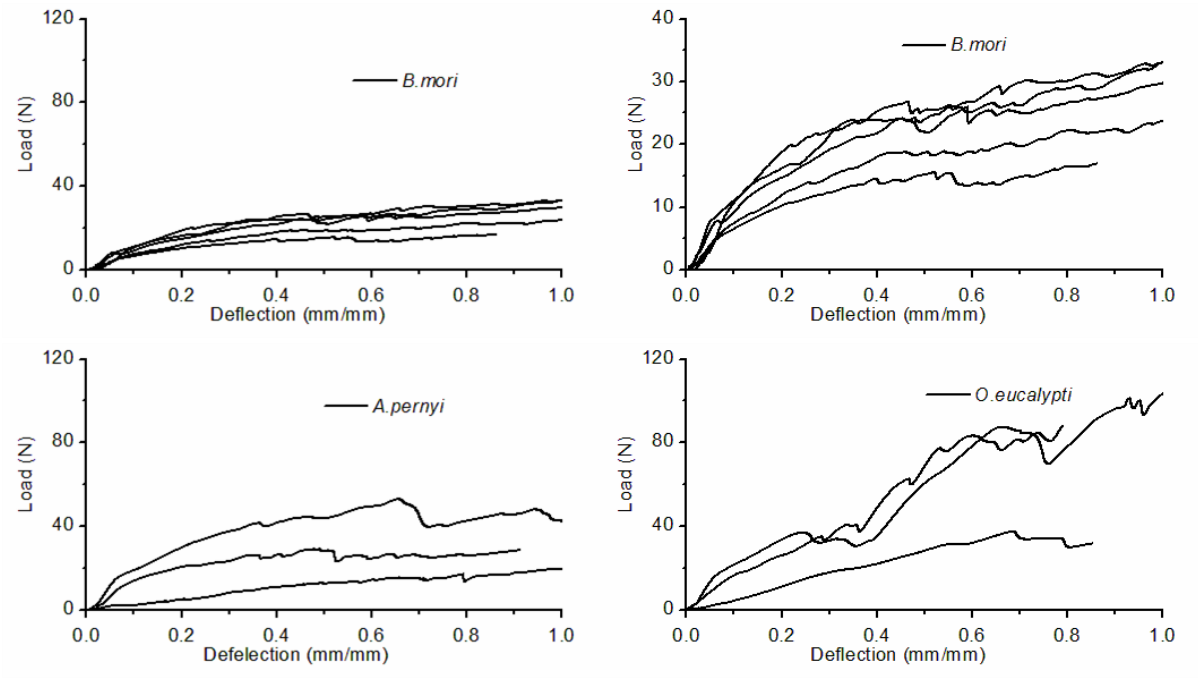

Figure 6.4 Load-deflection curves for impact tests on cocoons from three species. Above left: *B. mori* curve was scaled to the same load level as *A. pernyi* (Bottom left) and *O. eucalypti* (Bottom right) for comparison. Above right: The same *B. mori* curve with a smaller load scale to show more details.

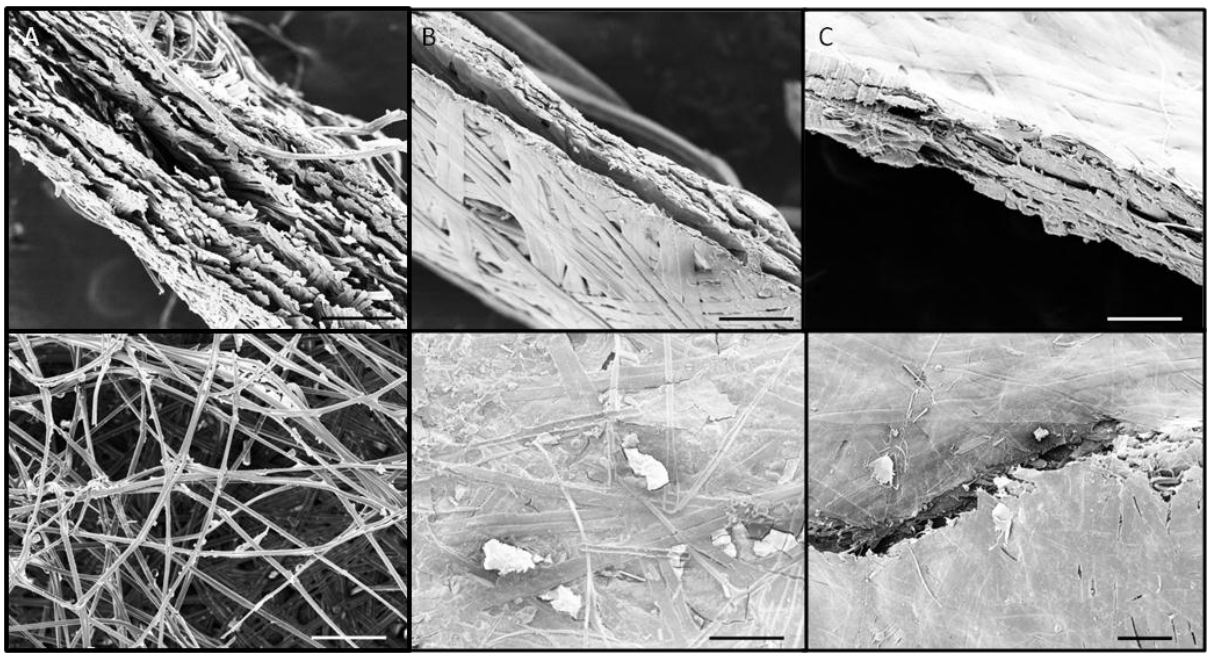

Figure 6.5 SEM pictures of cocoon microstructures. Above: delamination in cocoon concave area. Scale bar: 20 μmBottom: Huge magnification micrographs show fibre and sericin failure of the area under the impactor. (A) *Bombyx mori* (B) *Antheraea pernyi* (C) *Opodiphthera eucalypti*. *B. mori* and *A. pernyi* cocoons show sericin facture of some fibres, while *O. eucalypti* cocoon exhibit fibre fracture and penetration of the structure. Scale bar: 200 μm.

6.3.2 FEA: Constitutive model for materials

An open cell foam model was used to describe the tensile properties of cocoon walls in Chapter 4, based upon the similarity of cocoon morphology with that of cellular materials. In Chapter 3, we also showed that the compression behaviour of cocoon shells can be described again by an open cell foam model using the slightly different deformation geometry of the cell walls under compression. To complicate things further, we also saw in Chapter 5 that interlaminar debonding contributes to the mechanical properties of cocoon walls and should

thereby be included in the deformation and failure mechanisms, particularly where shear (hence bending) deformation is involved through the wall thickness.

The plastic compressibility of foams results from the collapse of the cell walls due to buckling, breaking or yielding [8]. A localized progressive crushing mechanism for foams is described by Li et al. [9], where the plastic deformation is usually localized into the weakest cell layer and the strain increases rapidly in this layer and then triggers the next layer to crush. This process is very similar to the bond fission and delamination processes of cocoon damage. Since such foam compression simulations have been described in literature using ABAQUS, we assumed that we would find an appropriate constitutive model in the software that would implicitly include damage occurring in the plasticity of the irreversible process of cocoon indentation.

A number of different constitutive plasticity models in ABAQUS were tested for their ability to reproduce the experimental tensile stress-strain relations discussed in Chapter 4. The most appropriate deformation plasticity model available in our version of ABAQUS is the Ramberg-Osgood plasticity model, which describes the strain response to an applied stress through a yield process

$$\varepsilon = \frac{\sigma}{E} + \alpha \frac{\sigma_0}{E} \left(\frac{\sigma}{\sigma_0}\right)^n \tag{6.1}$$

where σ is the stress, ε is the strain, E is the Young's modulus, α is the yield offset parameter, σ_0 is the yield stress, n=hardening exponent, and $\alpha \frac{\sigma 0}{\mathrm{E}}$ = yield offset strain.

All these parameters come from fitting experimental tensile stress-strain data as shown in Figure 6.6 and Table 6.1. This deformation plasticity model is a modified elastic model to

include yielding behaviour and we thought that it would be the simplest model with nonlinear behaviour to represent damage in our version of ABAQUS, since it describes itself as a 'plastic' model. However, we later realised that it is a simple empirical model to fit data using simple maths, and it does not actually incorporate plastic flow and damage, since when $\varepsilon = 0$, $\sigma = 0$ under all deformation paths in equation (6.1). Also, the model does not include the rapid drop in stress at the percolation damage point in each experimental curve, but with very limited time and no better options, we chose this model to try simulations on the basis that the nonlinear stress response may at least suggest mechanisms for initiation of the cocoon collapse in areas where modulus reduces significantly under load.

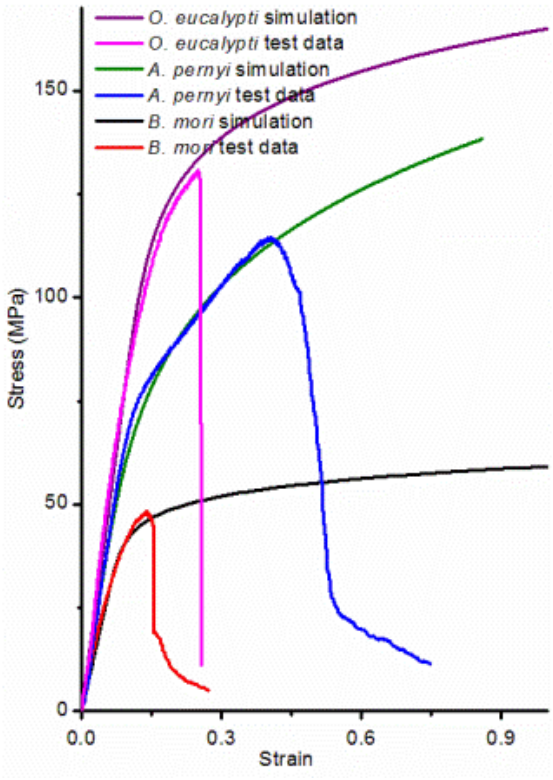

Figure 6.6 Stress-strain curves for cocoon samples tested and simulated in uniaxial tension from the deformation plasticity model

Table 6.1 Parameters of plasticity constitutive model of FEA simulations

	Thickness (mm)	Modulus (MPa)	Poisson's ratio	Yield stress (MPa)	Exponent	Yield offset parameter
B. mori	0.61	500	0.1	43.5	11.6	0.28
A. pernyi	0.43	730	0.1	77. 5	4.9	0.38
O. eucalypti	0.25	850	0.1	128.0	10.2	0.40

6.3.3 FEA simulation results of cocoon samples

Figure 6.7 reports the evolution of the stress on the outer surface of the cocoons at three increasing indentation loads and also the stress through the thickness of the cocoon wall in a cross-section through the long axis, with red being the highest stress and blue the lowest. We see clear differences in the deformation shapes due to the combinations of wall thickness, cocoon shape, and material properties.

In *B. mori*, the cocoon has a highly deformed zone, which is localized around the indenter, while other parts of the cocoon undergo far less deformation. The highest tensile stress is concentrated on the outer surface of the minor axis of the cocoon.

At small deflections of the *A. pernyi* cocoon, the stress first develops in the radial direction. The indentation process is characterized by formation of a stressed zone which propagates

gradually down to the base of the cocoon. The concave shape develops at higher applied indenter load and the minor axis of the cocoon suffers the maximum tensile stress.

For *O. eucalypti* cocoon, the indentation effects are localized in the vicinity of the indentor. The stress distributes on the surface of the cocoon, and a broad collapse of the cocoon structure can be seen. When the ability of the cocoon to distribute the load in the minor axis is exceeded, the stress begins to grow in the major axis.

	B. mori	*A. pernyi*	*O. eucalypti*
Surface Stress	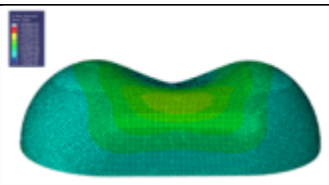	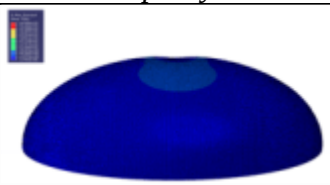	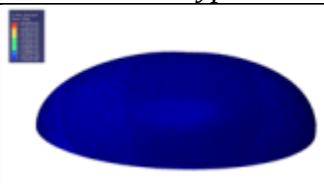
Cross Section Strain	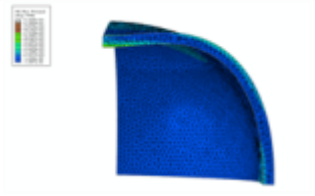	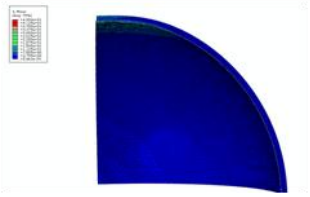	
	Applied Load: 16.73N Max Strain: 3.3%	Applied Load: 4.01N Max Strain: 0.48%	Applied Load: 2.31N Max Strain: 0.24%
Surface Stress	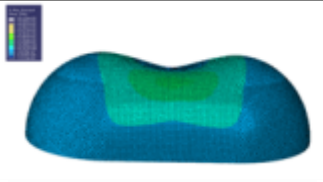	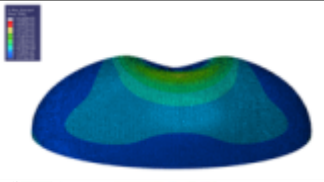	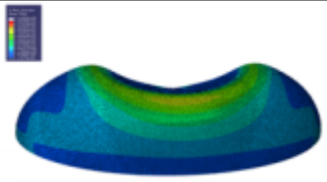
Cross Section Strain	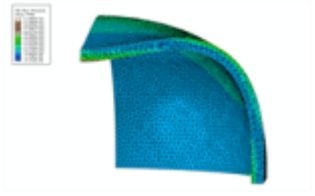	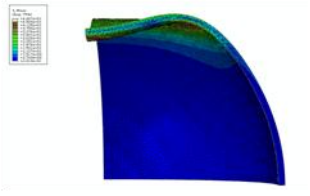	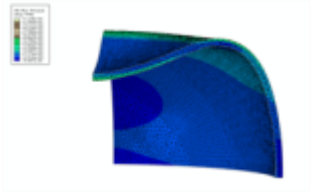
	Applied Load: 29.18N Max Strain: 4%	Applied Load: 11.99N Max Strain: 4%	Applied Load: 20.51N Max Strain: 6.5%
Surface Stress	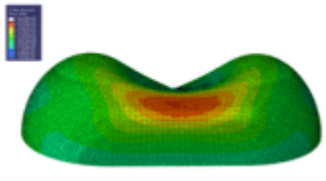	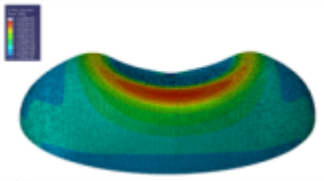	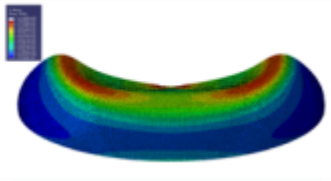
Cross Section Strain	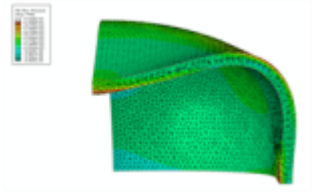	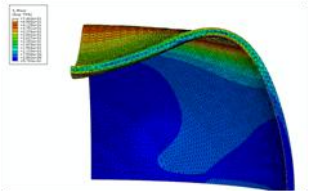	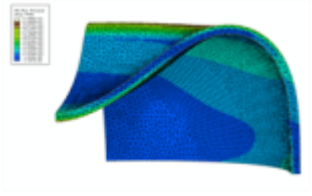
	Applied Load: 57.3N Max Strain: 5.6%	Applied Load: 20.51N Max Strain: 6.1%	Applied Load: 29.18N Max Strain: 9.2%

Figure 6.7 Evolution of the cocoon's indentation deduced from the numerical modelling.

Three applied loads were selected from load-deflection curves from each cocoon, and the

stress level in the concave and the strain level in the cross-section of the cocoon minor axis are shown. The simulation calculates the maximum strain in the cocoon structure

6.3.4 Indentation: Comparison between experiments and simulations

Since most experiments and simulations of cocoon indentation were carried out on *Bombyx mori* cocoons, the discussion here concentrates on these results to try to deduce some general trends that will be useful in future work. A comparison between the experimental results and simulation is made in this section, which starts by comparing the general cocoon shapes under indentation, and then load-deflection curves are compared. Since the direct simulations did not reproduce the experimental results well using the fitted constitutive model of equation (6.1), the simulation modelling approach is investigated by using different material parameters and examining the detailed form of the predicted stress distributions to try to understanding the underlying problems that were not envisaged at the start of the work.

The measured and simulated static indentation responses of *B. mori* cocoon are shown in Figure 6.8. The simulation can generally reproduce the concave shape deformation in the cocoons observed experiment all at small deflections. However at high deflection, the shape deformation in the simulations tends to concentrate too much around the indenter. In the experiments, the indenter produced a broader deformation in the cocoon, with a lower height.

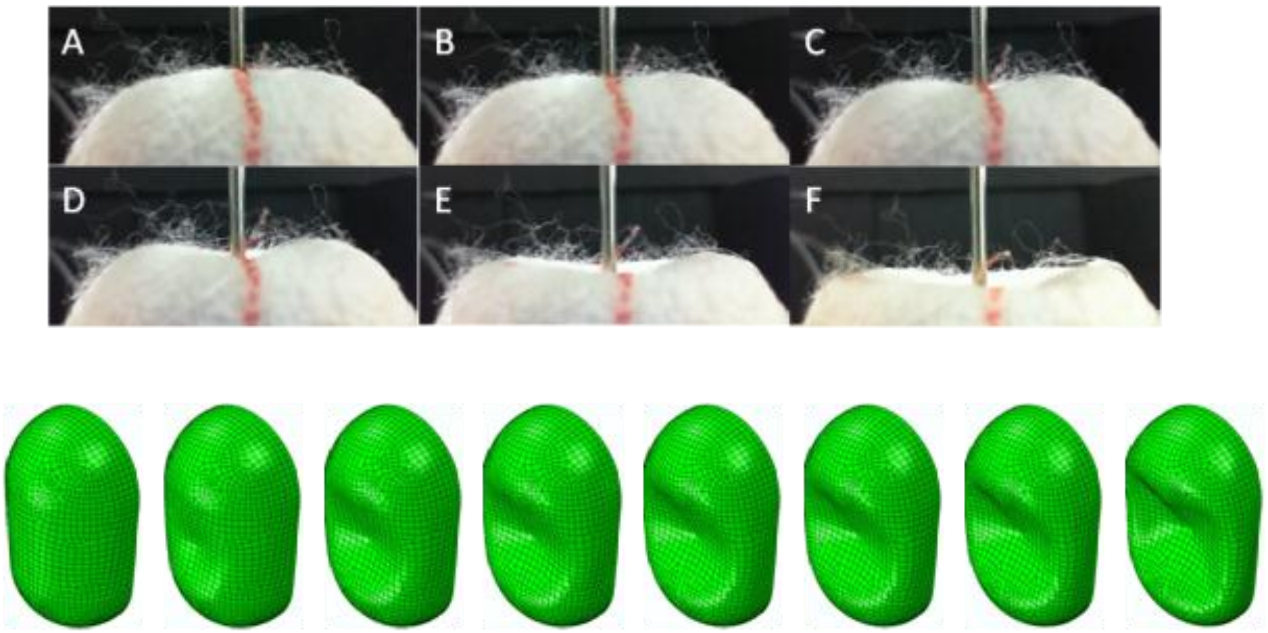

Figure 6.8 Comparison of *B. mori* cocoon shape between experiments (Above) and simulations (Bottom)

Interestingly, different constitutive models were tried for the cocoon wall material, including hyperelastic models and even simple rubber models, on this FEA model of *B. mori* cocoon shape. It turns out that this general concave shape of the cocoon indentation crater can be reproduced almost universally, but clearly with poor predictions of the load. It suggests that the general cocoon response behaviour is generic and quite independent of the material properties. The geometric shape of the cocoon appears to have more effect on its indentation behaviour.

The measured and the simulated static indentation load responses with the same cocoon geometries are given in Figure 6.9, but using different sets of material parameters in the constitutive model. For *B. mori* material data shown in Figure 6., the initial elastic slope of the simulated load-indentation curve is in good agreement with the experimental results.

However, at large deflections the numerical simulations do not reproduce the overall 'yielding' profile; the finite element modelling and the experimental study diverge at about 20% deflection. Using the constitutive model parameters for *A. pernyi* simply shifts the simulation to higher loads due to the higher modulus.

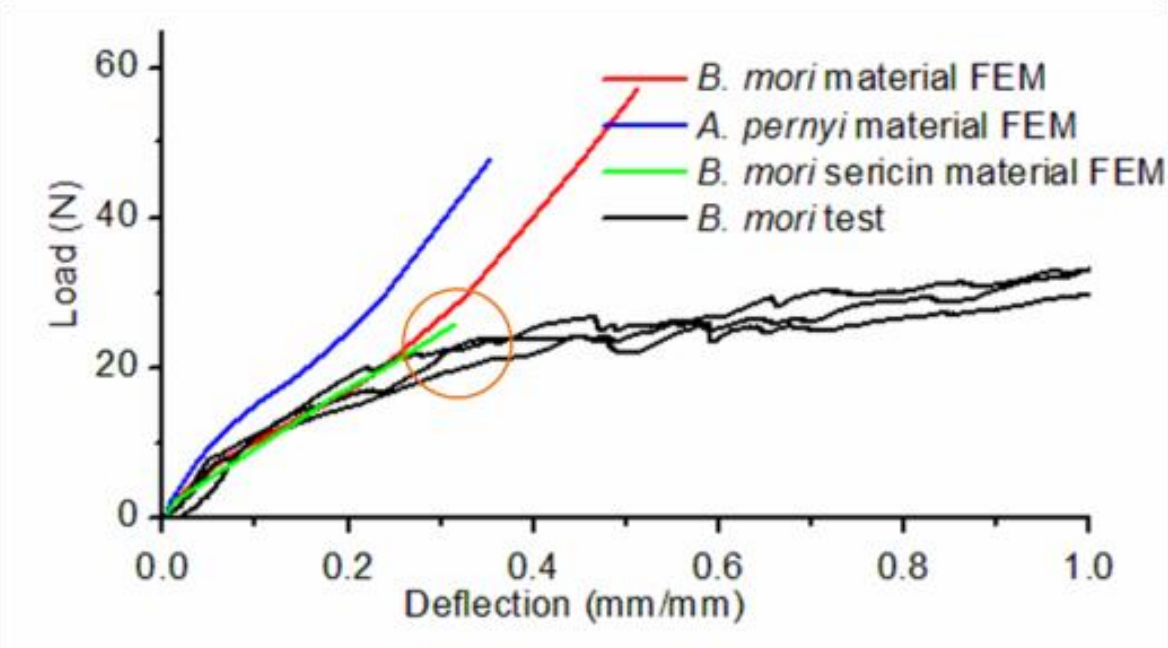

Figure 6.9 Comparison between impact load-deflection curves predicted by the finite element modelling with the experimental impact data for *Bombyx mori.* Circle shows the divergence between experiment and modelling which is attributed sericin breakage.

Figure 6.10 shows the distribution of the stress and strain which corresponds to the divergent point between the experimental results and the numerical simulation at about 20% cocoon deflection. The inner surface of the cocoon centre, which is localized under the indenter, has a highly deformed zone. The outer surface of the edge of the bending concave crater (circled) also develops the highest general strain, which is locally above 4% strain due to the tensile force distribution on the outer surface. This happens to be the breaking strain of sericin which has been discussed in detail in Chapter 4.

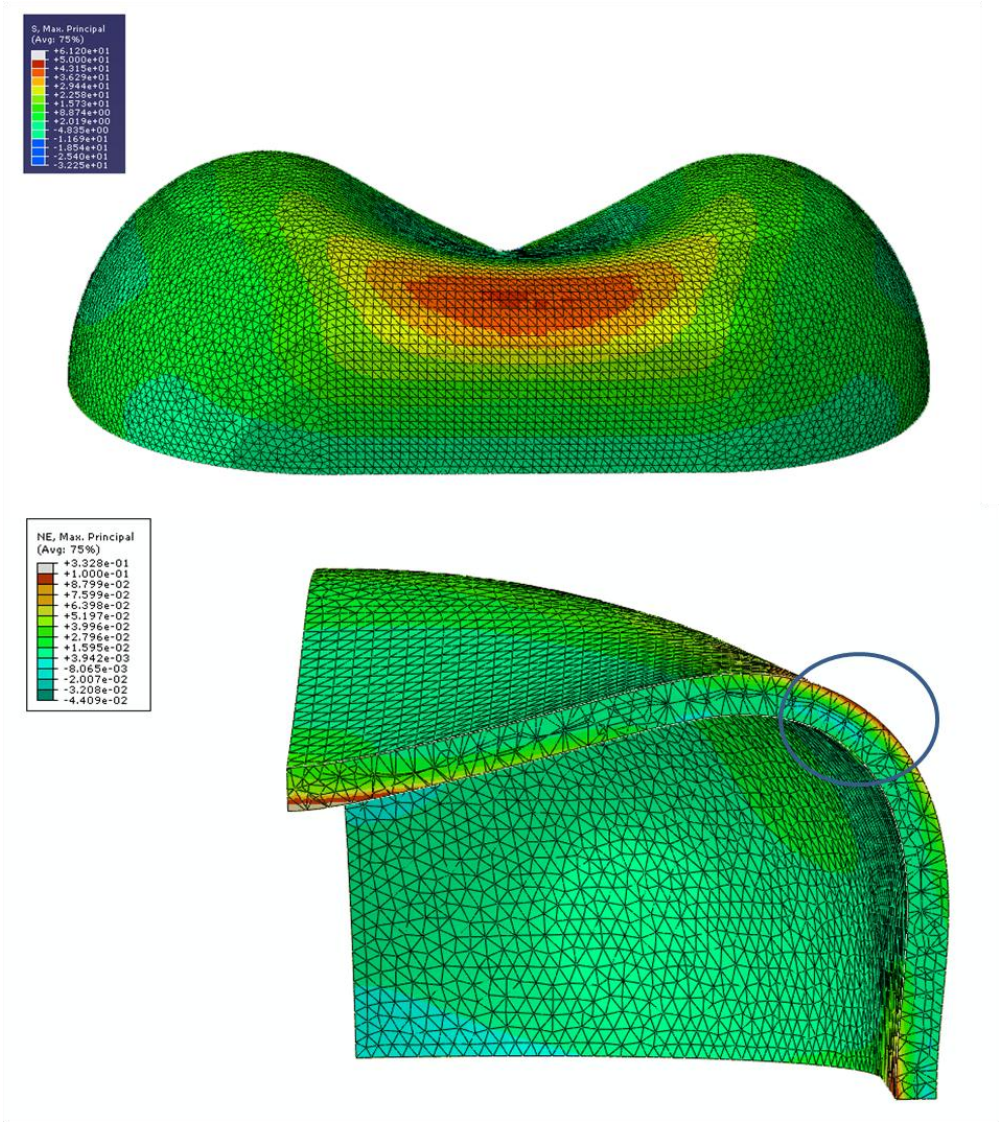

Figure 6.10 Distribution of the stress and strain corresponding to the maximum indentation load obtained from *B. mori* cocoon in the finite element analysis. Above: stress in the cocoon concave. Below: strain in the cocoon cross section.

The experimental observations suggest this divergence between simulation and experiments may indicate the model cannot predict the initiation of the damage. In the cocoon, our observations in the previous chapters suggest that the initiation of the damage is the sericin breakage between the layers at the surface of the cocoon. To explore this hypothesis, a *B.*

mori sericin model was used in the indentation simulations. This model has the same stress-strain behaviour as *B. mori* cocoon material at low strain, but is constrained to yield at 4% strain as for pure sericin (Figure 6.11). We thereby hope to examine whether the local stress-strain response in the cocoon walls is dominated by sericin failure.

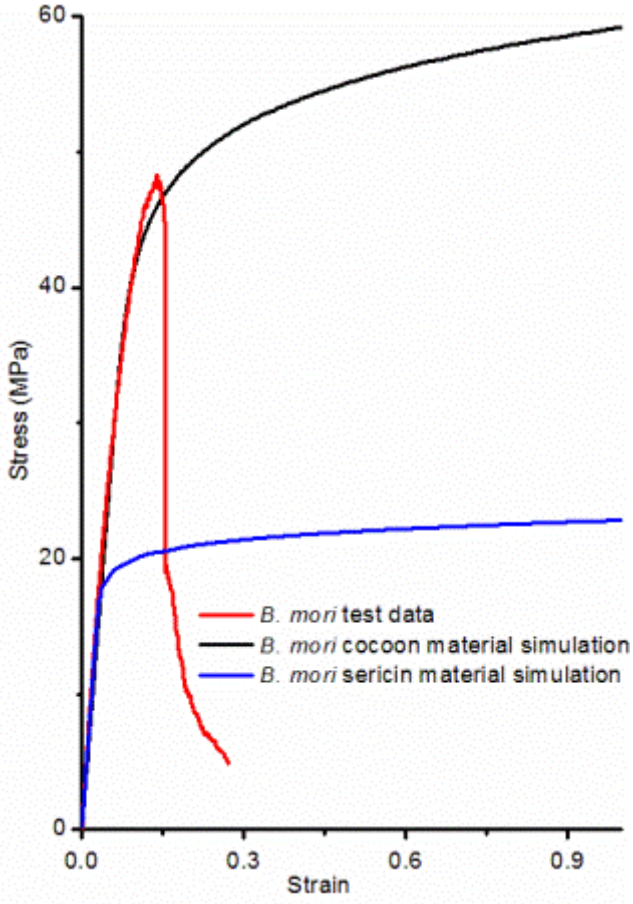

Figure 6.11 Stress-strain curve for *B. mori* cocoon samples tested, cocoon material simulation and sericin material simulation

The sericin model can reproduce the experimental results at low deformation (up to a deflection of 0.3 mm) shown in Figure 6.8. But the simulation does not converge above this deformation, which corresponds to a local strain on the outer surface of 4.5%, which is the failure strain of the sericin binder material. Therefore. we conclude that the point at which the

simulation diverges from the experiment is the initiation of the sericin fracture, which is irreversible fracture damage in the cocoon structure that is not included in the constitutive model. The point at which the sericin damage threshold is reached should correspond to delamination of the cocoon and loss of connectivity in the planar interfibre bonding. At this point the composite material cannot sustain load, and the stress is transferred in a cascade to ever deeper layers of the cocoon structure to propagate the damage process through the full cocoon thickness, resulting is no more increase in the indenter load.

In the limited time available, *A. pernyi* and *O. eucalypti* cocoon were simulated in initial trials. The measured and the simulated static indentation responses are given in Figure 6.12. Due to the variable size and shape of the cocoons, one specific cocoon geometry was taken for each type and compared simulations with the experimental results on those specific cocoons (shown as solid lines, with other experimental plots from Figure 6.3 shown for reference as dashed lines). Both the simulations of *A. pernyi* and *O. eucalypti* cocoons do not reproduce the experimental results particularly well, although the general magnitude and form are reasonable, bearing in mind that statistical damage events cannot be reproduced in the deformation process.. The simulations indicate that the response of the cocoon indentation should be approximately linear before and after a yield event, but the experiments show a gradual nonlinear behaviour.

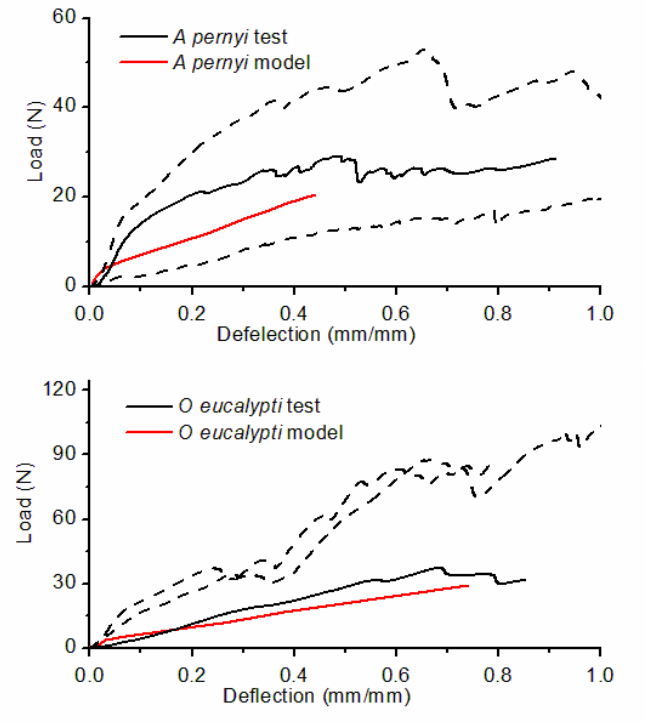

Figure 6.12 Comparison between stress-strain curves deduced from the finite element modelling and from the impact test. The solid lines are experimental results which have the same cocoon geometry as the model simulation, and the dashed lines are from other experiments of other cocoon geometries of the same species.

6.3.5 Problems of the FEA modelling

We had hoped to use the natural example of indentation of a cocoon by a simplified predator attack as a demonstration that future development and application of nonwoven composites based upon cocoon structures and morphology could be supported by engineering FEA simulations. While we were able to demonstrate that the indentation deformation of cocoons can be analysed at least qualitatively and to some extent quantitatively by the use of FEA simulations by careful selection of material property parameters, we must admit that direct simulation of such structures as potential engineering structures has been of limited success

here. However, we have learned a number of important lessons from the process, which should be valuable in future work.

At the end of section 6.3.3 in the discussion of *Bombyx mori* deformation, it was suggested that the key problem with this work on simulating impactor damage in cocoons is that the damage growth to the cocoon has not been included and the consequent inability to sustain load in the constitutive model for the cocoon wall composite material. The experiments clearly showed extensive damage from SEM pictures and the damage developing through the indentation process could even be heard. To model this damage phenomenon, an FE code specialized in modelling continuum damage mechanics would be required, such as DYNA-3D, PAMCRASH, RADIOSS or AUTODYNE. This is rather complex and expensive and goes beyond the scope of the present research work. It is clear that future work would require the advice of FEA modellers who are experienced in this area. Such codes might also allow us simply to use experimental data, instead of fitting a constitutive model, which would allow better use of our models for cocoon deformation to guide material properties.

Another problem with the simulations appears to be how the constitutive model deals with the yield conditions that we thought had been implicitly included in the tensile stress-strain profiles of the material. Although the graphic output for stress suggested stresses higher than nominal yield points, the material continued to behave in simple elastic mode. Attempts to explore the detailed results files for each element suggested that the stress output was showing values dominated by hydrostatic stress, which is not part of the tensile yield response and the deviatoric stress component never actually reaches the yield stress of the constitutive model. Hence, strain was used to judge if damage might occur at any point in a simulation.

Part of the problem with simulations was that only tensile deformation was considered in the choice of constitutive model, and chose material parameters within a constitutive model based upon fits only to tensile data. Since it was already clear from experimental observations that delamination through shear deformation through the cocoon wall thickness was an important damage mechanism, and results from Chapter 5 show that modulus, or the ability to sustain load, is reduced significantly by such damage, shear criteria should also have been included into the material model. In retrospect, this means that 3- and 4-point bending tests on the cocoon walls should have been conducted and a constitutive model found that reproduced both the tensile and bending modes deformation. This is particularly important, since the critical failure areas are on the outside surface at the point of maximum curvature. Such a constitutive model would also need to include the compressive analysis of the cocoon walls discussed in Chapter 3, which was not considered in the work reported here.

6.4 Discussion

The present study demonstrates that the silk moth cocoons are adapted to resist an impact force that is similar to those generated by predators. The moth larvae appear to employ a number of different strategies while building the cocoons to increase their impact resistance and damage tolerance by combining its macro structural shape, micro layer structure and properties, and component materials. Hierarchical organization and complicated engineering properties are inherent to their design.

Bombyx mori cocoon is the simplest example among all of the species studied in this work [11], so it has been extensively studied here for analysing its impact resistance and damage tolerance. Experimental and modelling results both suggest that the silk cocoon may indeed

be mechanically suited to withstand impact force. This is because of (1) the ellipsoid shape of the cocoon, (2) component material properties, (3) laminated layer structure, and (4) graded layer properties. Both the experiments and models show that a loading at the centre of the cocoon leads to a concave shaped deformation (Figure 6.8). The ellipsoid shape of the cocoon allows a certain level of elastic deformation of the cocoon wall, and then restricts the deformation to avoid propagation of damage. On the other hand, the FEA simulations suggest that the deformation process and the deformed shape of the cocoon is relatively independent of its material properties. The damage is localized at the edge of the concave crater without excessive propagation of damage. The material properties have effects only on the elastic deformation rather than the damage area. This feature helps to keep the cocoon structure intact (damage tolerance), and provides a good support to inhibit the massive deformation which would damage the pupa inside the cocoon by using limited materials.

In biological structures, the component material properties usually closely link with the structure, as they evolve together to fit the biological functions. This is also found from *B. mori* cocoon in its relation between component properties and laminated structure. The damage of *B. mori* cocoon can be described by two coupled failure modes: sericin bond fracture and delamination. FEA shows that sericin fracture is the first fracture event around the edge of the cocoon concave during an impact process due to its relatively low breaking strain compared to the fibres. After extensive breakage of sericin bonds, delamination (the crack in the sericin bonds between layers) develops, inducing separation of the individual layers which has been observed from the experimental results. This sacrificial breakage allows each fibre layer to deform semi-independently rather than transferring the stress through the layers. On the other hand, silk fibre with a high strain to failure adapts within this

individual layer structure. The fibre layer can have an elastic deformation without damaging the fibre to maintain its own mechanical properties in the fibre directions. This gives maximum energy absorption and increases the toughness of the structure.

The graded layer structure is another feature which may have evolved to improve the impact resistance of the cocoon. This is based on the FEA simulation results that the largest deformation of the cocoon happens at the innermost layer of the area under the impacter. After delamination damage, the individual layer would be able to deform independently, and the properties of each layer would determine its own damage mechanism. It was shown in Chapter 5 that the mechanical properties of cocoon layers decrease from inner to outer direction [12]. FEA simulation, on the other hand, shows that the deformation of layers decreases from inner to outer layers. It has been pointed out by Zhao et al. [13] that this material-structure relation may have evolved to adapt to the cocoon bending behaviour, which is part of the impact deformation, as the inner layer would sustain more tensile force than the outer layers.

A. pernyi cocoon has a similar breakage mechanism as *B. mori* cocoon, where the damage initiates at the brittle sericin and leads to an extensive delamination between the layers. The separated layers deform to absorb the impact energy and the relatively strong inner layers provide stiffness and stress to the structure. Given the species-specific geometry and identical loading regimes, peak stress was lower in *A. pernyi* cocoon because of its larger size, leading to less damage and higher impact resistance. On the other hand, the calcium oxalate crystals found on the cocoon surface [11] may also help to improve the hardness of the materials and therefore the impact resistance.

In comparison, *O. eucalypti* cocoon seems to employ another strategy to protect the pupa. The cocoon material has a high stiffness as a result of a high fibre connectivity and low porosity. This reduces its ability to deform the structure and damage of the materials, resulting in a high impact resistance. Apart from sericin fracture, fibre breakage is its significant energy absorbing mechanism. This leads to a catastrophic penetration when the sericin crack propagates to the fibres and the failure reaches a critical extent. This mechanism localises the damage under the impacter, avoids excessive damage and maintains the structure integrity in other undamaged areas. In nature, *O. eucalypti* seems to have a tolerance to holes in the cocoon, as it fabricates woven holes around its attachment in the cocoon construction. This may be a compensating strategy for ventilation as it has very low porosity in the cocoon walls compared with other species. These fabricated holes appear not to interfere with the structure and mechanical properties of the rest of the cocoon wall, unlike other nonwoven cocoons. In this case, it is not surprising that *O. eucalypti* cocoon would employ a penetration breaking mode in its cocoon impacting behaviour.

The impact behaviour of cocoon composites is very similar to conventional composite laminates, where layers of aligned unidirectional carbon fibres stack with epoxy matrix bonding between the fibres [14]. It has been an important concern in structural design in composite engineering for impact resistance and damage tolerance of the structure. Materials and structural design are essential for energy absorption and toughness of the structure. These design principles in composites engineering can be used to understand the design criteria of cocoon structure by connecting the materials and structure with their engineering functionality. Comparative analyses of cocoons from a broader sample of wild species are essential to test whether the observed cocoon properties and structures are a result of

adaptations to predators employing different strategies to penetrate the cocoon walls. On the other hand, as a complicated engineering product arisen from millions of years of evolution to fit their individual functions, silk cocoons may be able to provide a tool to apply these biomechanical engineering principles in the design of synthetic structural composites.

References

[1] Danks HV. The roles of insect cocoons in cold conditions. E J Entomol. 2004;101(3):433-437.

[2] Lyon BE, Cartar RV. Functional significance of the cocoon in two arctic Gynaephora moth species. Proc R Soc Lond Ser B-Biol Sci. 1996;263(1374):1159-1163.

[3] Blossman-Myer B, Burggren WW. The silk cocoon of the silkworm, *Bombyx mori*: Macro structure and its influence on transmural diffusion of oxygen and water vapor. Comparative Biochem Physiol A-Mol Integrative Physiology. 2010;155(2):259-263.

[4] Scarbrough AG, Waldbauer GP, Sternburg JG. Response to Cecropia Cocoons of Mus musculus and Two Species of Peromyscus. Oecologia. 1972;10(2):137-144.

[5] Waldbauer GP. Differential predation on cocoons of Hyalophora cecropia (Lepidoptera: Saturniidae) spun on shrubs and trees. Ecology. 1967;48(2):312.

[6] Hieber CS. Spider Cocoons and Their Suspension Systems as Barriers to Generalist and Specialist Predators. Oecologia. 1992;91(4):530-535.

[7] Marsh FL. Ecological observations upon the enemies of Cecropia, with particular reference to its hymenopterous parasites. Ecology. 1937;18(1):106.

[8] Rizov V, Shipsha A, Zenkert D. Indentation study of foam core sandwich composite panels. Composite Structures. 2005;69(1):95-102.

[9] Li QM, Mines RAW, Birch RS. The crush behaviour of Rohacell-51WF structural foam. International journal of solids and structures. 2000;37(43):6321-6341.

[10] Gilchrist A, Mills NJ. Impact deformation of rigid polymeric foams: experiments and FEA modelling. Int J Imp Eng. 2001;25(8):767-786.

[11] Chen F, Porter D, Vollrath F. Morphology and structure of silkworm cocoons. Mat Sci Eng C. 2012;32(4):772-778.

[12] Chen F, Porter D, Vollrath F. Silk cocoon (*Bombyx mori*): Multi-layer structure and mechanical properties. Acta Biomaterialia. 2012; 8(7):2620-2627.

[13] Zhao HP, Feng XQ, Yu SW, Cui WZ, Zou FZ. Mechanical properties of silkworm cocoons. Polymer. 2005;46(21):9192-9201.

[14] Chen F, Hodgkinson JM. Impact Damage. Encyclopaedia of Composites: Wiley Publishing, 2011.

Chapter 7

Synthetic Cocoon Composites

7.1 Introduction

Silk fibre is an interesting candidate as a reinforcement material for natural fibre composites, as it is not only a natural fibre which is biodegradable and environmentally friendly, but also an engineering fibre with an attractive combination of strength and toughness [1]. However, as a biological product, it evolves in nature to form a nonwoven structure as a cocoon for protecting the silkmoth [2]. A cocoon can be regarded as a sheet construction, which is easy to handle and cheap for composite manufacturing processes.

Most of the 'silk composites' developed so far use regenerated silk protein with inferior mechanical properties, rather than native silk fibres [3]. Silk protein can be regenerated into different forms, e.g. regenerated fibre, film, foam, hydrogel and sphere. They are then used to make composites by combining with other synthetic polymers and biopolymers, and even inorganic particles. These biocomposites are used for textiles and biomedical applications. However, silk protein loses its distinctive molecular structure, e.g. ß sheet structure, and mechanical advantages through the regeneration process [4], and such a material is not applicable for conventional fibre reinforced composites. There are also studies on natural silk fibre reinforced composites. Most of the work focuses on short fibres or wasted fibre fabric reinforced composites (Table 7.1). These reinforcements do not have good mechanical properties, since the unique advantages of silk fibres, e.g. high toughness, cannot be

expressed efficiently in the form of short fibres in the composites. These reinforcements can only marginally improve the composite properties.

Table 7.1 Literature survey of silk fibre composites.

Resin	Fibre	Mechanical properties	Reference
Poly(butylene succinate) (PBS)	30wt% short fibres	Tension and flexure	Lee et al. [5]
Poly(butylene succinate) (PBS)	20-50wt% short fibres	Tension and flexure	Han et al. [6]
Poly(butylene succinate) (PBS)	5-40wt% short fibre paper laminate	Tension, flexure and impact	Song et al. [7]
Poly(ε-caprolactone) (PCL)	15-65wt% short fibres	Tension and flexure	Li et al. [8-10]
Polypropylene (PP) and natural rubber	20wt% short fibre layer	Tension, flexure and impact	Shubhra et al. [11, 12]
Nitrile rubber	5-25wt% short fibre	Tension, tear, abrasion and compression	Setua et al. [13]
Gelatin	20wt% short fibre layer	Tension, flexure and impact	Shubhra et al. [14]
Poly(lactic acid) (PLA)	5-95wt% short fibres	Tension	Cheung et al. [15, 16]
Poly(lactic acid) (PLA)	5wt% short fibres	Tension and flexure	Ho et al. [17]
HDPE	3-6vt% short fibres	Tension	Kocak et al. [18]
Epoxy	5-25wt% fabric	Tension, compression, flexure and impact	Priya et al. [19-21]
Polyester (UPE)	Sisal/silk short fibres Coir/silk short fibres	Tension, compression and flexure	Noorunnisa et al. [22, 23]
Regenerated silk fibroin	10-25wt% long fibre laminate	Tension and compression	Yuan et al. [24]

In this Chapter, silk cocoon is used as a reinforcement to develop artificial nonwoven composites with different compatible matrix resins, and study the bonding, processing and mechanical properties of the modified composites.

7.2 Background of Composites

Polymer matrix composites now make up a very broad and important class of engineering materials. They are used in a wide variety of applications, such as aerospace, automotive and wind turbines. A polymer composite usually consist of a continuous resin matrix reinforced by fibres. In structural applications, the fibres sustain the external applied load in the composite structure and provide the mechanical strength and stiffness. The polymer matrix usually transfers the load and keeps the general structural form [25].

7.2.1 Resin Matrix

In this project, resin matrix systems are selected based on their potential chemical compatibility to silk fibres. Epoxy, polyurethane and regenerated silk fibroin are chosen because they all have hydroxyl groups in their molecular structures, which can be used for bonding silk fibres/sericin.

7.2.1.1 Epoxy

Epoxy resin is a common thermosetting resin used for composite manufacturing. It can crosslink during curing, i.e. strong covalent bonds form between polymer chains after application of heat, pressure or catalysts through a curing agent or hardener [25]. Epoxy resin is generally considered to have good mechanical properties and high adhesive strength for high performance composites.

The molecular structure of epoxy resin is based on the epoxy, or oxirane, ring group, consisting of two carbon atoms bridged by an oxygen atom, which opens to bond pairs of molecules and leave a polar hydroxyl group. Many commercial epoxy resins are based on diglycidylethers of bisphenol A (DGEBA). The epoxy group is reacted with amine groups,

for example, in a hardener to form a crosslinked thermoset resin during the cure process. Curing agents may be necessary as they accelerate amine reactions, especially when room temperature, pressure and short curing time are required in contact moulding processes, for example [26]. The number of hydroxyl groups, which is potentially important for bonding silk fibres, varies with different kinds of epoxy.

7.2.1.2 Polyurethane

Polyurethane is not often used for conventional composite processing. However, its advantages as a resin matrix also attract some interest. Polyurethane crosslinks rapidly, usually within a few minutes, and it requires only room temperature to cure. It can be used as a tough matrix, as it has a much greater impact strength and strain to failure compared to most of other resins. Also, it generally adheres very well to fibres [26].

Polyurethane is made by a reaction of an organic isocyanate with a polyol, which contains multiple hydroxyl groups. Isocyanate generally has a form of [R-N=C=O] in which R is a large aromatic group. The [-N=C=O] group is also extremely reactive and can react with any hydroxyl group to combine and form many different polymer structures. Polyurethanes are generally good adhesives [26].

7.2.1.3 Regenerated silk fibroin

Silk fibroins can be dissolved in aqueous systems, and then reprocessed into different material forms. This is so called regenerated silk fibroin (RSF). In the standard procedures, degummed silk fibres are dissolved in lithium bromide and then cleaned by dialysis in water

to obtain the protein aqueous solution. Regenerated silk film can be cast by drying the solution in the air [27].

The properties of this RSF silk film depend on its molecular and morphological structure, which consists of amorphous and ß-sheet crystal domains [28]. There is no clear conclusion yet how these two structures quantitatively control the mechanical behaviour of regenerated silk film, but loss of the intrinsic nanoscale semicrystalline morphology during solvation of the native silk fibres seems to be important in the loss of strength and toughness relative to native fibres. Literature shows that both protein size (molecular weight) [29], [30] and [31], and protein conformation [29] and [32] can be altered significantly by the elevated temperatures and highly chaotropic agents during the processing, leading to a wide range of different properties reported for RSF films [33-38].

7.2.2 Reinforcement

Traditional composite properties are strongly dependent on the fibre architecture, i.e. the arrangement and the distribution of the fibres. This includes features of fibres, e.g. diameter and length, as well as the fibre volume fraction and their alignment and packing arrangement [39]. The most widely used fibre architecture is lamina, which is a sheet containing aligned long fibres, and laminated composites are built up from stacking the laminae with adjacent plies at different angles to each other. Continuous fibres can also be produced in a variety of geometrical forms using textile technology, e.g. weaving, braiding and knitting. The incorporation of the reinforcement is usually aimed at enhancing the stiffness and strength of the matrix for high-performance structural applications. In this case, the fibre alignment and fibre volume fractions are important for the mechanical properties of the composites [39].

The other commonly used form of fibre distribution is chopped strand mat. Bundles of relatively long fibres are assembled together with aligned or random in-plane orientations. The shear lag model is probably the most widely used model for analyzing the mechanical properties of short fibre composites with aligned fibres. Originally proposed by Cox [40] and then developed by others, it describes the effect of loading a composite in which the tensile stress transfers from matrix to fibre by means of interfacial shear stresses (See Chapter 4 for more literature reviews). However, the connectivity model in Chapter 4 shows that the bonded interconnections between the fibres, is more important for the mechanical properties of a random fibre composite. The strain transfers from the fibre to the relatively weak matrix bonding, leading to the collapse of the connectivity and then the stiffness and strength of the composite structure [41].

7.2.3 Interfacial wettability

The interface between fibre and matrix is very important for the mechanical properties of composites. The load acting on the matrix is transferred to the fibre via the interface. In this case, the fibre has to be strongly bonded to the matrix to provide its mechanical properties to the composites. The fracture behavior also depends on the properties of the interface. A strong interface could have the reinforcement imparting its mechanical strength and modulus to the composite, but it could also induce a brittle failure mode and a low resistance to fracture. A weak interface could produce low mechanical strength and modulus but a high resistance to fracture and a tough failure mode [25, 39].

An intimate contact is essential for adhesion between the fibre and matrix. Usually matrix is applied in a form capable of flowing and behaving like a liquid. In this case, a key concept of

wettability is brought in for illustrating the spread of the liquid matrix on a solid reinforcement. A good wettability means a matrix can flow over the reinforcement and cover the whole surface. This can initiate the bonding and formation of the interface. It can only happen if the viscosity of the matrix is relatively low and a thermodynamic driving force exists [25, 39].

Surface energy, Υ, is often used to express the spreading coefficient, SC, as

$$SC = \gamma_{SG} - (\gamma_{SL} + \gamma_{LG}) \tag{0.15}$$

$\gamma_{SG}, \gamma_{LG}, \gamma_{SL}$ refer to solid-gas, liquid-gas and solid-liquid interfaces respectively. The gas phase is usually air. Usually, SC is positive for wetting, which means that if γ_{SG} is similar to or less than γ_{LG} then wetting cannot occur [25].

Contact angle, θ is a term which is used as a measure of the degree of the wettability. It is obtained by a balance of horizontal forces

$$\gamma_{SG} = \gamma_{SL} + \gamma_{LG} \cos\theta \tag{0.16}$$

For a contact angle of 180°, the liquid drop is spherical and no wetting occurs. On the other hand, perfect wetting takes place if the contact angle is 0°. In most cases, θ would have an intermediate value, i.e., 0°< θ <180°. The degree of wetting goes up as θ decreases [25].

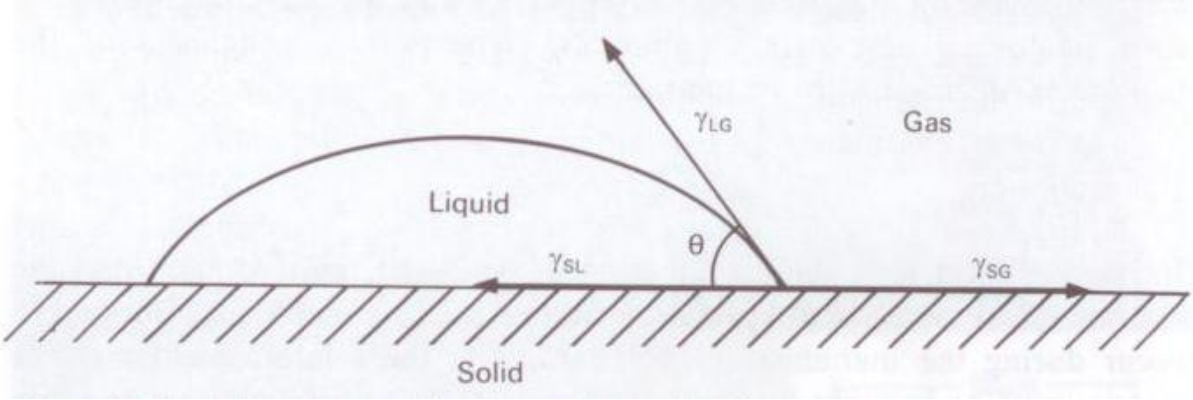

Figure 7.1 Contact angle θ and surface energies Υ for a liquid drop on a solid surface [25]

However, contact angle not only reflects the energy of a solid surface but also the topography. On a rough surface, the contact angle is larger than on chemically identical and smooth surfaces. If roughness is the main contributor, equation (0.16) would not be appropriate [42].

If a fibre interfaces with a liquid resin, the angle of the droplet may be greater than the contact angle between these two phases with the same material with a simple film surface due to the geometry. Literature suggests that liquid spreading increases both surface area and the hydrostatic pressure inside the droplet, which changes the local balance indicated by equation (0.16) [43].

7.3 Materials and Methods

7.3.1 Materials

Bombyx mori silkworms were raised in a laboratory (23±2 °C, 60% relative humidity) and fed with mulberry leaves until they spun cocoons in a dark environment. Their cocoons were collected after the pupae had left them through one end.

Epoxy Ampreg 20 system from Gurit was used in this project. The resin and the hardener from the system were mixed in a weight ratio of 4:1. Silk cocoons were cut into tensile test samples (See Section 3.2.3), and then placed in in 50 ml falcon tubes, submerged inside the aqueous resin. A Jouan MR 1812 Centrifuge was used to mix the resin and the cocoon samples. After spinning in the centrifuge for 5 mins in a speed of 5000 rpm, the samples were taken out of the resin and allowed to cure at room temperature for 16 hours.

AP10/65 polyurethane from Tiranti was mixed with its hardener in a weight ratio of 2.4:1. This resin was cured at room temperature for 5 minutes, so it was applied to the silk materials immediately after being mixed. The sample manufacturing method is the same as epoxy composite sample manufacturing.

Regenerated silk fibroin (RSF) solution was prepared from degummed cocoons dissolved in lithium bromide solution. The fresh cocoons were cut open to obtain two hemispheres. The pupae and other debris were removed from the cocoons. The cocoons were chopped into small pieces, and then put into 0.5 %w Na_2CO_3 solution. The solutions with the cocoon pieces were heated at 70°C for 1 hour with vigorously agitation for degumming the silk fibres. Then they were washed with cold tap water for 45 minutes three times and dried at 40°C for 24 hours. The cocoon pieces were then dissolved in 9 mol l^{-1} lithium bromide solution with a concentration of 250mg/ml, and then dialysed and dried at 5°C. RSF solutions were collected after different times to obtain different protein concentrations, and preserved at 5°C. Their protein concentrations were calculated by drying the solutions in air for 24 hours and comparing the wet and dry weights. The complete protocol for the preparation of RSF, developed by Mr Maxime Boulet-Audet, is given in Supplementary Information. Three

batches of RSF solution were produced in this project. Their silk fibroin protein content are 4.2%, 13.6% and 22.5%.

7.3.2 Contact angle measurement

Cocoons samples were cut to have a relatively flat surface and bonded on slides using double sided adhesive tapes. Resin liquid was placed in a disposable syringe. Water was also used for reference. A drop was placed on the cocoon sample each time by pushing the syringe. A camera was used to obtain an initial live image. The height of the camera was adjusted to look horizontally at the drop and pictures were taken for analysis using Adobe Photoshop CS4. The RSF solution used in this experiment has 22.5% of silk protein.

7.3.3 Single fibre coating and testing

The fibre-matrix bonding was measured through a fibre coating test. Natural cocoon silk fibres were carefully unravelled from the surface of an intact cocoon using standard techniques (See Chapter 3). A fibre was then fed though a pipette tip and the two ends were fixed. Resin solution was poured into the pipette tip and run down the fibre length thus coating the fibre, which was air-dried for 12 hours. The coated fibres were then collected for mechanical testing to evaluate the interfacial bonding. The RSF solution used in this experiment has 22.5% of silk protein.

Degummed silk fibres were used for RSF coating for comparison between the coatings of natural sericin and manmade RSF. The silk fibres were degummed by 0.5%w sodium carbonate (Na_2CO_3) solution for 2 hours to remove the sericin before coating with RSF. Instron 5582 was used to show the fracture process of silk fibres. Both natural fibres and RSF

coated fibres were mounted onto paper frames with a gauge length of 10 mm by supergluing their two ends. They were then fixed by the clamps of the Instron and pulled with a speed of 0.01min^{-1}. The tests were stopped at different tensile strains, and samples with different fracture degree were then collected for SEM observation and comparison. The average fragmented length was measured using SEM. The RSF solution used in this experiment has 22.5% of silk protein.

7.3.4 Composites manufacturing

In this study, undegummed silkworm cocoon strips were cut by using a blade to create bone-shape samples with a width of 5 mm and a length of 15 mm. The samples were submerged individually in 2 cm^3 resin in Eppendorf tubes, and then put in a centrifuge for spinning for 10 mins to push the resin into the cocoon. The composites were then transferred on a plate and covered by peel plies and breathing cloths from Easycomposite Co. on two sides for curing. After curing, the cocoon composites were transferred and the excess matrix was cut away. Both cocoon samples and composites were weighed to calculate the fibre content of the composites.

7.3.5 Thermogravimetric analysis (TGA)

TGA studies were conducted with a TA instruments Q500 Thermogravimetric Analyser at the rate of 10 ºC min^{-1}. The TGA was weight calibrated at ambient temperature using 100 mg & 1g weights. A two point (154 & 358ºC) temperature calibration was carried out prior to sample analyses to ensure accuracy in the temperature scale. Certified Curie standards (Nickel & Alumel) were used for the purpose of temperature calibration. The samples were prepared using a hole punch to cut disks from the bulk sample with a diameter of 4.5 mm.

The samples were then placed directly into the Platinum TGA sample holders, loaded onto the TGA and heated at 10°C/min in a flowing Nitrogen gas atmosphere (100 ml/min).

7.3.6 Mechanical testing and scanning electron microscopy (SEM)

All samples were produced and initially tested using the standardised protocols as outlined in Chapter 3. The specifics of each experiment will be introduced as they are encountered in the chapter.

7.4 Results

7.4.1 Fibre-matrix bonding

RSF droplets spread spontaneously along the undegummed fibre as the surface tension favours wetting, but it forms an uneven coating layer on the surface of the fibre. However, both epoxy and polyurethane form regular droplets on the fibre surface and not much resin coating can be found on the fibres (Figure 7.2).

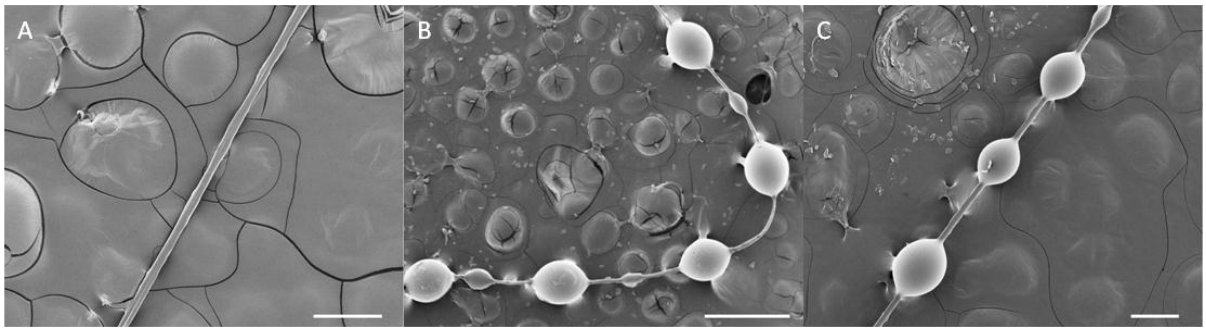

Figure 7.2 Silk fibre coating by matrix solution: (A) 22.5% regenerated silk fibroin solution (RSFS), scale bar: 200 μm (B) epoxy, scale bar: 500 μm (C) polyurethane, scale bar: 200 μm

Quéré [44] summarized in his review that the coating film can break into a periodic array of droplets because of the liquid surface tension when coating fibres. It is still debated whether a film can remain between the drops. From our experimental result, both epoxy and polyurethane cannot properly interact with the individual fibres, unlike the RSF due to the liquid surface tension.

Both the natural sericin and RSF coating on the fibre surface break at 3-5% strain when the fibres are stretched. Interestingly, the breaking strains of both coatings are about the same as the breaking strains of the coating matrices (Table 7.5) [41]. The average length of coating fragments is 3.19±1.77 μm and 2.03±0.80 μm for RSF and sericin, respectively (Figure 7.3). As the RSF coating performs similar to the natural sericin coating, it indicates good bonding strength between RSF and the silk fibroin fibres.

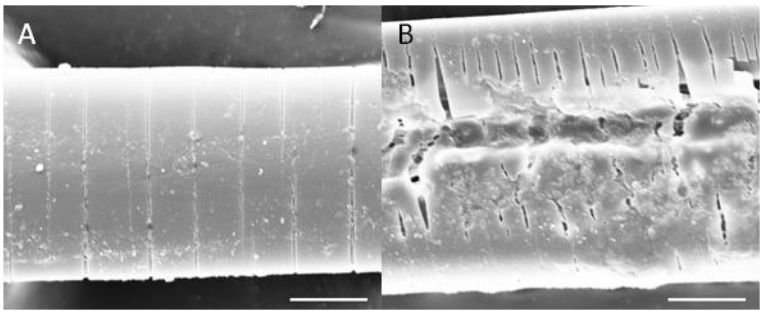

Figure 7.3 Silk fibre coating breakage under tensile force: (A) degummed silk fibre coated by regenerated silk fibroin (22.5%) at 4% strain (B) natural silk fibre at 5% strain. Scale bar: 10μm

This sericin fragmentation effect has been observed by Jauzein et al. [45]. They measured the critical half length between sericin sheath cracks as 17.8 μm to estimate a maximum shear stress at the interface of 145 MPa. This study was based on silk yarns consisting of multiple fibres bonded together by their sericin sheaths, somewhat like a parallel fibre composite.

Also, the material property values they used in their analysis, such as a modulus of 14.8 GPa for the tensile modulus of sericin and a radius of 22.4 μm for the radius of the silk yarns are very different from observations in our laboratories, where the sericin does not actually contribute to the measured tensile modulus of individual undegummed fibres [46, 47]. The original Kelly-Tyson model for composite fibre fragmentation in a matrix material [48] is inappropriate for a layer of matrix material coating a single fibre, where the matrix material sheath is weaker than the fibre. Bazhenov *et al* [49] looked at the fragmentation of a relatively brittle coating on a ductile layer and showed that the Kelly-Tyson approach of a stress balance at the interface between fibre and coating can be adapted for short coating fragmentation lengths with an approximate form

$$l_c \approx \frac{4\,h\,\sigma_m}{\sigma_f} \qquad (7.3)$$

Where l_c is the critical coating fragment length, h is the thickness of the coating, σ_m is the ultimate tensile strength of the coating, and σ_f is the stress in the fibre substrate layer, assuming a simple planar geometry as a first approximation.

The ratio σ_m/σ_f can be taken to be the ratio of the tensile moduli of the sericin and fibroin materials in GPa as about 4/10 = 0.4 at the failure strain of about 4% for the sericin, such that for a sericin coating thickness is about 1 μm (very approximately and very varied) then the critical fragmentation length must be about 1.6 μm, which is of the correct order for the observed fragmentation of about 2 μm. A more detailed geometrical analysis of the Bazhenov model may give some improvements to the analysis presented here, but the overall framework shows that the Kelly-Tyson model as used by Jauzein is probably inappropriate as

a direct application of the original single fibre fragmentation model to the observations on single fibres presented here.

7.4.2 Contact angle measurement

Both water and RSF solution are found to form a droplet on the cocoon surface, and their contact angles are shown in Table 7.2. But both epoxy and polyurethane resin with hardeners can be completely absorbed by cocoon materials within seconds once they were applied to the undegummed natural cocoons (Figure 7.4).

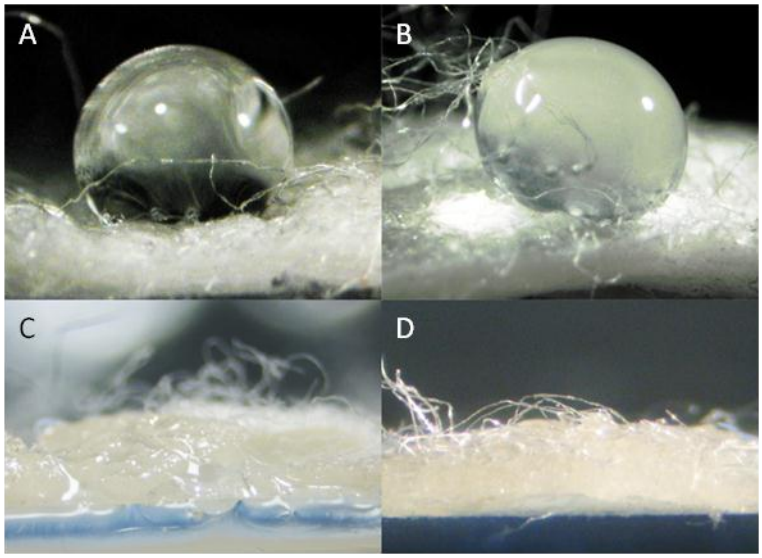

Figure 7.4 Wettability of cocoons with different matrix solution: (A) water, (B) regenerated silk fibroin solution, (C) epoxy, (D) polyurethane

The results of measured contact angle can only be used as a qualitative reference comparison. Cassie et al. [50] have proposed the factors controlling wettability on porous surface are (1) solid-liquid contact angle and (2) relative size of the fibre and the hole between fibres. A cocoon surface follows this model whereby the apparent surface tension is modified from the original silk fibre surface tension due to the cocoon porosity. It helps to reduce the difference

of surface tension between epoxy/polyurethane and silk for the resin to impregnate the cocoon. On the other hand, a cocoon has evolved to have a surface tension which can protect the silkmoth from being drowned by preventing water from remaining on its surface, despite silk sericin coating on the fibre being hydrophilic. Although there is no report on surface energy of RSF, we can deduce its high surface tension as its water content is more than 70%. In our composite manufacturing process, we used centrifuge spinning to force the RSF into the cocoon to interact with the silk fibres.

Table 7.2 Contact angles against cocoons with different binders

Materials	Water	Regenerated silk fibroin solution (13.6%)
Contact angle against cocoon (°)	43.7±5.2	26.3±1.5

Table 7.3 Surface energies of different liquid in air [25]

Materials	Water	Regenerated silk fibroin	Epoxy	Polyurethane
Surface Tension ϒ in air (dynes/cm)	72	-	47	43

7.4.3 Cocoon composites morphology

Figure 7.5 shows the morphologies of the silk cocoon composites. All the chosen resins manage to form bonding between fibres. Epoxy cocoon composites have the least porosity, which indicates the epoxy can significantly increase the connectivity on the cocoon surface. All the other resins can also increase the bonding connections in the composites to different

degrees. The matrix contents of RSF composites increase with the protein content of RSF (Table 7.4). A RSF resin with 36.2% silk fibroin protein content was unable to permeate the silk cocoons, so it was not used to manufacture composites.

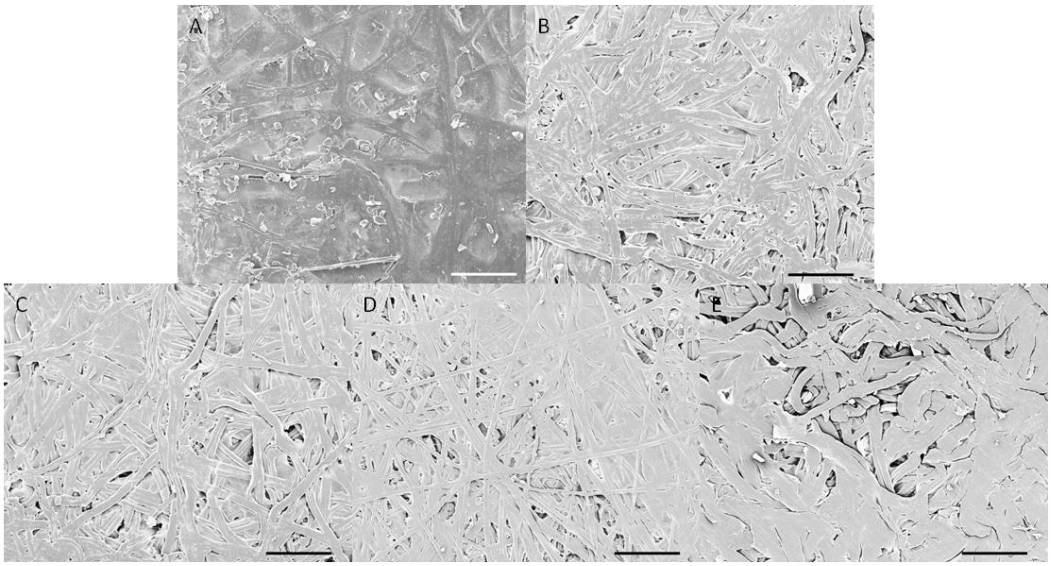

Figure 7.5 Silk cocoon composites with different resin matrix (A) epoxy (B) polyurethane (C) regenerated silk fibroin 4.2% concentration (D) regenerated silk fibroin 13.6% concentration (E) regenerated silk fibroin 22.5% concentration. Scale bar: 200 μm

7.4.4 Thermal properties

Figure 7.6 shows the TGA thermal degradation profiles of different types of Resin-Cocoon composite matrices. The Cocoon (control sample) was found to have a weight loss of 7.5% between ambient and 141°C (T_w) which contribute to water loss from its structure. Water was found to leave the cocoon as soon as heating commenced with a maximum rate of weight loss at 41°C. This is observed in the derivative weight loss signal. The rate of thermal degradation of the cocoon was a maximum at 311°C (T_d). The RSF cocoons were found to have a similar water content and onset of thermal degradation to that observed for the cocoon, which is expected since structurally they are very similar in nature. In this case fibre volume fractions of RSF cocoon composites with different protein content cannot be

quantified through this technique. The cocoon composite constructed with epoxy was found to have greater thermal stability, with the maximum of thermal degradation increasing by over 30°C compared to the cocoon and RSF composites. It also had significantly lower water content (approx. 3%). The polyurethane composite also exhibited lower water content (approx. 5%) and interestingly it was found to have a lower thermal degradation temperature (approx. 180°C) than all other samples investigated in this study. The main decomposition of the polyurethane composite was found to compare well with the cocoon and RSF composite samples (between 250 & 350°C).

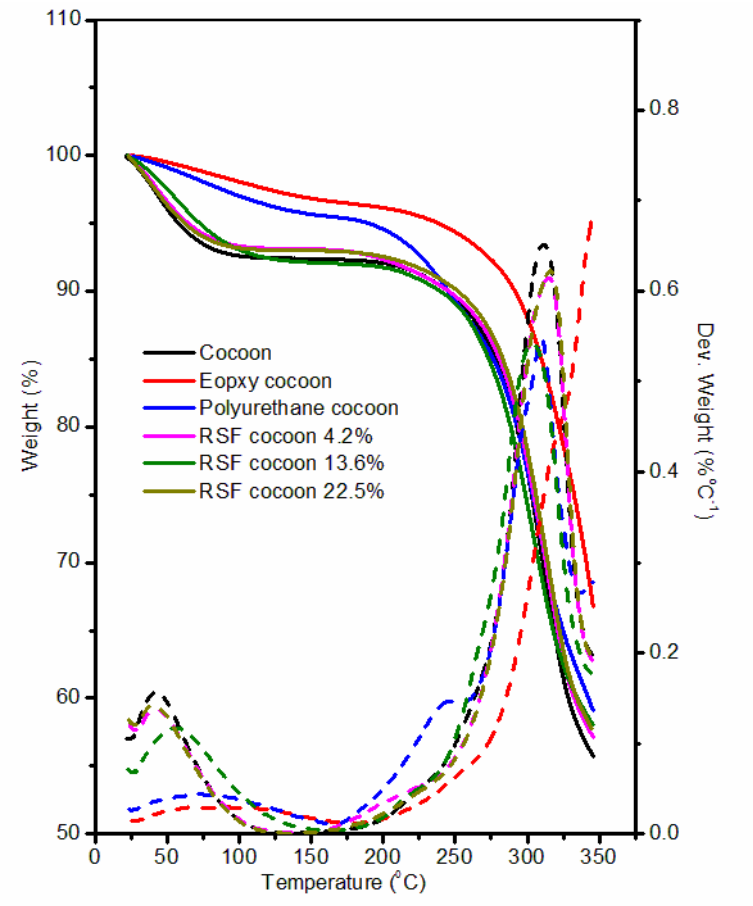

Figure 7.6 TGA thermograms of cocoon and composites

7.4.5 Mechanical properties

The stress-strain curves of silk cocoon composites are shown in Figure 7.7 and the breaking mechanisms of cocoon composites are shown in Figure 7.8. When the epoxy composite is stretched, the failure of epoxy propagates into the fibres, leading to a fibre breakage in the composite system. In the polyurethane and RSF cocoon composites, the resin bonding breaks within the sericin layer, and the fibres debond from each other when the strain increases. After the bonding percolation threshold occurs, the composite fails and the fibres disentangle with the increasing strain.

The effects of different resins on cocoon composites are shown in Figure 7.9 and Table 7.4. Considering the variation of the results, the resin matrices only marginally affect the cocoon modulus. Epoxy cocoon composites have a relatively high modulus before the strain reaches 3%. The epoxy resin with a breaking strain of 3.3% (Table 7.5) breaks along the fibres and only the silk cocoons themselves sustain the force at higher strains. This appears as a drop in the modulus in stress-strain curves and a similar mechanical strength of the composite is observed compared to natural cocoon. The matrixes also have little effect on composites strength, given the big statistical variations.

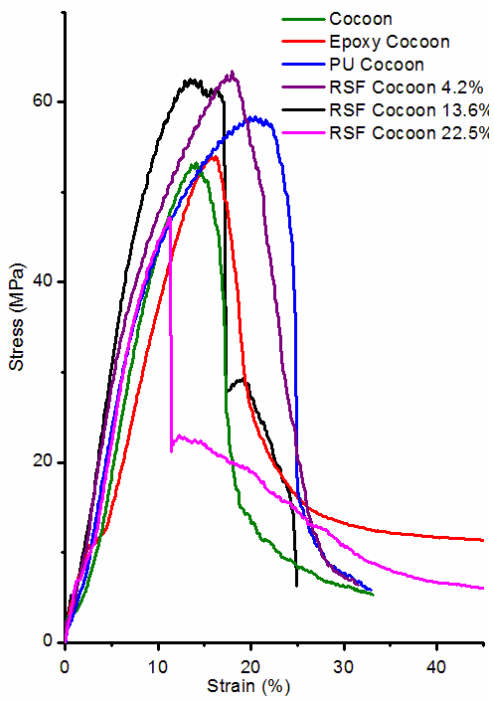

Figure 7.7 Mechanical behaviour of silk cocoon composites

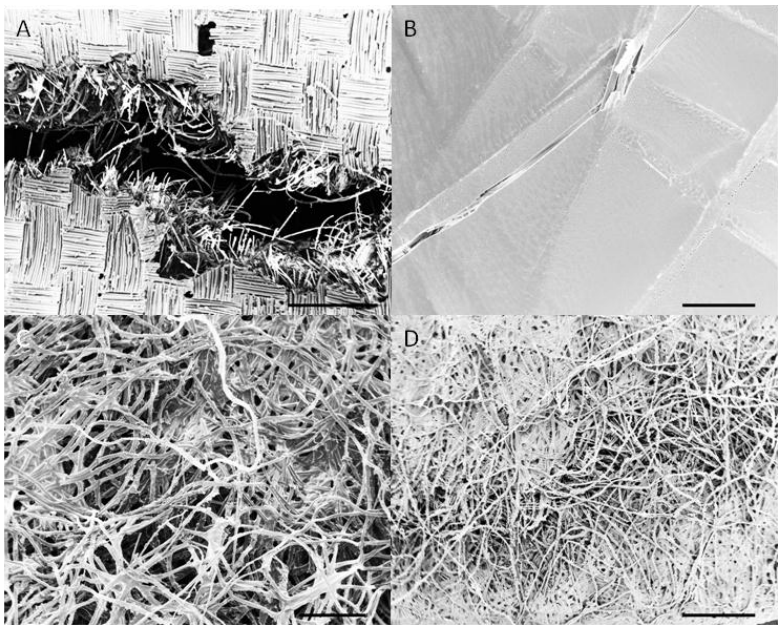

Figure 7.8 Fracture mechanism of silk cocoon composites with resin matrix (A) epoxy, scale bar: 1mm (B) epoxy at 3%strain, scale bar: 100 μm (C) polyurethane, scale bar: 500μm (D) regenerated silk fibroin, scale bar: 1mm

However, the effects on the strain at maximum stress of cocoon of resin matrixes are statistically significant. It implies that the increasing connectivity in the cocoon could change the percolation threshold of the composite system (Figure 7.9). For RSF cocoon composites, the strain at maximum stress of the composite decreases with the increasing concentration of RSF resin. Although cocoon composites with low-concentration RSF have a fibre debonding and disentanglement mechanisms, the composite with RSF-22.5% has a dramatic drop in stress level at about 50 MPa, which is the breaking stress of the RSF (Table 7.5). A model to describe the damage mechanism of cocoon composites has been developed in Chapter 4 [41, 51]. It shows the cocoon connectivity could break in a brittle mode if the stress level has reached the threshold failure stress of the binder, which fits the results of composites with high-concentration RSF.

Polyurethane resin significantly increases the percolation strain of composites due to its ductile nature (Table 7.5). From our model in Chapter 4, the properties of the bonding agent would change the first activation strain of the cocoon. A bonding agent with a high breaking strain can increase toughness and percolation strain of the composites.

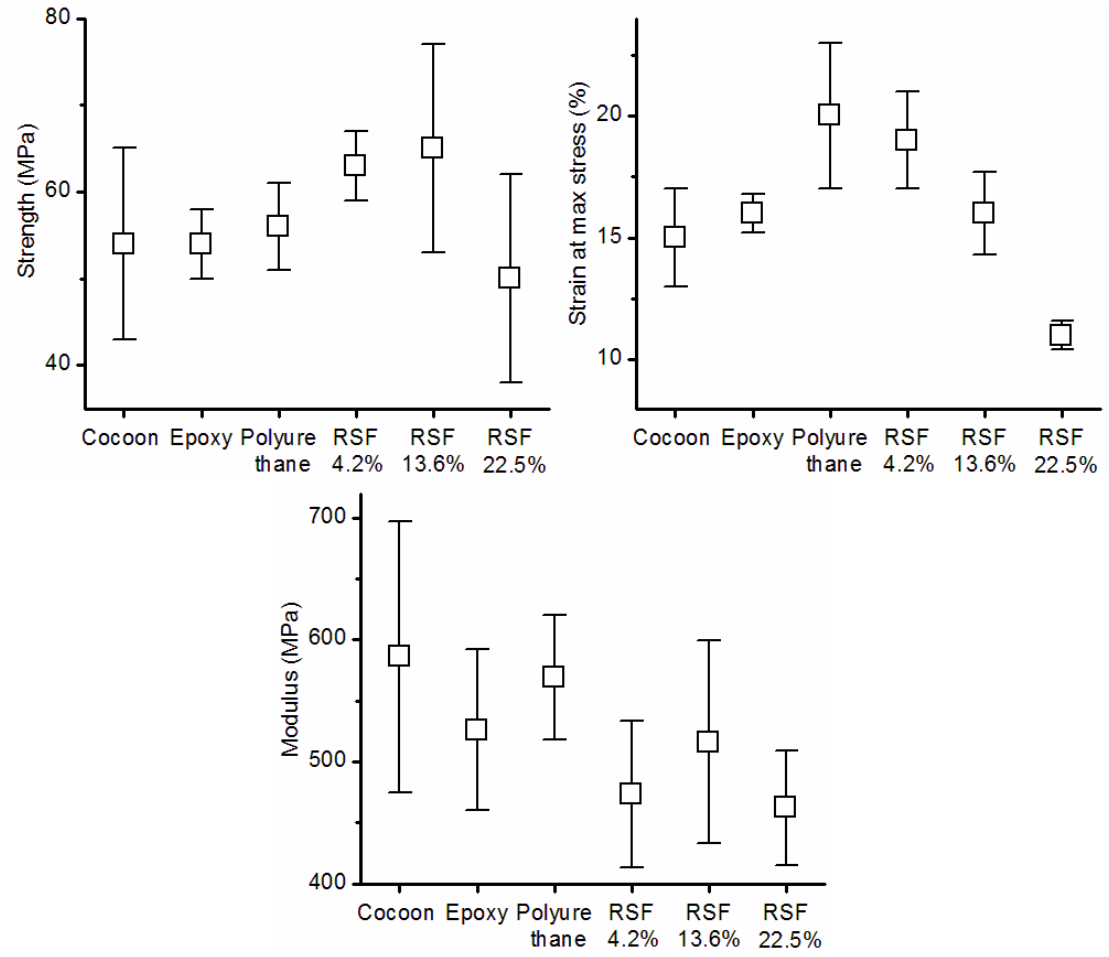

Figure 7.9 Relationship between mechanical properties and composites resin matrix

Table 7.4 Mechanical properties of silk cocoon composites

	Matrix weight content (%)	Max load (N)	Strength (MPa)	Breaking strain (%)	Modulus (MPa)	Strain at max stress (%)

Cocoon (*B. mori*)	-	115±36	54±11	35±8	586±111	15±2
Epoxy cocoon	71±1	376±13	54±4	44±1	526±66	16±1
Polyurethane cocoon	55±3	162±21	56±5	40±6	569±51	20±3
RSF 4.2% cocoon	6±1	159±30	63±4	34±11	473±60	19±2
RSF 13.6% cocoon	13±2	106±11	65±12	33±10	516±83	16±2
RSF 22.5% cocoon	51±2	151±12	50±10	67±4	442±55	11±1

Table 7.5 Mechanical properties of resin matrixes

	Density (kg/m3)	Strength (MPa)	Breaking strain (%)	Modulus (MPa)
Ampreg20 cast epoxy [52]	1148	72	3.3	3700
Polyurethane [53]	1050	4	932	0.8
RSF cast film [54, 55]	1345	47.2	1.9	3900

7.5 Discussion and Conclusions

As silk cocoon is a highly evolved nonwoven material system. It has a multi-layer porous structure with strong and tough properties for protecting the pupa from environmental threats, such as penetration, tearing or indentation of the cocoon wall. In this case, a silk fibre is optimised to be tough for bending but not necessarily stiff for stretching. It adapts to the cocoon nonwoven structure in which the fibre bears little load compared to parallel fibre laminate composites. In contrast, cellulose fibre, which is another candidate for developing natural fibre composites, evolved to have high stiffness and low flexibility for supporting

biological structures rather than unravelling in a fibre mat structure. It is proposed that silk cocoon can be a good candidate for making nonwoven natural fibre composites with these material and structural benefits.

As a nonwoven fibre mat, silkworm cocoon composite has a similar failure mechanism to manmade fibre mats from other natural fibres, e.g. hemp [56], sisal [57], flax [58], alfa [59]. The failure of the composites initiates in the interfibre bonding, which is expressed as a drop in modulus in stress-strain curves. The fibres gradually debond and the structure unravels, until the fibres support the applied force and fracture. This mechanism is mainly due to the bonded random fibre structure rather than the fibre properties. The weaker resin gradually breaks and transfers the load to the rotating fibres, leading to a gradual loss of modulus and increasing toughness. If the fibres are too strongly bonded and cannot rotate, the nonwoven system would expect a catastrophic failure in a brittle mode [41].

Based on an understanding of the cocoon system, synthetic cocoon composites were developed by increasing the connectivity in the natural cocoon using different resin bonding. It started from testing the wetting of fibres and cocoons with different resins. The promising results indicated a good interaction between the silk cocoon and the matrix. Good thermal stabilities were also found from cocoon composites with different matrix resins. Polyurethane increased the toughness of the cocoon by adding more tough bonds in the cocoon system, while brittle epoxy does not have much effect on the mechanical behaviour of cocoons. RSF can vary the composite properties from brittle to tough behaviour, depending on its concentration, i.e. the amount of the bonding it adds in the cocoon nonwoven system.

Supplementary Information

Silk fibroin reconstitution protocol

- Prepare 1L of 70°C Na2CO3 solution.(5g/L)
- Weigh 20g of dry cocoon to degum
- Add 500mL of Elix type II water into the food processor (with the blades).
- Turn on the food processor at maximum speed and pour in the cocoons one by on leave for 15 minutes. It is necessary to cut roughly the cocoons before doing the degumming otherwise fibres can entangle the blender's shaft
- Using gloves, take the blade out before taking the fibres out. Filter the blender's content using coarse mesh to recover most of the fibres before cleaning the food processor with Elix water. Filter the washing water to recover most of the fibres. Wash the fibres by poring helix water in the filter. Wring the fibres and put then in a clean plastic box.
- Fill the food processor with 500 mL of 70°C Na_2CO_3 solution.(5g/L)
- Turn on the food processor at minimum speed and gradually pour in the wrung fibres little by little and leave for 60 minutes (use timers).
- Using gloves take the blade out before taking the fibres out. Filter the blender's content using coarse mesh to recover most of the fibres before cleaning the food processor with Elix water. Filter the washing water to recover most of the fibres. Wash the fibres by poring helix water in the filter. Wring the fibres and put then in a clean plastic box.
- Fill the food processor with 500 mL of 70°C Na_2CO_3 solution.(5g/L)
- Turn on the food processor at minimum speed and gradually pour in the wrung fibres little by little and leave for 60 minutes (use timers).
- Using gloves take the blade out before taking the fibres out. Filter the blender's content using corse mesh to recover most of the fibres before cleaning the food processor with Elix water. Filter the washing water to recover most of the fibres. Wash the fibres by poring helix water in the filter. Wring the fibres and put then in a clean plastic box.
- Fill the food processor with 500 mL of Elix type II water.
- Turn on the food processor at minimum speed and gradually pour in the wrung fibres little by little and leave for 15 minutes (use timers).
- Using gloves take the blade out before taking the fibres out. Filter the blender's content using corse mesh to recover most of the fibres before cleaning the food processor with Elix water. Filter the washing water to recover most of the fibres. Wash the fibres by poring helix water in the filter. Wring the fibres and put then in a clean plastic box.
- Fill the food processor with 500 mL of Elix type II water.
- Turn on the food processor at minimum speed and gradually pour in the wrung fibres little by little and leave for 15 minutes (use timers).
- Using gloves take the blade out before taking the fibres out. Filter the blender's content using corse mesh to recover most of the fibres before cleaning the food processor with Elix water. Filter the washing water to recover most of the fibres. Wash the fibres by poring helix water in the filter. Wring the fibres and put then in a clean plastic box.
- Fill the food processor with 500 ml of Elix type II water.
- Turn on the food processor at minimum speed and gradually pour in the wrung fibres little by little and leave for 15 minutes (use timers).
- Using gloves take the blade out before taking the fibres out. Filter the blender's content using corse mesh to recover most of the fibres before cleaning the food processor with Elix water. Filter the washing water to recover most of the fibres. Wash the fibres by poring helix water in the filter. Wring the fibres thoroughly and put then in a clean plastic box.
- Replace the food processor steel blade by the mixing plastic blade.
- Place the fibres in the blender and blend for 5 minutes until they become small bits.
- Put the fibres in the Mini Oven (blue, under the freeze dryer) at 50°C for drying overnight and label/date the batch.

- Replace the food processor steel blade by the mixing plastic blade.
- Place the fibres in the blender and blend for 5 minutes until they become very small fluffy bits.
- Put the fibres in the vacuum oven overnight and label/date the batch.
- Replace the food processor steel blade by the mixing plastic blade.
- Place the fibres in the blender and blend for 5 minutes until they become a fluffy mass.
- Store the fibres in a clean plastic box with desiccant packs and leave at 5°C.
- Fill in the XP Metadata spreadsheet (degumming section).
- Dialysis tube preparation:
- Cut a 25cm long dialysis tube and immerge in Elix water of few minutes.
- Put tie a strings at the tube base and attach an eppendorf.
- Rinse the tube twice with elix water and test its permeability.
- Keep the tube in Elix water
- Drying tube preparation:
- Cut a 30cm long dialysis tube and immerge in Elix water of few minutes.
- Cut the tip of a 10 mL at its 2 mL mark.
- Cut and seal a needle that fit the syringe.
- Insert the syringe tip inside the dialysis tube and tie with three strings, one at the tip, on the base and one just after the syringe.
- Seal the bottom with parafilm
- Rinse the tube twice and test its permeability.
- Keep the tube in Elix water

Dissolving the silk:

- Prepare 9M LiBr solution (100ml -> 80g LiBr). Place a large beaker and on the balance weight the desired volume of solution (1g = 1mL)
  Draw a line on the beaker, remove half of the water. Add the required amount of LiBr slowly. Attention! Exothermic reaction! Complete the volume to the marked line
  Store in a glass bottle for further use.
- Weight no more than 25% (w/w) of dried and degummed silk. Note the fiber on LiBr ratio (the standard concentration is 250mg/mL)
- Finely cut the fibers using scissors or an herb chopper to obtain fiber less than 1 mm long. The fiber shouldn't have enough entanglement to flow freely thought a liquid funnel. The fibers that don't pass through the funnel must be cut again.
- Heat a water bath to 70°C (or less, note the temperature) with a smaller 40 mL beaker containing 20mL of LiBr solution. Make the water of the bath is stirred and than the bottom of the beaker is not touching the bath to prevent any local heating. The goal is to uniformly heat the beaker.
- Mount the dialysis bag at the end of the funnel while keeping the bag immersed in tall container filled with Elix water.
- Pour the silk fibers in the funnel and stir gently with a glass rod.
- Soak the silk as quickly as possible (2-3 min) to ensure that the whole batch has a similar exposition to the LiBr solution.
- Let solubilise the fibres without stirring for 20 min (note the duration, between the first fibre is soaked and the moment the solution is poured in the funnel).
- Once solubilised pour the silk solution in the funnel into the dialysis bag.
- Once the dialysis bag is filled, seal the top end with a string and a clamp. Close the tall container.

Dialysis:

- Leave the dialysis container in the cold room (~5°C).
- Change the water after 2h, 4 times and leave overnight for a 4th dialysis.
- 1st 2nd 3rd4th 5th (Overnight)
- Test for remaining traces of LiBr by adding silver nitrate to the bottom fraction of the washing water.

Drying:

- Attach the drying bag to a funnel with a filter. Not the type of filter used. Pierce the dialysis bag and transfer the RSF to the drying bag.
- Hang the dialysis bag in the cold room in front a spinning fan.
- Silver nitrate test for LiBr:
- Test wash water by taking 1ml in an eppendorf an adding one-two grains of silver, If it turns black after some time (exposure to light) it is still LiBr in there.

References

[1] Vollrath F, Porter D, Holland C. There are many more lessons still to be learned from spider silks. Soft Matter. 2011;7(20):9595-9600.

[2] Chen F, Porter D, Vollrath F. Morphology and structure of silkworm cocoons. Mat Sci Eng C. 2012;32(4):772-778.

[3] Hardy JG, Scheibel TR. Composite materials based on silk proteins. Progress in Polymer Science. 2010;35(9):1093-1115.

[4] Vollrath F, Porter D. Silks as ancient models for modern polymers. Polymer. 2009;50(24):5623-5632.

[5] Lee SM, Cho D, Park WH, Lee SG, Han SO, Drzal LT. Novel silk/poly(butylene succinate) biocomposites: the effect of short fibre content on their mechanical and thermal properties. Comp Sci Technol. 2005;65(3-4):647-657.

[6] Han OS, Lee MS, Won HP, Cho D. Mechanical and thermal properties of waste silk fiber-reinforced poly(butylene succinate) biocomposites. Journal of Applied Polymer Science. 2006;100(6):4972-4980.

[7] Song R, Kimura T, Ino H. Papermaking from Waste Silk and Its Application as Reinforcement of Green Composite. Journal of Textile Engineering. 2010;56(3):71-76.

[8] Li W, Qiao XY, Sun K, Chen XD. Mechanical and viscoelastic properties of novel silk fibroin fiber/poly(epsilon-caprolactone) biocomposites. Journal of Applied Polymer Science. 2008;110(1):134-139.

[9] Qiao X, Li W, Watanabe H, Sun K, Chen X. Rheological behavior of biocomposites of silk fibroin fiber and poly(ε-caprolactone): Effect of fiber network. Wiley Subscription Services, Inc., A Wiley Company; 2009. p. 1957-1970.

[10] Li W, Qiao XY, Sun K, Chen XD. Effect of Electron Beam Irradiation on the Silk Fibroin Fiber/Poly(epsilon-caprolactone) Composite. Journal of Applied Polymer Science. 2009;113(2):1063-1069.

[11] Shubhra QTH, Alam AKMM, Khan MA, Saha M, Saha D, Gafur MA. Study on the mechanical properties, environmental effect, degradation characteristics and ionizing radiation effect on silk reinforced polypropylene/natural rubber composites. Composites Part A: Applied Science and Manufacturing. 2010;41(11):1587-1596.

[12] Shubhra QT, Saha M, Alam A, Beg M, Khan MA. Effect of matrix modification by natural rubber on the performance of silk-reinforced polypropylene composites. Journal of Reinforced Plastics and Composites. 2010;29(22):3338-3344.

[13] Setua DK, De SK. Short silk fibre reinforced nitrile rubber composites. Journal of Materials Science. 1984;19(3):983-999.

[14] Shubhra QTH, Alam AKMM, Beg MDH. Mechanical and degradation characteristics of natural silk fiber reinforced gelatin composites. Materials Letters. 2010;65(2):333-336.

[15] Cheung H-Y, Lau K-T, Tao X-M, Hui D. A potential material for tissue engineering: Silkworm silk/PLA biocomposite. Com Pt B Eng. 2008;39(6):1026-1033.

[16] Cheung H-Y, Lau K-T, Pow Y-F, Zhao Y-Q, Hui D. Biodegradation of a silkworm silk/PLA composite. Com Pt B Eng. 2010;41(3):223-228.

[17] Ho M-p, Lau K-t, Wang H, Bhattacharyya D. Characteristics of a silk fibre reinforced biodegradable plastic. Com Pt B Eng. 2010;42(2):117-122.

[18] Kocak D, Tasdemir M, Usta I, Merdan N, Akalin M. Mechanical, Thermal, and Microstructure Analysis of Silk- and Cotton-Waste-Fiber-Reinforced High-Density Polyethylene Composites. Polym-Plast Technol Eng. 2008;47(5):502 - 507.

[19] Priya SP, Ramakrishna HV, Rai SK, Rajulu AV. Tensile, flexural, and chemical resistance properties of waste silk fabric-reinforced epoxy laminates. Journal of Reinforced Plastics and Composites. 2005;24(6):643-648.

[20] Priya SP. Impact, Compression, Density, Void Content, and Weight Reduction Studies on Waste Silk Fabric/Epoxy Composites. Journal of Reinforced Plastics and Composites. 2005;24(15):1605.

[21] Priya SP, Rai SK. Studies on the Mechanical Performance of PMMA Toughened Epoxy-Silk and PC Toughened Epoxy-Silk Fabric Composites (vol 25, pg 33, 2006). Journal of Reinforced Plastics and Composites. 2009;28(2):247-248.

[22] Noorunnisa Khanam P, Mohan Reddy M, Raghu K, John K, Venkata Naidu S. Tensile, Flexural and Compressive Properties of Sisal/Silk Hybrid Composites. Journal of Reinforced Plastics and Composites. 2007;26(10):1065-1070.

[23] Noorunnisa Khanam P, Ramachandra Reddy G, Raghu K, Venkata Naidu S. Tensile, Flexural, and Compressive Properties of Coir/Silk Fiber-reinforced Hybrid Composites. Journal of Reinforced Plastics and Composites. 2010;29(14):2124-2127.

[24] Yuan Q, Yao J, Chen X, Huang L, Shao Z. The preparation of high performance silk fiber/fibroin composite. Polymer. 2010;51(21):4843-4849.

[25] Matthews FL, Rawlings RD. Composite materials: engineering and science. CRC Press, 1999.

[26] Bunsell AR, Renard J. Fundamentals of fibre reinforced composite materials. Institute of Physics Publishing, 2005.

[27] Nazarov R, Jin HJ, Kaplan DL. Porous 3-D scaffolds from regenerated silk fibroin. Biomacromolecules. 2004;5(3):718-726.

[28] Vepari C, Kaplan DL. Silk as a Biomaterial. Progress in Polymer Science. 2007;32:991-1007.

[29] Zuo B, Dai L, Wu Z. Analysis of structure and properties of biodegradable regenerated silk fibroin fibers. Journal of Materials Science. 2006;41(11):3357-3361.

[30] Yamada H, Nakao H, Takasu Y, Tsubouchi K. Preparation of undegraded native molecular fibroin solution from silkworm cocoons. Mater Sci Eng C-Biomimetic Mater Sens Syst. 2001;14(1-2):41-46.

[31] Iridag Y, Kazanci M. Preparation and characterization of *Bombyx mori* silk fibroin and wool keratin. Journal of Applied Polymer Science. 2006;100(5):4260-4264.

[32] Asakura T, Kuzuhara A, Tabeta R, Saito H. Conformation Characterization of Bombyx-Mori Silk Fibroin in the Solid-State by High-Frequency C-13 Cross Polarization Magic Angle Spinning Nmr, X-Ray-Diffraction, and Infrared-Spectroscopy. Macromolecules. 1985;18(10):1841-1845.

[33] Martel A, Burghammer M, Davies R, DiCola E, Panine P, Salmon JB, Riekel C. A microfluidic cell for studying the formation of regenerated silk by synchrotron radiation small- and wide-angle X-ray scattering. Biomicrofluidics. 2008;2(2):024104-024111.

[34] Jin LW, Claborn KA, Kurimoto M, Geday MA, Maezawa I, Sohraby F, Estrada M, Kaminsky W, Kahr B. Imaging linear birefringence and dichroism in cerebral amyloid pathologies. Proceedings of the National Academy of Sciences of the United States of America. 2003;100(26):15294-15298.

[35] Viney C. Natural silks: archetypal supramolecular assembly of polymer fibres. Supramol Sci. 1997;4(1-2):75-81.

[36] Knight DP, Vollrath F. Method and Apparatus Performing Objects. Great Britain; 2002.

[37] Foo CWP, Bini E, Huang J, Lee SY, Kaplan DL. Solution behavior of synthetic silk peptides and modified recombinant silk proteins. Applied Physics A: Materials Science & Processing. 2006;82(2):193-203.

[38] Inoue S, Tanaka K, Arisaka F, Kimura S, Ohtomo K, Mizuno S. Silk fibroin of Bombyx mori is secreted, assembling a high molecular mass elementary unit consisting of H-chain, L-chain, and P25, with a 6 : 6 : 1 molar ratio. Journal of Biological Chemistry. 2000;275(51):40517-40528.

[39] Hull D, Clyne TW. An introduction to composite materials. Cambridge University Press, 1996.

[40] Cox HL. The elasticity and strength of paper and other fibrous materials. British Journal of Applied Physics. 1952;3:72.

[41] Chen F, Porter D, Vollrath F. Silkworm cocoons inspire models for random fiber and particulate composites. Physical Review E. 2010;82(4):041911-041917.

[42] Kwok DY. Contact angle measurement and contact angle interpretation. Advances in Colloid and Interface Science. 1999;81(3):167.

[43] Hodzic A. Droplet on a fibre: Surface tension and geometry. Composite interfaces. 2001;8(6):415.

[44] Quéré D. Fluid coating on a fiber. Annual review of fluid mechanics. 1999;31(1):347.

[45] Jauzein V, Bunsell A. Bio-composite aspects of silk: the sericin sheath acting as a matrix. Journal of Materials Science. 2012;47(7):3082-3088.

[46] Guan J, Porter D, Vollrath F. Silks cope with stress by tuning their mechanical properties under load. Polymer. 2012.

[47] Perez-Rigueiro J, Viney C, Llorca J, Elices M. Silkworm silk as an engineering material. Journal of Applied Polymer Science. 1998;70(12):2439-2447.

[48] Kelly A, Tyson WR. Tensile properties of fibre-reinforced metals: Copper/tungsten and copper/molybdenum. J Mech Phys Solids. 1965;13(6):329-350.

[49] Bazhenov SL, Volynskii AL, Alexandrov VM, Bakeev NF. Two mechanisms of the fragmentation of thin coatings on rubber substrates. Journal of Polymer Science Part B: Polymer Physics. 2002;40(1):10-18.

[50] Cassie ABD, Baxter S. Wettability of porous surfaces. Transactions of the Faraday Society. 1944;40:546-551.

[51] Chen F, Porter D, Vollrath F. A nonwoven composite model based on silkworm cocoon (*Bombyx mori*). Journal of Materials Science and Engineering. 2010;4(9):28-33.

[52] Gurit Ampreg 20 Epoxy Wet Laminate System, Product datasheet.

[53] Varghese S, Gatos KG, Apostolov AA, Karger-Kocsis J. Morphology and mechanical properties of layered silicate reinforced natural and polyurethane rubber blends produced by latex compounding. Journal of Applied Polymer Science. 2004;92(1):543-551.

[54] Jin H-JP, Jaehyung; Valluzzi, Regina; Cebe, Peggy; Kaplan, David L. Biomaterial Films of Bombyx Mori Silk Fibroin with Poly(ethylene oxide). Biomacromolecules. 2004;5:711-717.

[55] Freddi G, Romano M, Massafra M, Tsukada M. Silk fibroin/cellulose blend films - preparation, structure, and physical-properties. Journal of Applied Polymer Science. 1995;56(12):1537-1545.

[56] Dhakal HN, Zhang ZY, Richardson MOW. Effect of water absorption on the mechanical properties of hemp fibre reinforced unsaturated polyester composites. Composites Science and Technology. 2007;67(7):1674-1683.

[57] Zhong LX, Fu SY, Zhou XS, Zhan HY. Effect of surface microfibrillation of sisal fibre on the mechanical properties of sisal/aramid fibre hybrid composites. Composites Part A: Applied Science and Manufacturing. 2010;42(3):244-252.

[58] Bodros E, Pillin I, Montrelay N, Baley C. Could biopolymers reinforced by randomly scattered flax fibre be used in structural applications? Composites Science and Technology. 2007;67(3):462-470.

[59] Marrakchi Z, Oueslati H, Belgacem MN, Mhenni F, Mauret E. Biocomposites Based on Polycaprolactone Reinforced with Alfa Fibre Mats. Composites Part A: Applied Science and Manufacturing. 2012;43(4):742-747.

Chapter 8

Summary

8.1 General summary

The goal of this DPhil work was to look at engineering aspects of silk cocoons as a structural biological composite system. This research, interdisciplinary in scope, sets out to answer a number of questions. What are the morphologies, structures and physical properties of the cocoons? What are the general structure-property relationships for cocoons? How are cocoons engineered to fit their biological functions? Can we use these engineering relationships to explain other synthetic materials? What can we learn from silk cocoons to develop biomimetic silk composites? This thesis sets out my contribution to partially answer these questions.

Silk cocoons can be described very broadly as nonwoven fibre composites made of silk fibres bonded by sericin binder, although the variety of species can show a diversity of structural features of the layers, porosity, degree of orientation, binding density and presence of crystals etc. These structural differences lead to a range of mechanical behaviour in cocoons. Tensile and compressive properties of cocoons were tested, and different types of cocoon behaviour were summarized due to the inter-fibre and inter-laminate bonding and density. Gas diffusion through the cocoon walls is controlled by the combination of thickness and density, and contributions due to features such as calcium oxalate crystals were identified.

A fundamental quantitative model was developed that links directly the structures and mechanical properties of silk cocoons. The gradual loss of connectivity of the inter-fibre bonding is the key mechanism in cocoons. This connectivity can be quantified as a strain activated function for the gradual loss bonding up to a critical failure criterion, where either a percolation threshold of 50% of these bonds or the failure stress of the binder is reached. In *Bombyx mori* cocoons, which have a graded-layer structure, the model was extended to quantify the contribution of interlayer and intralayer bonding in the system. This model can also be applied to other nonwoven fibre and particulate composites using a small number of physically realistic model parameters.

Based on this understanding of structure-mechanical property relationships in silk cocoons, an engineering approach of Finite Element Analysis was used to examine cocoons as impact resistant structural materials, which provide mechanical protection from environmental threats. In addition, silk cocoons were used as a nonwoven lattice material to develop engineering composites by increasing the matrix bonding connectivity in the cocoons. Using polyurethane or regenerated silk fibroin infusions of medium concentration can increase the toughness of cocoons, and epoxy or regenerated silk fibroin at high concentrations leads to a brittle system.

8.2 General discussion

Silk cocoons, which are complicated hierarchical structural composites, were studied in this thesis. In order to adapt to different environmental pressures, silk cocoons evolved to use a limited number of materials (silk fibre and sericin) to produce a diversity of structural features and consequent physical properties. Like other natural materials, the quality of the

silk fibres is not always consistent due to the animal behaviour and environmental factors. However, a silk cocoon as a composite structure evolved to have a high tolerance to the variation of its components, and the structure itself should be able to cover the weaknesses of the components and ensure relatively consistent properties. In this case, the morphological structure is more important for the composite properties than the individual component properties. This is very different from industrial fibre reinforced composites, where the properties of the components would be far more critical for the composite properties. With these unique features, silk cocoon provides a good starting point for me to study structure-property relationships for non-conventional composites. Together with my colleagues, I studied the components, morphologies and mechanical properties of the silk cocoons, and explored a fundamental structural mechanism that is able to explain these properties.

If I were to condense all my main findings in this thesis into a single concept, I would call it 'Properties Controlled by Connectivity'. The idea of connectivity has been developed from the sericin binder between silk fibres in the cocoon. The mechanical properties of a silk cocoon are determined by the fibre layup and by the properties of the sericin binder and its location as a binder between the fibres in the cocoon. Although not a completely novel idea, we have been able here to develop a physically realistic and quantitative model to describe it. By quantifying the loss of connectivity in the structure, we are able to predict the failure processes of that structure. With an understanding of the form of the connectivity, we can predict the properties and control them by modifying the structures.

Interestingly, this concept is independent of structural dimensions. Here the connectivity is the binder in a nonwoven or particulate structure. However, any structure always has a multidimensional connectivity from atomic to bulk scales. For silk, it could be the hydrogen

bonds between molecules, the disordered regions between nanocrystals, the sericin between fibres in a cocoon, or the fibre interconnects in a spider's web. We can easily extend this idea from across scales, and calculate the connectivity and the activation conditions for its loss at any specific scale to quantify properties. It is interesting to see that the stress-strain curves of silk fibres have a similar form to those of cocoon composites, with strain activated loss of intermolecular bonding replacing sericin binder.

This connectivity concept is especially crucial for biological structures. Many biological structures have evolved to have light weight through porous structures, namely a limited amount of connectivity in the structure, for minimum energy consumption and multifunctionality. Typical examples are cellular structures that are prevalent in feathers, beak interior, cancellous bone and wood. Even for high density ceramic composites like shells, teeth, bones, diatoms and spicules of sponges, porous structures can also be found. In this case, we can predict the properties of these biological materials by understanding their properties in terms of the amount of connectivity in their structures.

This thesis also demonstrate how this connectivity concept is useful for synthetic structural materials, e.g. nanofibre mat, nonwoven fabric, concrete, polymer bonded explosives etc. Although these materials have different morphologies, they can all be seen as a connected structure using various binders. Their properties are all determined by the amount of the connections in the structure and the properties of the binders, which themselves are controlled by the bonding connectivity. The concept is a very useful tool for fundamentally understanding of the structure-property relationships for these technologically important synthetic materials.

As a structural materials engineer, it seems that understanding of the connectivity concept can be applied in a self-consistent way to develop new synthetic materials by altering or modifying properties of the 'binders' and the connectivity numbers in the structures, as the example of synthetic cocoon composites shown in this thesis. Unlike biological systems where the design of the structure and component materials are intimately connected through evolution, synthetic materials design often has a disciplinary separation between component materials and structures across the scales, based largely on tradition. Originated from biological structure, our connectivity concept can be applied to synthetic structures by connecting component material properties and structure for predicting structural properties. It could be a fundamental bioinspired design principle for novel synthetic structural materials from first principles. For example, it may be possible to develop a mathematical formalism for linked scales of connectivity such as the simple relation of equation (4.8) for multiple processes, i

$$\sigma = Y\ \varepsilon\left[1-\sum_i f_i \exp\left(-\left(\frac{\varepsilon_{ai}}{\varepsilon}\right)^2\right)\right] \text{ where } \quad f_i = \frac{Y_i}{Y}$$

where each process has a magnitude , here Y_i, and an activation strain, ε_i, that quantify the connectivity effects. Without learning from the design principles of nature, it is unlikely that we will be able to copy or use natural materials to their full capability.